

The effects of mechanical loading and carbonation on
properties of soils treated with the Stabilization/Solidification
(S/S) method

by

Ghassan ABURAAS

THESIS PRESENTED TO ÉCOLE DE TECHNOLOGIE SUPÉRIEURE IN
PARTIAL FULFILLMENT OF THE REQUIREMENTS FOR THE DEGREE
OF DOCTOR OF PHILOSOPHY
Ph.D.

MONTREAL, DECEMBER 19, 2023

ÉCOLE DE TECHNOLOGIE SUPÉRIEURE
UNIVERSITÉ DU QUÉBEC



(Ghassan Aburaas, 2023)



This Creative Commons licence allows readers to download this work and share it with others as long as the author is credited. The content of this work can't be modified in any way or used commercially.

BOARD OF EXAMINERS

THIS THESIS HAS BEEN EVALUATED

BY THE FOLLOWING BOARD OF EXAMINERS

Mr. François Duhaime, Thesis Supervisor
Department of Construction Engineering, École de technologie supérieure

Mr. Jean-Sébastien Dubé, Thesis Co-supervisor
Department of Construction Engineering, École de technologie supérieure

Mrs. Elmira Moosavi, President of the Board of Examiners
Department of Systems Engineering, École de technologie supérieure

Mr. Yannic Éthier, Member of the jury
Department of Construction Engineering, École de technologie supérieure

Mr. Matthieu François, External Evaluator
SNC-Lavalin

THIS THESIS WAS PRESENTED AND DEFENDED

IN THE PRESENCE OF A BOARD OF EXAMINERS AND PUBLIC

ON DECEMBER 11, 2023

AT ÉCOLE DE TECHNOLOGIE SUPÉRIEURE

ACKNOWLEDGMENTS

I would like to begin by expressing my sincere gratitude to my supervisors, Professor Francois Duhaime and Professor Jean-Sébastien Dubé, for their invaluable guidance and supervision throughout this study. Without their dedicated efforts, this dissertation would not have been possible. I am truly grateful for their teachings, which instilled in me the virtues of perseverance, patience, attention to detail, a thirst for knowledge, and openness to criticism during my doctoral studies.

I would also like to extend my thanks to the members of my Ph.D. committee, namely Professors Elmira Moosavi, Yannic Éthier, and Matthieu François. Their careful review of this thesis and their valuable comments and suggestions have greatly enhanced the quality and substance of this dissertation.

I am also indebted to the technicians of ETS and my colleagues at LG2 group for their assistance and practical support and camaraderie throughout this journey.

I humbly extend my heartfelt gratitude and dedicate this work to my beloved wife, Eman, whose unwavering love, infinite patience, unwavering support, and profound understanding have been indispensable throughout the arduous journey of my doctoral research. To my cherished children, Alharith, Jana, Atika, and my precious angel Talyh, you are the epitome of inspiration and joy in my life. Your presence and unwavering belief in my abilities have been a constant source of motivation and strength.

I reserve the closing words of this dedication for my family, whose unyielding support has been instrumental in shaping my academic path. To my parents, your boundless love and unwavering support from the earliest stages of my educational journey have been invaluable. I cannot forget to thank my brothers and my sisters for their encouragement which helped me a lot to face the difficulties.

Les effets de la charge mécanique et de la carbonatation sur les propriétés des sols traités avec la méthode de stabilisation/solidification (S/S)

Ghassan Aburaas

RÉSUMÉ

Au cours des dernières décennies, on a constaté une augmentation significative de l'accumulation de déchets dangereux dans différentes régions du monde. Une partie du problème réside dans le fait que ces déchets sont générés quotidiennement et que leurs caractéristiques chimiques limitent l'application de certaines méthodes de remédiation. La solidification/stabilisation (S/S) représente une méthode de traitement de divers contaminants, y compris les déchets dangereux tels que les métaux traces. Notamment, cette technique a suscité l'intérêt en tant qu'alternative prometteuse grâce à sa capacité à offrir des solutions pratiques pour la santé humaine et environnementale (Al Tabbaa & Stegemann, 2011). Les techniques de solidification/stabilisation à base de ciment ont été largement utilisées pour produire des formes stables de sols contaminés et limiter le transfert des contaminants dans l'environnement.

Cependant, les structures de matrice solidifiée/stabilisée présentes sur les sites sont continuellement exposées à diverses conditions agressives, notamment des charges fluctuantes et du dioxyde de carbone atmosphérique. De plus, il existe un manque d'informations concernant les performances à long terme des techniques de S/S dans ces conditions environnementales spécifiques. La présence de charges externes favorise la propagation des fissures, facilitant la pénétration d'agents agressifs tels que l'eau dans la matrice S/S. Ce phénomène accélère la détérioration de la structure S/S. En revanche, la carbonatation entraîne la précipitation de calcite (produits de carbonatation) dans ces fissures, réduisant la porosité et permettant des processus d'autoguérison. L'autoguérison, à son tour, a le potentiel d'améliorer les propriétés hydrauliques de la matrice S/S. Par conséquent, l'étude de l'impact de la charge et de la carbonatation sur les propriétés chimiques et mécaniques de la matrice S/S est importante pour comprendre la stabilité à long terme de la structure.

L'objectif principal de ce projet consistait à simuler les conditions environnementales, telles que la charge et l'exposition au CO₂, sur du sable solidifié. La simulation de la matrice solidifiée a été réalisée en induisant des altérations physico-chimiques grâce à la mise en œuvre de divers scénarios expérimentaux, à savoir : aucune carbonatation/ aucune charge (NC/NL), carbonatation seule (C), charge mécanique seule (L), carbonatation suivie de charge mécanique (C/L), et charge mécanique suivie de carbonatation (L/C). Des échantillons solidifiés avec un rapport eau/ciment (W/C) de 2 ont été préparés et soumis à des tests de lixiviation à l'aide d'une configuration de lixiviation en continu. Ces simulations ont été réalisées à l'aide d'une cellule triaxiale modifiée. Les résultats expérimentaux présentés dans cette thèse ont mis en évidence la détérioration résultant des scénarios susmentionnés, qui englobaient des contraintes mécaniques et la carbonatation. De plus, une étude sur la cicatrisation physico-chimique des microfissures au sein de la matrice S/S a été réalisée grâce à des tests de conductivité hydraulique et à la tomographie par rayons X. Par ailleurs, les effets de ces scénarios

VIII

expérimentaux ont été examinés en ce qui concerne la résistance à la compression, la conductivité électrique, le pH, la lixiviation de l'aluminium, du silicium, du calcium et du cuivre, ainsi que l'analyse thermogravimétrique.

Lors de l'application de divers scénarios de test sur les échantillons, des résultats distincts ont été observés. Le scénario de contrôle a présenté une légère diminution de la conductivité hydraulique, indiquant un impact négligeable. En revanche, la carbonatation a présenté des avantages significatifs en réduisant la conductivité hydraulique et en diminuant la porosité, facilitant ainsi les processus d'autoguérison. Les contraintes mécaniques ont provoqué des fractures et des dommages sur le sable solidifié, qui, bien qu'impossible à éliminer complètement, ont été atténués dans une certaine mesure grâce à l'autoguérison induite par la carbonatation, réduisant ainsi la formation de fissures. De plus, l'ordre des opérations, tel qu'indiqué par l'analyse CT, a révélé des différences perceptibles (par exemple, la carbonatation par rapport à la charge), principalement attribuées aux effets d'autoguérison qui favorisent une récupération partielle des propriétés physiques des échantillons.

Les conclusions de cette thèse ont également montré différents comportements en termes de lixiviation du calcium. Les scénarios sans carbonatation ont présenté une lixiviation stable du calcium sur une période prolongée. Cependant, la présence de carbonatation dans les scénarios C, C/L et L/C a entraîné une diminution significative de la lixiviation du calcium. En ce qui concerne la lixiviation du cuivre, elle était modeste et stable, comme en témoigne le scénario NC/NL. Cependant, lors de l'exposition à la carbonatation, trois phases distinctes de lixiviation du cuivre ont été observées, à savoir une augmentation notable, suivie d'une diminution partielle, pour finalement atteindre un état stable. Les contraintes mécaniques avaient tendance à réduire la lixiviation du cuivre, avec une concentration de cuivre non détectable dans les effluents du scénario L après une courte durée. De plus, le test de lixiviation a révélé une légère augmentation du volume des pores dans le scénario NC/NL, tandis que la carbonatation réduisait significativement la porosité globale de l'échantillon. En revanche, l'effet de charge augmentait la porosité totale dans les scénarios L, C/L et L/C.

Les résultats indiquent que l'influence des facteurs de stress sur la lixiviation, la distribution de la taille des vides, la résistance à la compression et la perméabilité est complexe et caractérisée par des interactions entre les contraintes.

Mots-clés: Solidifié/stabilisé, conductivité hydraulique, carbonatation, chargement mécanique, scan micro-CT aux rayons X, résistance à la compression non confinée, métaux lourds, cellule triaxiale modifiée, phénomène d'autoguérison, test de lixiviation en continu

The effects of mechanical loading and carbonation on properties of soils treated with the Stabilization/Solidification (S/S) method

Ghassan Aburaas

ABSTRACT

In the last few decades, there has been a significant increase in the accumulation of hazardous wastes across various areas of the world. Part of the problem is that these wastes are generated daily, and their chemical characteristics limit the application of some remediation methods. Solidification/Stabilization (S/S) represents a method for treating diverse contaminants, including hazardous wastes like trace metals. Notably, this technique has garnered attention as a promising alternative owing to its capacity to offer practical resolutions for both human and environmental health (Al Tabbaa & Stegemann, 2011). Cement-based solidification/stabilization techniques have gained extensive utilization in producing stable forms of contaminated soils and curtailing the movement of contaminants into the environment.

However, the solidified/stabilized matrix structures present at sites are continually exposed to various aggressive conditions, including fluctuating loads and atmospheric carbon dioxide. Moreover, there is a lack of information regarding the long-term performance of S/S techniques under these specific environmental conditions. The presence of external loads promotes crack growth, facilitating the penetration of aggressive agents such as water into the S/S matrix. This phenomenon accelerates the deterioration of the S/S structure. Conversely, carbonation leads to the precipitation of calcite (carbonation products) into these cracks, reducing porosity and enabling self-healing processes. Self-healing, in turn, has the potential to enhance the hydraulic properties of the S/S matrix. Therefore, investigating the impact of loading and carbonation on the chemical and mechanical properties of the S/S matrix is important for comprehending the long-term stability of the structure.

The primary objective of this project entailed the simulation of environmental conditions, such as loading and exposure to CO₂, on solidified sand. The simulation of the solidified matrix was achieved by inducing physicochemical alterations through the implementation of various experimental scenarios, namely: no carbonation/no loading (NC/NL), carbonation only (C), mechanical loading only (L), carbonation followed by mechanical loading (C/L), and mechanical loading followed by carbonation (L/C). Solidified samples with a water-to-cement ratio (W/C) of 2 were prepared and subjected to leaching tests using a flow-through leaching setup. These simulations were conducted using a modified triaxial cell. The experimental findings presented in this thesis elucidated the deterioration resulting from the aforementioned scenarios, which encompassed mechanical stresses and carbonation. Moreover, an investigation into the physicochemical healing of micro-cracks within the S/S matrix was carried out through hydraulic conductivity testing and X-ray CT scanning. Furthermore, the effects of these experimental scenarios were examined in relation to compressive strength, electrical conductivity, pH, leaching of aluminum, silicon, calcium, and copper, as well as thermogravimetric analysis.

Upon subjecting the samples to various test scenarios, distinct results were observed. The control scenario exhibited a marginal decrease in hydraulic conductivity, indicating a negligible impact. Conversely, carbonation exhibited significant advantages by reducing hydraulic conductivity and lowering porosity, thereby facilitating self-healing processes. Mechanical stresses induced fractures and inflicted damage upon the solidified sand, which, albeit impossible to completely eliminate, were mitigated to some extent through carbonation-induced self-healing, thereby reducing crack formation. Furthermore, the order of operations, as revealed by the CT analysis, demonstrated perceptible differences (e.g., carbonation versus loading), primarily attributed to the self-healing effects that promote partial recovery of the physical properties of the samples.

The findings of this thesis also showed different behaviors in terms of calcium leaching. The non-carbonation scenarios exhibited stable calcium leaching over an extended period. However, the presence of carbonation in the C, C/L, and L/C scenarios resulted in a significant decrease in calcium leaching. In the case of copper leaching, it was modest and stable, as evidenced by the NC/NL scenario. However, upon exposure to carbonation, three distinct phases of copper leaching were observed, namely a notable increase, followed by a partial decrease, and ultimately reaching a steady state. Mechanical stresses tended to diminish copper leaching, with no detectable copper concentration in the leachate of the L scenario after a short duration. Furthermore, the leaching test revealed a slight increase in pore volume in the NC/NL scenario, while carbonation significantly reduced the overall porosity of the sample. Conversely, the loading effect increased the total porosity in the L, C/L, and L/C scenarios.

The results indicate that the influence of stressors on leaching, void size distribution, compressive strength and permeability is complex and characterized by interactions between the stressors.

Keywords: Solidified/stabilized, hydraulic conductivity, Carbonation, Mechanical loading, X-ray micro-CT scan; Unconfined compressive strength; Heavy metals; Modified triaxial cell, Self-healing phenomenon, Flow-through leaching test

TABLE OF CONTENTS

	Page
INTRODUCTION	1
CHAPTER 1 LITERATURE REVIEW	5
1.1 Waste Management.....	5
1.1.1 Waste storage in deep mines.....	6
1.1.2 Use of chemical methods.....	6
1.1.3 Bitumen encapsulation.....	7
1.1.4 Solidification/Stabilisation.....	7
1.2 Portland Cement.....	8
1.2.1 Portland cement and its hydration.....	8
1.2.2 Mechanical and hydraulic properties of cement-based materials.....	13
1.2.3 pH of the pore solution of the concrete matrix.....	15
1.3 Microstructure and Permeability of Solidified Sand	16
1.3.1 Microstructure of solidified matrix.....	16
1.3.2 Hydraulic conductivity of concrete.....	17
1.4 Stabilization/Solidification Processes (S/S).....	18
1.4.1 Interactions between S/S Binder and Contaminants.....	19
1.4.1.1 Immobilization mechanisms of contaminant.....	19
1.4.1.2 Immobilization of metals in cement-based S/S	21
1.4.1.3 Retention of copper.....	22
1.5 Carbonation.....	24
1.5.1 Natural carbonation phenomenon.....	24
1.5.1.1 Carbonation of portlandite.....	25
1.5.1.2 Carbonation of calcium silicate hydrate	27
1.5.2 Factors influencing the carbonation process.....	28
1.5.2.1 Factors related to the surrounding environment.....	28
1.5.2.2 The influence of composition parameters.....	29
1.5.2.3 Concentration of CO ₂ and pore saturation.....	30
1.5.3 Main consequences of carbonation on cement-based materials	32
1.5.3.1 Change in pH.....	32
1.5.3.2 Modification of the microstructure.....	33
1.5.3.3 Modification of hydraulic conductivity.....	34
1.5.3.4 Influence of carbonation on metals leachability.....	35
1.6 Mechanical Stresses.....	36
1.6.1 Causes of cracks formation.....	36
1.6.1.1 Shrinkage	37
1.6.1.2 Chemical reactions.....	38
1.6.1.3 External loads	38
1.6.2 Influence of cracking on concrete permeability.....	39

1.7	Leaching.....	40
1.7.1	Selecting leaching test.....	40
1.7.1.1	Flow-through leaching test	42
1.8	Self-healing Phenomenon	43
1.8.1	Self-healing mechanisms	43
1.8.1.1	Formation of calcium carbonate (CaCO_3)	45
1.8.1.2	Continued hydration phenomenon.....	45
1.8.1.3	Accumulation of particles.....	46
1.8.2	Parameters influencing the self-healing.....	46
1.8.2.1	Influence of crack width on self-healing	46
1.8.2.2	Influence of matrix properties: pH, age, and W/C ratio	47
1.8.2.3	Influence of humidity	48
1.8.3	Effect of healing on concrete properties	48
1.9	X-Ray Micro-Tomography (CT Scans).....	49
1.9.1	Principle of tomography	49
1.9.2	Micro-CT applications in geotechnical engineering.....	50
1.10	Summary and Research Objectives	55
CHAPTER 2 MATERIALS, METHODS, AND EXPERIMENTAL FRAMEWORK		59
2.1	Leaching Protocols and Stressor Scenarios	59
2.1.1	Leaching protocols.....	59
2.1.2	Stressor scenarios.....	61
2.2	Experimental Setup and Devices	62
2.2.1	The modified triaxial cell.....	62
2.2.2	Test system for stressor scenarios.....	64
2.2.2.1	Accelerated carbonation	64
2.2.2.2	Mechanical Loading	65
2.2.2.3	Flow-through leaching test (FTL)	65
2.3	Materials	67
2.3.1	Silica Sand	67
2.3.2	Cement (GU).....	70
2.3.3	Contaminant.....	71
2.3.4	Preparation of solidified/stabilized samples	71
2.4	Experimental Characterization Tests	73
2.4.1	Mechanical and hydraulic characterization	73
2.4.1.1	Unconfined compressive strength (UCS).....	73
2.4.1.2	Hydraulic conductivity test.....	74
2.4.2	Chemical analysis of pore solution.....	75
2.4.3	Techniques for carbonation detection.....	76
2.4.3.1	Colour Indicator (Phenolphthalein)	76
2.4.3.2	Thermogravimetric analysis (TGA).....	76
2.4.4	Observation by X-ray CT.....	78
2.4.4.1	Image configuration and acquisition	79
2.4.4.2	Image processing	80

CHAPTER 3	EXPERIMENTAL RESULTS.....	85
3.1	Hydraulic conductivity.....	85
3.2	Compressive strength.....	87
3.3	Evaluation of chemical properties	88
3.3.1	pH.....	88
3.3.2	Electrical conductivity	89
3.3.3	Aluminium leaching.....	91
3.3.4	Silicon leaching.....	93
3.3.5	Calcium leaching	95
3.3.6	Leaching behaviour of Copper (Cu)	97
3.4	Carbonation detection	100
3.4.1	Phenolphthalein test.....	100
3.4.2	Thermogravimetric analysis (TGA).....	104
3.5	Evolution of the microstructure observed in X-ray tomography	110
3.6	Influence of carbonation and loading on the sample appearance	116
CHAPTER 4	ANALYSIS OF EXPERIMENTAL RESULTS.....	119
4.1	Leaching.....	119
4.2	Carbonation.....	123
4.3	Mechanical strain.....	128
4.4	Interactions between leaching, loading and carbonation.	131
CONCLUSION AND RECOMMENDATIONS		139
BIBLIOGRAPHY.....		149

LIST OF TABLES

	Page
Table 1.1	Composition of Portland cement8
Table 1.2	Composition and properties of cement phases9
Table 1.3	Influence of carbonation on porosity34
Table 2.1	Chemical composition of silica sand (Atlantic Silica Inc)69
Table 2.2	Geometric characteristics of silica sand69
Table 2.3	Chemical composition of Portland cement (GU)70
Table 2.4	Physical properties of Portland cement (GU).....71
Table 2.5	Decomposition of hydration products78
Table 3.1	Percentage of CO ₂ and CaCO ₃ before and after leaching test (NC/NL and L scenarios)108
Table 3.2	Percentage of CO ₂ and CaCO ₃ after leaching test (first procedure)109
Table 3.3	Percentage of CO ₂ and CaCO ₃ before and after leaching test (C, C/L and L/C scenarios).....109
Table 3.4	Percentage of total pores before and after the leaching tests.....111
Table 3.5	Variations of a sample volume before and after the leaching test.....116

LIST OF FIGURES

	Page
Figure 1.1	Stages of hydration as a function of heat flux11
Figure 1.2	Strength development in a cement matrix14
Figure 1.3	Tortuosity of the concrete matrix for different aggregate sizes.....18
Figure 1.4	Solubility of metal hydroxide21
Figure 1.5	Main chemical species involved in the carbonation phenomenon26
Figure 1.6	CO ₂ distribution during the continuous and cyclic process.....27
Figure 1.7	Relationship between the depth of carbonation and RH29
Figure 1.8	Relation between CO ₂ concentration and carbonation depth31
Figure 1.9	Micro-cracks due to shrinkage of paste38
Figure 1.10	Water flowing (a) around the matrix; (b) through the matrix.....42
Figure 1.11	Self-healing mechanisms44
Figure 1.12	Water flow as a function of crack width.....47
Figure 1.13	Schematic of the micro-CT and its elements.....50
Figure 1.14	2D images (a) original image and (b) segmented image51
Figure 1.15	Distribution of healing products in 3D images.....52
Figure 1.16	Image pre-processing procedure.....53
Figure 1.17	CT images of the crack healing54
Figure 1.18	3D distribution of a) small pores (grey) and macropores (blue), b) cracks (red), and c) healing products (yellow)55
Figure 2.1	Stressor scenarios for the continuous water injection protocol60
Figure 2.2	Stressor scenarios for the intermittent water injection protocol60
Figure 2.3	Cross-section of the modified triaxial cell.....62

Figure 2.4	Equipment required for the test sample	63
Figure 2.5	The system of CO ₂ injection into the sample	64
Figure 2.6	Schematic diagram of flow-through leaching test.....	66
Figure 2.7	Accelerated leaching test: a) collection reservoir during the night, b) collection tube during the day, c) membrane syringe filters, and d) the initial set of leachate tests.....	67
Figure 2.8	Silica sand from Atlantic Silica Inc.....	68
Figure 2.9	Grain size distribution of the tested silica sand	70
Figure 2.10	Stages of solidified sample preparation: a) copper oxide and tap water mixed, b) electric mixer, c) manual mixing, d) samples in a plastic bag in a humidity room	72
Figure 2.11	Compacting tools used to prepare S/S samples	73
Figure 2.12	Uniaxial compression test on a cylindrical sample.....	74
Figure 2.13	Equipment of triaxial cell: a) control panel, b) sample placed on the base of the cell, c) the sample under the test, and d) the hydraulic conductivity panel (burettes)	74
Figure 2.14	Example of phenolphthalein on concrete	77
Figure 2.15	S/S sample placed on CT system at École de technologie supérieure.....	79
Figure 2.16	Stages of image observation and pores detection	79
Figure 2.17	2D images processing and segmentation: A) original image; B) image filtering; C) Material with pores; D) pores filled; E) pores obtained	82
Figure 3.1	Hydraulic conductivity for the intermittent water injection protocol.....	86
Figure 3.2	Variation of electrical conductivity values (scenarios NC/NL and L)	89
Figure 3.3	Variation of electrical conductivity values (scenarios C).....	90
Figure 3.4	Variation of electrical conductivity values (scenarios C/L, and L/C)	90
Figure 3.5	Variation of Al values (scenarios NC/NL and L).....	91

Figure 3.6	Variation of Al values (scenario C).....	92
Figure 3.7	Variation of Al values (scenarios C/L and L/C).....	93
Figure 3.8	Variation of Si concentrations (scenarios NC/NL and L)	94
Figure 3.9	Variation of Si concentrations (scenarios C, C/L, and L/C).....	95
Figure 3.10	Variation of Ca concentrations (scenarios NC/NL, C and L).....	96
Figure 3.11	Variation of Ca concentrations (scenarios C/L and L/C)	97
Figure 3.12	Variation of copper as a function of cumulative time for NC/NL and L scenarios	98
Figure 3.13	Variation of copper as a function of cumulative time for C scenario.....	99
Figure 3.14	Variation of copper as a function of cumulative time for C/L and L/C scenarios	99
Figure 3.15	S/S sample stained with the phenolphthalein solution (NC/NL scenario)	101
Figure 3.16	S/S sample stained with the phenolphthalein solution (L scenario).....	101
Figure 3.17	Sample before being cut into three discs, each with a thickness of 3 cm	102
Figure 3.18	Solidified sample stained with the phenolphthalein solution (C scenario).....	103
Figure 3.19	Solidified sample stained with the phenolphthalein solution (C/L scenario).....	103
Figure 3.20	Solidified sample stained with the phenolphthalein solution (L/C scenario).....	104
Figure 3.21	DTG curves of all scenarios before any tests (initial stage).....	105
Figure 3.22	DTG curves of the NC/NL before and after the leaching test.....	106
Figure 3.23	DTG curves for the loading (L) scenario before and after the leaching test	106
Figure 3.24	DTG curves for C, C/L, and L/C scenarios after the leaching test.....	107

Figure 3.25	Pores and cracks on the S/S matrix after multiple cycles of loading and carbonation.....	111
Figure 3.26	Pore size distribution before and after the leaching test (NC/NL scenario)	112
Figure 3.27	Pore size distribution before and after the leaching test (L scenario).....	113
Figure 3.28	Pore size distribution before and after the leaching test (C scenario).....	114
Figure 3.29	Pore size distribution before and after the leaching test (C/L scenario)	115
Figure 3.30	Pore size distribution before and after the leaching test (L/C scenario)	115
Figure 3.31	Comparison of the changes in sample colour in each test scenario: carbonated samples (buff) and un-carbonated samples (gray)	117
Figure 4.1	Vertical CT scan sections for the NC/NL scenario A) before and B) after FTL test.....	120
Figure 4.2	Variations of Ca concentrations as a function of pH.....	121
Figure 4.3	Variations of Si concentrations as a function of pH.....	122
Figure 4.4	Vertical CT scan sections for the C scenario A) before and B) after FTL test.....	123
Figure 4.5	Relationship between porosity and hydraulic conductivity.....	125
Figure 4.6	Variations of Cu concentrations as a function of pH.....	127
Figure 4.7	Vertical CT scan sections for the L scenario A) before and B) after FTL test	128
Figure 4.8	Vertical CT scan sections for the C/L scenario A) before and B) after FTL test	133
Figure 4.9	Vertical CT scan sections for the C/L scenario A) before and B) after FTL test	134

LIST OF ABBREVIATIONS

C	Carbonation Only
C/L	Carbonation followed by mechanical loading
CAH	Hydrates calcium aluminate
CEPA	Canadian environmental protection act
CT	Computed tomography
C-S-H	Calcium silicate hydrate
CH	Portlandite
DI	Deionized water
EC	Electrical conductivity
FTL	Flow-through leaching test
GU	General Use cement
ICP-OES	Inductively coupled plasma optical emission spectroscopy
L	Mechanical loading only
L/C	Mechanical loading followed by carbonation
MSW	Municipal Solid Waste
NC/NL	No carbonation / no mechanical loading
OWC	Optimum water content
SCE	Sequential chemical extraction tests
S/S	Stabilization/solidification
TCLP	Toxicity characteristic leaching procedure test
TGA	Thermogravimetric analysis

UCS	Unconfined compressive strength
W/C	Water to cement ratio
μ -CT	X-ray microcomputed tomography

LIST OF SYMBOLS

Al	Aluminum
°C	Degree Celsius
Ca	Calcium
CaCO ₃	Calcium carbonate
Ca(OH) ₂	Portlandite/ calcium hydroxide
Cc	Coefficient of curvature
m/s	Meter/second
CO ₂	Carbon dioxide
Cu	Coefficient of uniformity
Cu	Copper
h	Hour
k	Hydraulic conductivity
kN	Kilo newton
kPa	Kilopascal
mg/L	Milligram Per Litre
mm	Millimeter
MPa	Megapascal
Pb	lead
Si	Silicon
SW	Well-graded sand
Zn	Zinc
µg	Microgram

μm	Micrometre
β	Skempton coefficient
2D	2 Dimension
3D	3 Dimension

INTRODUCTION

Cement-based stabilization/solidification (S/S) has been used in the USA to treat contaminated soils since the early 1970s (Conner & Hoeffner, 1998b). The S/S technique creates a composite material composed of waste materials or soil mixed with Portland cement. The S/S microstructure varies based on the material, cement type, water/cement ratio, and degree of hydration. The monolithic material produced from the S/S technique prevents the waste from contaminating the surrounding air, water and soil by limiting the rate of transport of contaminants (Catalan, Merlière & Chezick, 2002). The S/S technique also enhances the durability of the treated material in the S/S matrix (Al-Tabbaa & Boes, 2002).

Many factors can influence the long-term stability S/S-treated wastes. Some factors affect the physical integrity of the S/S matrix, while other factors affect the chemical equilibrium of the S/S matrix. Carbonation is the primary chemical reaction that typically influences the long-term performance of S/S materials (Walton, Bin-Shafique, Smith, Gutierrez & Tarquin, 1997). It is a natural reaction between carbon dioxide and cementitious materials in the S/S matrix. This phenomenon commonly occurs when carbon dioxide dissolves in the pore solution of the S/S matrix and reacts with Portlandite to form calcium carbonate (CaCO_3) (Du, Wei, Reddy & Wu, 2016; Jiangying et al., 2008). In the long term, carbonation also decomposes the calcium silicate hydrate (C-S-H) gel into CaCO_3 and water (Du et al., 2016; Jiangying et al., 2008).

The precipitation of calcium carbonate in the pore space will prompt structural changes in the S/S material. Although these changes can enhance self-healing of S/S material since CaCO_3 precipitates in cracks and pores, CaCO_3 's binding properties are usually weak compared to the original cement phases (Li & Yang, 2007).

Carbonation also impacts the S/S materials' leaching performance. The precipitation of CaCO_3 decreases the pH of the pore solution. It reduces the solubility of certain metals (e.g., Pb, Ni and Zn). In contrast, carbonation can increase the release of copper and arsenic (Sanchez, Gervais, Garrabrants, Barna, & Kosson, 2003; Garrabrants, Sanchez & Kosson, 2004).

Over time, cracks can form in the S/S matrix, which can affect its physical integrity and result in the degradation of its properties, such as compressive strength, stiffness, and hydraulic conductivity. Cracks in S/S materials can be formed and worsened by external loading, hydraulic gradients, volume expansion, internal stresses, and temperature changes caused by chemical reactions and freezing temperatures. Griffith's theory assumes that cracks typically occur due to increased loading that causes higher stress in a material (Barenblatt, 1959). However, when stress is distributed over certain areas of a material, it creates an energy imbalance and begins to change the shape of voids and the coalescence of micro-cracks that exist in the matrix (Barenblatt, 1959; Chang & Lee, 2004).

Additionally, these fractures can intersect or combine to form networks of cracks known as linked cracks (Szelağ, 2018). These cracks can critically degrade the mechanical characteristics of the portions of the material that are subjected to stress. In particular, the permeability of S/S materials subjected to mechanical loading increases (Chang & Lee, 2004). The cracks are critical because they increase water flow, which induces the release of metals from the S/S material, calcium leaching and concrete degradation (Ekström, 2003). In addition, the dissolution of calcium hydroxide can increase the porosity and reduce the material strength (Ekström, 2003). The final outcome is the matrix's failure to isolate the waste.

Despite the encouraging results from the use of the S/S technique in many countries around the world, there is a lack of information regarding the long-term stability and retention properties of contaminants (Al Tabbaa & Stegemann, 2011), which could be caused by the lack of a standardized method for assessing long-term behaviour (Al Tabbaa & Stegemann, 2011). For example, some test methods (e.g., leaching mechanisms of metals) may not reflect the change in long-term monitoring of S/S materials in-situ conditions. In addition, the long-term environmental durability and stability of the S/S matrix are critical. Because most S/S matrices are underground, they are vulnerable to various external stresses, and accelerate the leaching mechanisms that can develop over time due to contact with groundwater (Du et al., 2010; Kogbara, 2014). However, some leaching tests (e.g., toxicity characteristic leaching

procedure, sequential chemical extraction test, and column test) may not be appropriate for monitoring the long-term stability of S/S materials (Catalan et al., 2002). The hydraulic conductivity of the S/S matrix is one of the main factors that can govern the transport system of the S/S matrix, particularly the leachate transport.

The main phenomena influencing the long-term performance of S/S materials that were studied in this thesis are carbonation and mechanical loading. These phenomena have been studied in the laboratory, but almost exclusively separately and without confining stress, which is known to influence the formation and the aperture of cracks. Cracks not only influence the microstructure and transport parameters of S/S materials, but it can also affect CO₂ penetration.

In this context, a triaxial cell was used to carry out CO₂ gas injection and to apply a strain on sand samples treated with the S/S method. The triaxial cell was also used to carry out leaching tests on the samples. Several leaching tests have been utilized for other geotechnical applications to evaluate environmental stability according to standardized tests such as the ASTM standards. However, there is no leaching test available that simulates environmental conditions and estimates the stability of solidified materials in the long term. Furthermore, since most tests do not consider any confining stresses, a flow-through leaching test must be conducted in order to assess the long-term stability of S/S (Butcher, Cheeseman, Sollars & Perry, 1993; Poon, Chen & Wai, 1999; Zhang, Wang, Dong, Feng & Fan, 2009). In the flow-through leaching test, the injected water is constantly renewed. This test can also simulate the way water comes in contact with S/S materials in environmental conditions.

This research project aims to investigate the impact of carbonation and loading on hydraulic conductivity, compressive strength, the leaching of metals, the change in microstructure, and the self-healing phenomenon of the solidified matrix. Given the need to simulate the environmental conditions such as carbonation and loading in a laboratory setting, specific experimental devices and protocols had to be developed. To this end, two different leaching test protocols were used to examine the solidified samples. Carbonation and mechanical

loading were also used with a modified triaxial cell and computed tomography (micro-CT) technique.

This thesis is organized into six chapters, as follows:

CHAPTER 1 presents a brief survey of existing waste treatment methods, as well as Canada's regulations and waste policy. An overview of the interactions between cement and soil, and the hydration of Portland cement is presented. Carbonation and mechanical loading, the two main long-term stressors studied in this thesis, are described with the factors that influence carbonation. The main consequences of carbonation on cement-based materials are listed, along with the causes of cracking in concrete structures. An overview of self-healing phenomena in cement-based materials is also presented. Finally, an overview of X-ray tomography applications in geotechnical engineering is presented. **CHAPTER 2** introduces the methods, materials and equipment used in this study. The proposed methodology consists of two protocols with either intermittent or continuous leaching. Each experimental protocol included five test scenarios combining different loading and carbonation stages. The test scenarios and leaching tests were conducted using a modified triaxial cell described in this chapter. The methodology for the tests used to characterize the hydraulic and mechanical properties of the S/S material are presented in this chapter. It also describes the methodology for the thermogravimetric analysis and X-ray tomography. Moreover, this chapter presents the materials and the preparation of the solidified sand samples. **CHAPTER 3** includes experimental results including the hydraulic conductivity, compressive strength, leachate analyses, thermographic analyses, and a description of the microstructure based on X-ray tomography. **CHAPTER 4** compares the result of the various test scenarios. Finally, the conclusion, recommendations and main contributions of this thesis are listed in **CHAPTER 5**.

CHAPTER 1

LITERATURE REVIEW

This chapter contains background information on waste treatment and waste regulations in Canada. It also reviews the S/S technique, as well as two important stressors: carbonation and mechanical loading. Information is also provided on self-healing mechanisms in concrete and X-ray tomography.

1.1 Waste Management

In recent decades, hazardous waste generation has dramatically increased in many areas of Europe and North America. It has become highly dangerous since it has a long-lasting adverse impact on humans and the environment (Blackman Jr, 2016). According to Section 64 of the Canadian Environmental Protection Act (1999), waste is considered toxic if it harms human life or the environment (Taylor & Chénier, 2003). In 1992, the government of Canada spent approximately \$3 billion on managing nearly 33.76 million tonnes of waste (Sawell, Hetherington & Chandler, 1996). The Canadian Government has since adopted successful strategies for reducing waste generation and, consequently, its financial strains. In 2008, it was estimated that it costs Canadians nearly \$1.8 billion to manage about 13 million tonnes of waste (Statistics Canada, 2008), which includes 8.5 million tonnes of waste sent to landfills and 4.4 million tonnes of recycled or composted waste (Statistics Canada, 2008). Despite the Government's efforts, it is clear that landfilling is still the predominant route for waste disposal in this country.

In Canada, three levels of government can share environmental protection responsibilities within their jurisdictions. Local governments establish disposal programs for waste, while provincial governments adopt criteria for licensing dangerous waste producers and treatment facilities. The federal government regulates the transboundary transportation of this waste and passes legislation that regulates contaminated site remediation (e.g., the Canadian

Environmental Protection Act). It should be noted that each province across Canada has policy frameworks in place for managing contaminated sites. In addition, all provinces establish their own guidelines. For example, the first province to publish guidelines for the management of contaminated areas was Nova Scotia. Ontario also established standard guidelines for a range of substances, while Yukon has a list of soil criteria that concentrate on metals (Bates & Hills, 2015). The treatment of contaminated soils requires advanced methods to reduce the release of their toxicity into the environment. Recently, several methods have been employed for the treatment of contaminated soils, and the selection of the best option depends on the contaminant category as well as the advantages and disadvantages of each technique.

1.1.1 Waste storage in deep mines

One possibility for the disposal of hazardous waste is underground storage in sealed capsules or mixing the hazardous waste with cement. Storing hazardous waste in deep salt mines is possible because these mines must be located below drinking aquifers (Lee & Lee, 2012). Geological and hydrological data should confirm that there is no hydraulic connection between pollutants and groundwater to ensure the long-term stability of waste and to avoid soil and water contamination (Hjelmar, 1996). Using former mines for long-term waste disposal is limited by space availability.

1.1.2 Use of chemical methods

Chemical methods can reduce the mobility of pollutants into the environment. These methods significantly reduce the leachability of metals, either through the precipitation of metal or by converting them into insoluble materials (Dhaliwal, Singh, Taneja & Mandal, 2020). Technology focused on chemical methods has been developed in recent years involving the Chemical Fixation Process (stabilization), the Chemical Leaching Process, the Ferrox Process, and the Acid Extraction-Sulfide Process (AES) (Dhaliwal et al., 2020; Katsuura, Inoue, Hiraoka & Sakai, 1996; Rani, Boccaccini, Deegan & Cheeseman, 2008).

1.1.3 Bitumen encapsulation

Some hazardous waste can be immobilized by using bitumen encapsulation. Although this technology has many advantages regarding chemical stability, impermeability to water, and resistance to micro-organisms and cracking, it can be very costly since it depends on the price of crude oil (Rani et al., 2008).

1.1.4 Solidification/Stabilisation

The Stabilization/Solidification (S/S) technique, which treats hazardous waste for safe disposal, includes both chemical and physical treatment. One way S/S contrasts with other hazardous waste management solutions is by immobilizing toxic components in waste rather than removing them. Solidification converts waste into solid form via the soil-cement matrix (Wuana & Okieimen, 2011) and changes in the physical properties of the matrix, such as permeability and compressive strength (Wiles, 1987). At the same time, stabilization limits the solubility of hazardous components, such as metals contained in the waste, by three main mechanisms: sorption, complexation and precipitation (Bone et al., 2004). The S/S technique has many advantages including its low cost, resistance to biodegradation, and low-water permeability.

S/S projects have been conducted in Canada since 1990. Applications include treating contaminated soils and managing mining sites (Conner & Hoeffner, 1998b). Most of these projects originated in western Canada, specifically in BC. For example (but not limited to) the Dockside Green project, the False Creek project, the Rifle Range project, and the Western Steel Mill project are notable solidification/stabilization projects in Canada (Bates & Hills, 2015). On the other hand, it is essential to note that Nova Scotia has the most significant S/S project in the world: the Sydney Tar Ponds (Bates & Hills, 2015; Walker, MacAskill & Weaver, 2013), which spans nearly 33 hectares. In Québec, S/S has been used to a limited

extent to treat contaminated soil with metals (St-Laurent, Burelle, Ouellette, Bonneau & Larue, 2012).

1.2 Portland Cement

Portland cement is one of the most common binders for S/S applications (Shi & Spence, 2004; Yousuf, Mollah, Vempati, Lin & Cocke, 1995). Table 1.1 outlines the main components of Portland cement (Paria & Yuet, 2006).

Table 1.1 Composition of Portland cement
Taken from Paria & Yuet (2006, p. 221)

Components	Typical Composition (%)
CaO	67
SiO ₂	22
Al ₂ O ₃	5
Fe ₂ O ₃	3
Other	3

Portland cement involves four main phases that govern the hardening of cement. These components are Alite (tricalcium silicate, Ca₃SiO₅), Belite (dicalcium silicate, β-Ca₂SiO₄), Aluminite (tricalcium aluminate, Ca₃Al₂O₆), and Ferrite (Ca₄Al₂Fe₂O₁₀), the properties of these components are shown in Table 1.2 (Dalton et al., 2004). Alite (C₃S) and Belite (C₂S) are the two key cement phases that contribute to strength development.

1.2.1 Portland cement and its hydration

Concrete is a multiphase material comprised of aggregates and cement paste. Cement paste is a combination of cement and water (Bullard et al., 2011). The chemical reaction between water and anhydrous cement that results in an amorphous paste is known as cement hydration. In the end, this paste grows stronger by transforming into a solid mass.

Table 1.2 Composition and properties of cement phases
Taken from Dalton et al. (2004, p. 230)

Cement phase	Typical composition	Contribution to the cement matrix
Alite (C ₃ S)	50-70 (%)	Rapid hydration and contribution to initial strength
Belite (C ₂ S)	15-30 (%)	Slow hydration and contribution to final strength
Aluminite (C ₃ A)	5-10 (%)	Rapid hydration and high heat of hydration, limited contribution to strength
Ferrite (C ₄ AF)	5-15 (%)	Slow hydration and low heat of hydration, limited contribution to strength

The hydration of cement is a complex process that corresponds to a series of chemical reactions between the anhydrous phases (cement components) and water (Al Tabbaa & Stegemann, 2011; Glasser, 1997). The hydration of C₃S and C₂S leads to the formation of two distinct products: the C-S-H phase, and calcium hydroxide (CH):



During cement hydration, CH and C-S-H form more than 70% of all products. According to Bullard et al., (2011), the hydration of the cement undergoes four main stages, as described in Figure 1.1.

1. Initial reaction stage

This stage begins upon contact between water and the anhydrous cement and lasts only a few minutes after mixing. This leads to hydrolysis of the surface causing ions to be released rapidly into the solution (Gartner, Young, Damidot & Jawed, 2002). During this stage, intense chemical activity takes place in the paste accompanied by significant release of heat

(-138 kJ/mol) due to the dissolution of C_3S (Bullard et al., 2011). According to the slow dissolution step hypothesis, Alite (C_3S) and Belite (C_2S) in cement grains react immediately with water, forming C-S-H (Bullard et al., 2011). As the amount of calcium silicate hydrate increases, it reduces the concentration of silicate and increases the molar ratio of $Ca^{2+}:SiO_2$ in the solution. According to Salami (2014), this increase in silicate is temporary and reduces rapidly, while the $Ca(OH)_2$ continues to rise. Scrivener, Ouzia, Juilland & Mohamed (2019) reported that at this point in the process, these formed hydrates could govern the pore solution.

2. Slow reaction stage

This stage is characterized by a decreased rate of hydration. This could be due to portlandite growth restricting C-S-H growth (Bullard et al., 2011). Also, this stage occurs at the end of the initial reaction but before the acceleration stage. During this stage, Ca^{2+} and OH^- ions are released (Gartner et al., 2002). This action leads to a pH increase and slows the C_3S dissolution rate. The chemical activity and the release of heat are minimal. The hydration products (e.g., C-S-H) gradually form a thin layer, primarily around the cement particles and on C_3S surfaces (Gartner et al., 2002). According to the metastable barrier hypothesis, this thin layer stops the C_3S surface from coming into contact with water and restricts the diffusion of the ions, which retards dissolution (Bullard et al., 2011; Gartner et al., 2002). The slow reaction stage ends when the thin layer is removed or becomes more permeable due to ageing (Taylor, 1997).

3. Acceleration stage

The acceleration stage typically occurs 5 to 10 hours after mixing. It begins when the Ca^{2+} and OH^- concentrations are high enough for Portlandite to be saturated. Following the delay stage, the C-S-H nanoparticles have a tendency to interpenetrate with one another and to aggregate to produce stable C-S-H for a long period of time (Bullard et al., 2011). Constantinides & Ulm (2004) observed two types of C-S-H (high and low density) that exist at this stage. They also concluded that the formation of C-S-H was highly reduced at the initial stage, followed by a gradual increase. During acceleration, the main hydration products (e.g., C-S-H and CH) grow rapidly and easily into available spaces (Gartner et al., 2002). These hydration products constantly remove ions from the solution, which must be replaced by additional C_3S

dissolution (Bullard et al., 2011). According to Taylor (1997), the growth and nucleation of the C-S-H during this stage regulates the rate of reaction. As time elapses, the concentrations of Ca^{2+} and OH^- in the solution rise, and Portlandite begins to precipitate when the solution reaches supersaturation (Taylor, 1997). The dissolution, nucleation and precipitation of the different phases then follow, allowing the formation of hydrates (Ettringite, Portlandite and C-S-H). This high chemical activity emits a significant amount of heat and creates a rigid solid. Additionally, the acceleration stage regulates the growth of strength and concrete permeability, as well as setting properties.

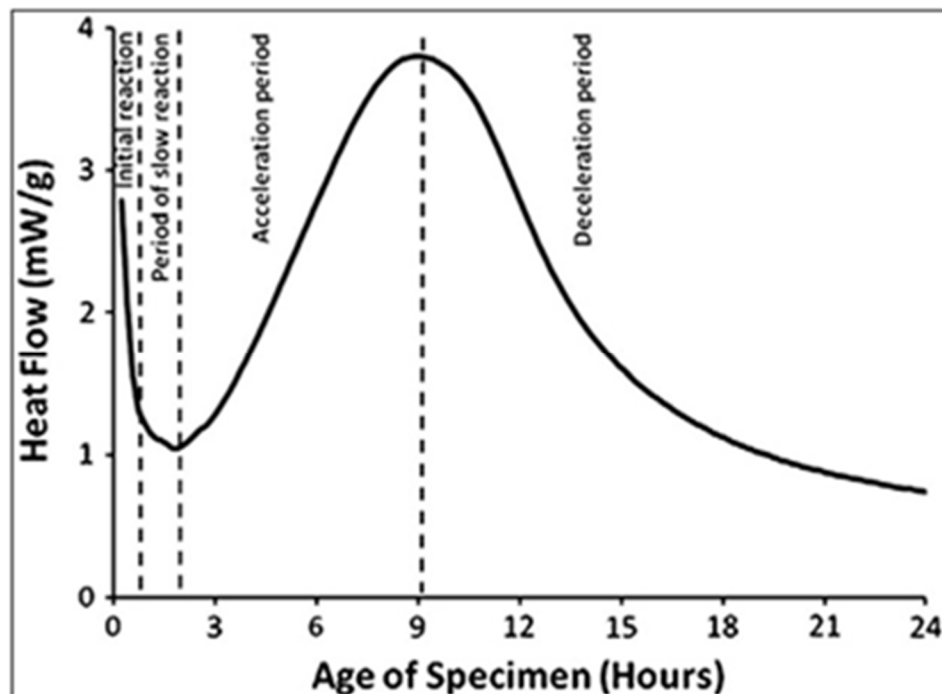


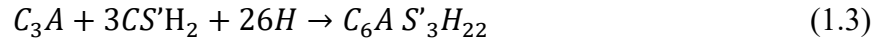
Figure 1.1 Stages of hydration as a function of heat flux
Taken from Bullard et al. (2011, p. 1210)

4. Deceleration stage

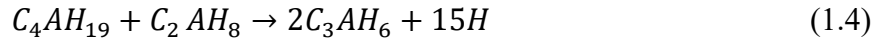
The deceleration stage typically extends to about 48 hours after mixing due to the accumulation of ions in the solution. During this stage, diffusion regulates the rate of hydration (Bullard et al., 2011; Hu, Ge & Wang, 2014). The deceleration stage is important because the lack of water can result in chemical shrinkage (Bullard et al., 2011). Additionally, the particle size

distribution has a significant influence on the rate of hydration at this time. Particles smaller than 3 μm are typically consumed in less than 10 hours while particles smaller than 7 μm require 24 hours to react completely (Bullard et al., 2011).

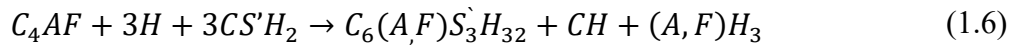
Tricalcium aluminate and water react to form ettringite and heat, as shown in Equation (1.3). Ettringite's stability depends on the quantity of gypsum present in the solution. However, the amount of gypsum is often insufficient for all C_3A to react.



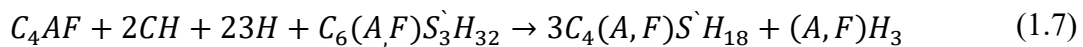
According to Meredith, Donald, Meller, & Hall (2004), ettringite loses its stability when all of the gypsum has been used in the reaction (1.4). It then reacts with any leftover C_3A to produce calcium aluminium monosulphate hydrate ($\text{C}_4\text{AS}'\text{H}_{12}$), also known as monosulphate:



Hydration of ferrite phase (C_4AF) in the presence of gypsum produces products similar to those of C_3A (Rose et al., 2006). In the presence of gypsum, C_4AF reacts with water to form ettringite, as outlined in the following equation:



The formed ettringite reacts with the remaining C_4AF to produce hydrous garnet (Rose et al., 2006; Xue, Liu, Ma, Teng & Guan, 2022). This new product (garnet) doesn't actually contribute to the strength development; it simply fills the space.



It is important to note that the simultaneous occurrence of multiple chemical reactions makes it challenging to understand the hydration process.

Contaminated soil can include varying quantities of metals such as Cu, Cr, Ni, Cd, Zn, and Pb, depending on industrial activities or the sources of waste. Many of these metals may have a detrimental effect on the cement hydration process, and thus they may affect the properties of the cement matrix (Chen et al., 2007; Shi & Spence, 2004; Thomas, Jameson, & Double, 1981). Tashiro & Oba (1979) indicated that some of metals reduced the hydration rate and the mortar's mechanical strength. According to Thomas et al. (1981), the presence of Cu, Zn, and Pb retards the cement hydration process at early stages (particularly tricalcium silicate). They also ranked the metals' ability to slow cement hydration in the following order: $Zn^{2+} > Pb^{2+} > Cu^{2+}$. Shi & Fernández-Jiménez (2006) prepared the S/S matrix by combining Portland cement with furnace dust that contained high quantities of metals. They found that 60% of the dust in the mixture seemed to delay the early hydration of the Portland cement. Tashiro & Oba (1979) argued that metals can have an impact on hydration by forming a thin film surrounding cement grains. The formation of these thin films is dependent on the concentration of the metal ions (hydroxy compounds). In other words, a high concentration of hydroxy compounds is required to form a highly coherent layer (Thomas et al., 1981). The hydration of C_3S (allite) in the presence of Zn could be different. For example, Chen et al. (2007) concluded that while Zn^{2+} slowed the hydration of C_3S in its earlier stage, it enhanced it after a year. On the other hand, the presence of small quantities of Cu^{2+} can accelerate C_3S hydration (Chen et al., 2007; Kantro, 1975). The study carried out by Chen et al. (2009) concluded that in the presence of Cu^{2+} , Pb^{2+} , and Cr^3 , the hydration of C_3S was accelerated.

1.2.2 Mechanical and hydraulic properties of cement-based materials

Cement-based materials are heterogeneous composite materials formed from aggregates (sand and gravel), water and cement (hydraulic binder). Cement hydration also plays a vital role in the mechanical properties of concrete, as well as strength development over time. The different cement phases do not contribute equally to the compressive strength increase during hydration.

Figure 1.2 illustrates that the hydration of two main cement phases (C_3S and C_2S) is responsible for strength development. The compressive strength increases gradually during the curing phase (28 days). After this period, the compressive strength development is slower. C_3S contributes to the early growth of strength while C_2S contributes to the development of strength after 28 days of hydration. Both C_3S and C_2S are responsible for the final long-term strength development (Neville & Brooks, 1987). The contribution of other phases, such as C_3A and C_4AF , is limited. It is worth noting that temperature conditions can affect the growth of matrix strength during the curing period. For instance, exposing the matrix to high temperatures in its early stages can accelerate the hydration process and result in rapid strength growth (James et al., 2011).

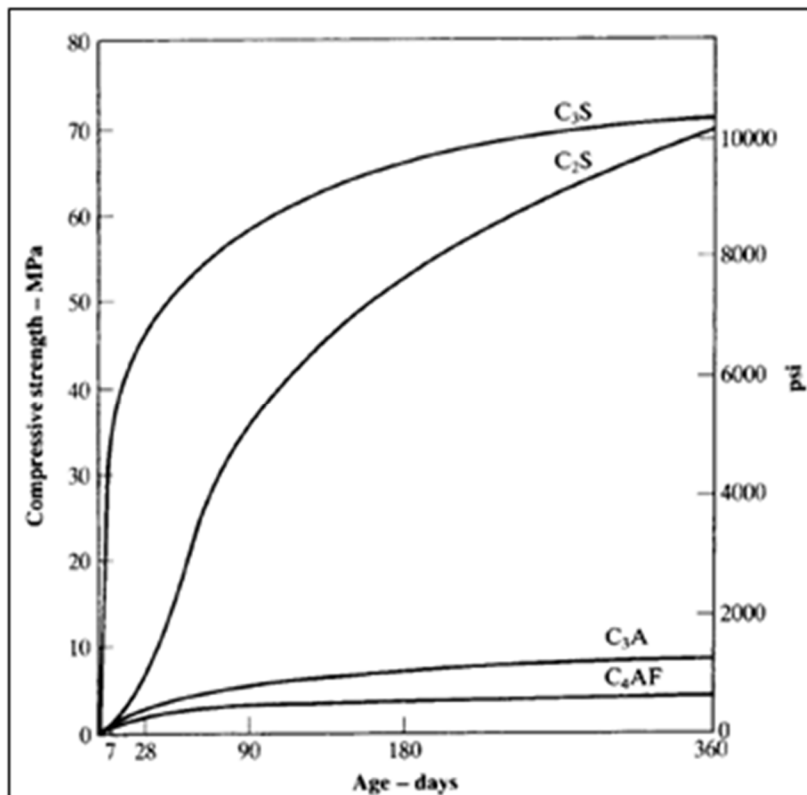


Figure 1.2 Strength development in a cement matrix
Taken from Neville & Brooks (1987, p. 15)

Many researchers have studied the relationship between the water-to-cement ratio (W/C) and the strength development of concrete (UCS). A higher W/C ratio generally causes a strength reduction of cement-based materials. Haach, Vasconcelos & Lourenço (2011) concluded that the mechanical characteristics of mortar decreased as the W/C ratio increased. The W/C ratio affects the porosity of the cement paste. A higher W/C ratio results in a higher porosity and a lower compressive strength (Haach et al., 2011; Popovics & Ujhelyi, 2008).

The fluctuating amount of water (i.e., W/C ratio) in the matrix plays a significant role in the hydraulic properties of cement-based materials. For example, the value of hydraulic conductivity increases as W/C ratios increase (Neville & Brooks, 1987). In the case of lower water content, there is a possibility of air voids being formed in the structure of the matrix, which would increase its hydraulic conductivity. Jolous Jamshidi (2014) demonstrated that in the case of high water content, there is also high porosity due to the paste bleeding, which raises permeability. The hydraulic properties of cement-treated materials are strongly influenced by the hydration process. For example, as cement hydration continues during the curing time, the C-S-H gel gradually forms and fills the pores in the cement paste. These products decrease porosity and hydraulic conductivity (Jing, Song, Zhang & Nowamooz, 2022; Jolous Jamshidi, 2014).

1.2.3 pH of the pore solution of the concrete matrix

The composition of the concrete pore solution is determined mainly by the solubility of the solid phases. It is critical to understand the composition of the pore solution because the mechanisms for the immobilization of waste materials are directly influenced by its pH (Brouwers, 2003). When water reacts with the cement and the aggregates in the matrix, it tends to raise the pH of the pore solution to 13 due to the dominance of highly soluble alkali hydroxides (Coumes et al., 2006).

1.3 Microstructure and Permeability of Solidified Sand

The microstructure of the solidified sand matrix comprises multiple components that are combined and compacted to form a monolithic matrix. These components include Portland cement, aggregates (such as gravel or sand), and water. Together, these components interact to create the complex microstructure of cement paste which essentially depends on its components (e.g., calcium silicate hydrate, portlandite, and non-hydrated clinker) as well as the presence of voids (e.g., air pores and capillary porosity). The microstructure controls the permeability of the cement-based material in the absence of cracking.

1.3.1 Microstructure of solidified matrix

Many factors can affect the microstructure of the solidified matrix. For example, the W/C ratio, particle size, relative humidity, curing conditions can influence the pore network. Yaman, Hearn, & Aktan (2002) divided the porous system of concrete matrix into two categories based on the porous activity: active pores (capillaries pores) and non-active pores (air pores). Air pores are formed during the mixing of the matrix due to air entering the paste, whereas capillary pores are formed during cement hydration. Despite being smaller than air pores, capillary pores are responsible for giving the concrete matrix its mechanical and hydraulic properties (i.e., mechanical strength and hydraulic conductivity) (Yaman, Aktan & Hearn, 2002; Yaman, Hearn, et al., 2002).

Various techniques are employed to quantify the porous network structure of cementitious materials. In recent years, non-destructive methods such as scanning electron microscopy and micro-tomography CT scans have become the preferred options due to their capacity to perform multiple measurements on a single sample without causing any damage to it (Bentz, Haecker, Peltz & Snyder, 2008; Burlion, Bernard & Chen, 2006).

1.3.2 Hydraulic conductivity of concrete

Henry Darcy (1856) proposed the following law to describe the flow of fluids in porous media:

$$q = \frac{-k(h_2 - h_1)}{l} \quad (1.8)$$

Where q is the Darcy velocity, h_1 and h_2 are the upstream and downstream hydraulic heads, respectively, l is the distance between the points where h_1 and h_2 are observed, and k is the hydraulic conductivity. Darcy's law assumes that the porous medium is completely saturated and that the flow forces are due to the fluid viscosity (Whitaker, 1986). The capacity of the solidified matrix to withstand the penetration of fluids and gases depends on its permeability. When the solidified matrix has a high permeability, it is more vulnerable to deterioration.

Hydraulic conductivity is the ability of a porous medium to transmit a fluid or gas under a pressure gradient. There are several factors that might affect concrete's hydraulic conductivity. For example, the use of additive materials, the W/C ratio, curing conditions, the size of the aggregate, and the porosity of the matrix all play a role in transport properties. The permeability of concrete is strongly influenced by porous medium parameters such as porosity, as well as the pore network tortuosity and connectivity (Dullien, 2012). A higher porosity and connectivity lead to a lower resistance to flow and a higher hydraulic conductivity (Zhong & Wille, 2016; Zhong, Xu, Netto & Wille, 2016). Large aggregate results in high hydraulic conductivity. According to Zhong et al. (2016) and Neithalath, Weiss & Olek, (2006), increasing the aggregate size increased porosity, which in turn increased connectivity. Additionally, they concluded that small aggregates provide a pore structure with a high tortuosity and vice versa, as shown in Figure 1.3. Additionally, they indicated that an increase in pore tortuosity hampers the flow of water along convoluted pathways, leading to reduced hydraulic conductivity in concrete.

1.4 Stabilization/Solidification Processes (S/S)

The main goal of the stabilization and solidification technique is to reduce leachability and limit the migration of contaminants from the monolith to nearby soil and groundwater (Poon, Qiao & Cheeseman, 2011). The objective of the S/S matrix is to create a monolithic solid that is less permeable to minimize fluids from entering (i.e., attacking) or leaving (i.e., leaching) the matrix. Fluids can flow through or around the solidified matrix depending on whether the surrounding materials are permeable or not (Poon & Chen, 1999).

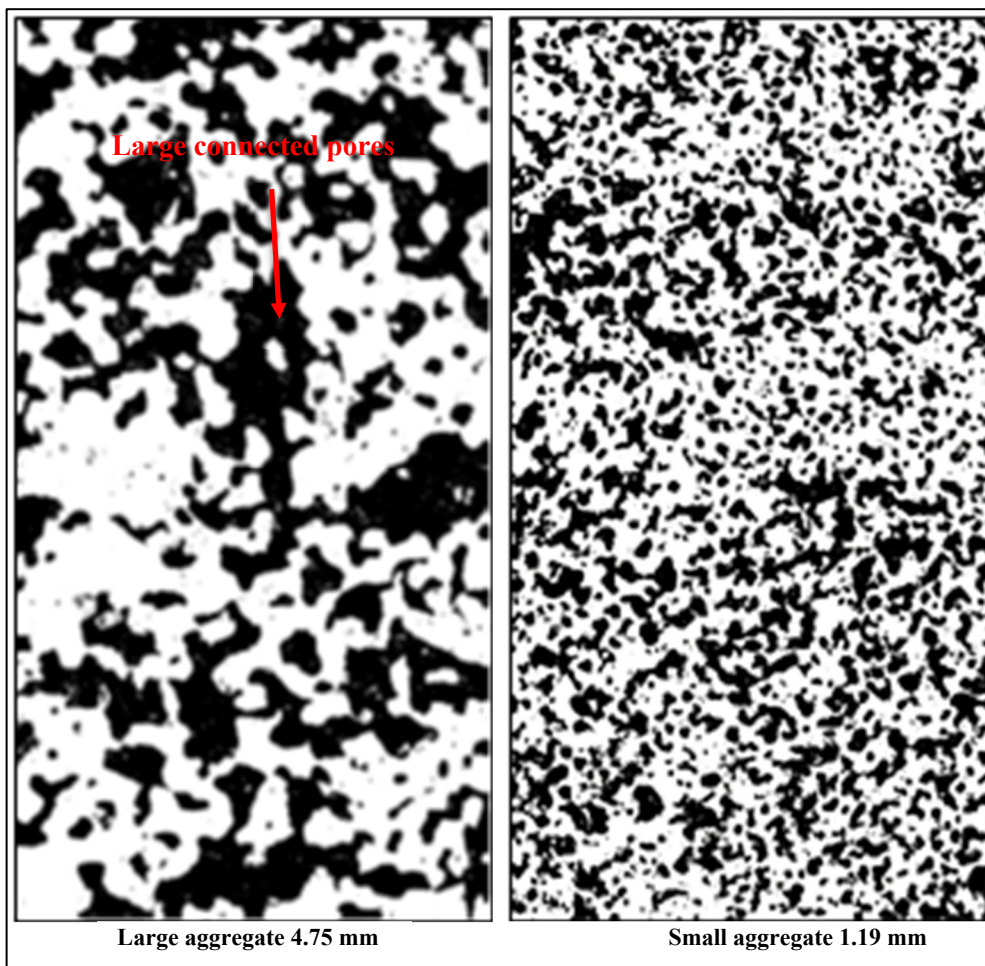


Figure 1.3 Tortuosity of the concrete matrix for different aggregate sizes
Taken from Zhong et al. (2016, p. 1161)

Hydraulic conductivity decreases as the process of cement hydration continues. In addition, the result may change in the long term in the presence of contaminated materials. Kogbara (2014) explained that the contaminants react with the matrix's components, affecting ongoing hydration and increasing hydraulic conductivity. For safe disposal, the acceptable limits of hydraulic conductivity values must be between 10^{-8} and 10^{-9} m/s, as specified in the Quebec provincial guidelines for managing contaminated soil treated by S/S (St-Laurent et al., 2012).

There is a strong correlation between the strength and the leachability of the S/S matrix. According to the Quebec provincial guidelines for managing contaminated soil treated by S/S, the compressive strength must be above 700 kPa for safe disposal in a site (St-Laurent et al., 2012). The physical characteristics of cementitious materials can be altered as a result of leaching (e.g., increase in porosity), which causes a reduction in the compressive strength (UCS) of the S/S monolithic (Ekström, 2003).

1.4.1 Interactions between S/S Binder and Contaminants

1.4.1.1 Immobilization mechanisms of contaminant

According to Young (1972), it is preferred to use S/S technology to immobilize metals rather than trapping organic compounds. This is due to the detrimental effects of organic compounds on the microstructure of the S/S matrix, such as an increase in porosity and a decrease in matrix strength (Paria & Yuet, 2006). However, recent research has indicated that this technique is effective in remediating certain metal contaminations (Al Tabbaa & Stegemann, 2011). Contaminants can be immobilized in the cement matrix by chemical mechanisms, such as precipitation and chemical fixation, and by physical mechanisms, such as adsorption (Al Tabbaa & Stegemann, 2011; Shi & Fernández-Jiménez, 2006; Levy, Barbarick, Siemer, & Sommers, 1992).

Chemical fixation limits the toxicity and mobility of metals by converting them to insoluble compounds (Al Tabbaa & Stegemann, 2011). Metals are immobilized chemically as a result

of their interactions with hydration products, such as calcium silicate hydrate (Du et al., 2010; Shi & Fernández-Jiménez, 2006). Precipitation is the most common mechanism for reducing metal mobility. Although metals precipitation occurs in many forms, such as sulphides, carbonates, and silicates, the most common form is hydroxide (Conner & Hoeffner, 1998a; Kogbara, 2014). Metals can precipitate from aqueous solutions in pores or on the surface of solid particles. It should also be noted that the stability of metal-bearing phases depends mainly on the pH of the solution in the S/S matrix. An important issue is that some metals may be released into the pore solution due to exposure to aggressive conditions over time, even if the majority of metal species are stable and precipitate as hydroxide (Al Tabbaa & Stegemann, 2011; Perera et al., 2011). For example, Portland cement increases the pH of the S/S matrix and converts the metal contaminants into metal hydroxides; however, under the effects of carbonation, the results will be different (Kogbara, Al-Tabbaa, Yi & Stegemann, 2013).

Adsorption is a surface phenomenon in which the molecules or ions of contaminants are attracted to the constituent surfaces of the matrix. This phenomenon might be caused by physical, chemical, or electrical forces (Al Tabbaa & Stegemann, 2011; Sakai, Yamada & Ohta, 2003). Some minerals, such as clays or zeolites, are excellent adsorbents because they have very large surfaces per unit mass. It is well known that calcium silicate hydrates have a large surface area and the ability to adsorb contaminants. This characteristic makes C-S-H appropriate to adsorb a wide variety of metals, such as cadmium and chromium (III) (Du et al., 2010; Park, 2000; Shao et al., 2020). In addition, certain metallic element ions have the capability to interact with C-S-H through surface substitution of Ca^{2+} . For instance, Cu^{2+} can replace Ca^{2+} in the C-S-H structure (Park, 2000). Dermatas et al. (2005) provided proof that C-S-H can successfully limit the release of metals such as Pb by up to 99%. For example, they found that immobilizing one mole of Pb required two moles of C-S-H. Moreover, Al Tabbaa & Stegemann (2011) discussed that for a cement-based matrix, the sorption of metals would depend on many factors such as pH and soil mineralogy, as well as type and concentrations of metals.

In addition to the above mechanisms, encapsulation is a physical process that uses cementitious materials to trap contaminants that remain soluble in the S/S matrix (Shi & Spence, 2004). These processes can protect the S/S structure, ensure immobilization, and limit the movement of contaminants into the surrounding environment (Kogbara et al., 2013). Additionally, CSH can encapsulate metal compounds (Chen et al., 2009). Moreover, redox mechanisms strongly affect the solubility of some metals, such as Ag, Cu, and Cd, as a function of pH (Al Tabbaa & Stegemann, 2011). For example, in acidic conditions, copper is typically present as soluble Cu^{2+} ions. As pH rises, copper may precipitate as $\text{Cu}(\text{OH})_2$, reducing solubility. Under highly basic conditions, complex ions like $\text{Cu}(\text{OH})_4^{2-}$ can form, increasing solubility compared to hydroxides.

1.4.1.2 Immobilization of metals in cement-based S/S

The pH value of the cement matrix has a major impact on metal retention. Figure 1.4 illustrates the impact of pH on the solubility of metal hydroxides (Paria & Yuet, 2006; Shi & Spence 2004).

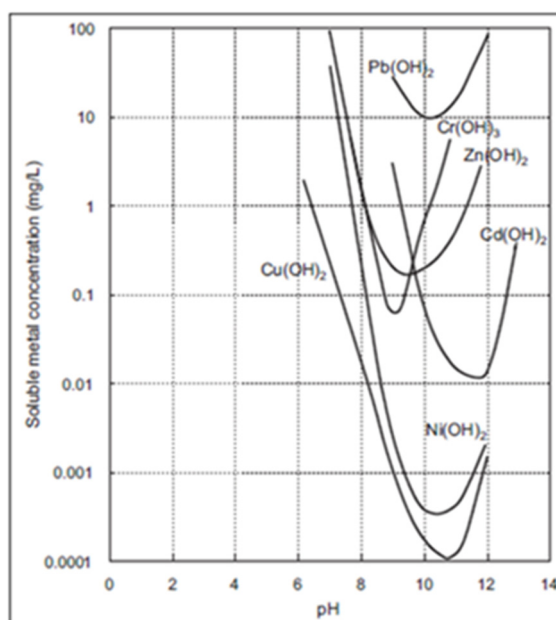


Figure 1.4 Solubility of metal hydroxide
Taken from Paria & Yuet (2006, p. 238)

Metal hydroxides of Cd, Cr, Cu, Pb and Zn are amphoteric: they are soluble in both acidic and basic solutions (Al Tabbaa & Stegemann, 2011; Bech et al., 2012). Hydroxide solubility decreases with increasing pH until a pH of between 9 and 11 depending on the metal. For higher pH values, the solubility increases with the pH. This variability in the solubility of hydroxides can influence the performance of an S/S matrix because the hydrated cement paste has a pH value of nearly 13. Maintaining a pH in the matrix above the pH corresponding to the minimum solubility can be challenging in the long term since surface water or groundwater, in certain cases, tends to be more acidic compared with the pore water in cement-based materials. Furthermore, as demonstrated in the subsequent section, carbonation tends to decrease the pH.

External conditions, such as loads and drying/wetting cycles, can degrade the microstructure of the matrix, leading to increased cracking and the release of metals. (Wang et al., 2022). Yvon et al. (2006) observed that the interconnected micro-cracks increase the permeability, which promotes the release of metals. According to Zha, Liu, Xu & Cui (2013), the porosity increased after five cycles of drying/wetting, which caused fractures to develop and significantly increased the release of metals in the pore solution.

Temperatures may also have an effect on waste solidification and stability. According to Yvon et al. (2006) the ability of the S/S matrix to trap metals improves when hydrates develop at low temperatures as compared to high temperatures. In contrast, researchers found that repeated freeze-thaw cycles had an impact on the S/S matrix's long-term stability. Zhongping et al. (2021) investigated the impact of freeze/thaw cycles on solidified/stabilized soils by repeating the cycles of freeze and thaw 180 times. They discovered that as the number of cycles rose, the release of metal gradually increased.

1.4.1.3 Retention of copper

Copper is considered one of the major trace elements that can cause harmful effects, even at low concentrations (Tchounwou, Yedjou, Patlolla & Sutton, 2012). For example, the US Environmental Protection Agency (EPA) has stipulated a maximum acceptable concentration

of copper in drinking water, setting the threshold at 1.3 mg/L. The presence of copper (Cu) in the environment can be of natural origin or linked to industrial activities. In calcareous soils, which are mostly composed of CaCO_3 , the retention of copper is mainly due to its precipitation in the form of malachite (copper carbonate hydroxide) (Plassard, Winiarski & Petit-Ramel, 2000). In acid soils, copper retention is governed by ionic exchanges with clay minerals such as kaolinite (Wu, West & Stewart, 2002). In addition, copper has a retarding effect on cement hydration and its forms $\text{Cu}(\text{OH})_2$ and $\text{CuSiO}_3 \cdot \text{H}_2\text{O}$. Furthermore, the retention patterns of Cu are comparable to those of Zn. It precipitated as hydroxides or hydroxycarbonates (Kakali, Tsivilis & Tsialtas, 1998).

Under sufficient alkaline conditions, copper can take the following forms: Cu^{2+} , CuOH^+ , $\text{Cu}(\text{OH})_2$, and CuCO_3 . According to Li, Poon, Sun, Lo & Kirk (2001), Cu may precipitate as copper hydroxide on the surface of C-S-H phase in the S/S matrix. Suo, Yao, Song & Dong (2022) used a copper nitrate solution with red mud, soil and cement to prepare the S/S-contaminated matrix. Their leaching results demonstrated that the metal release was within acceptable limits. Additionally, they concluded that hydration products including C-S-H, CaCO_3 , and ettringite gel are responsible for the retention of copper ions. According to Li et al. (2001), the presence of copper in the cement matrix may have an effect on strength development because of its interactions with silicate and aluminate. Bao, Wang & Xiao (2016) used cement, bentonite, and lime to solidify and stabilize contaminated sediments. They reported that the release of Cu before treatment was higher than 50 mg/L, then decreased to less than 50 mg/L after treatment.

Accelerated carbonation can have an impact on the leachability of the cement-based materials and the subsequent release of metals such as copper. For example, copper retention in the cement matrix can be enhanced by carbonation (Badreddine et al., 2004). Copper was released from the carbonated matrix more readily than other metals (e.g., Pb, Cd, and Zn) under acidic conditions such as those seen in the TCLP test (Pandey, Kinrade & Catalan, 2012). Chen, Zhang, Ke, Hills & Kang (2009) confirmed these findings by subjecting the S/S matrix to nitric acid. They concluded that when the pH fell below 6, the leaching of Cu increased significantly.

In general, the impact of carbonation on metal leaching from the cementitious matrix can be complex and dependent on a range of factors such as the pH of the leachate. According to some research, carbonation can reduce the release of copper (Lange, Hills & Poole, 1995; Sweeney, Hills & Buenfeld, 1998). Other research, on the other hand, determined that carbonation increased copper release (Sweeney et al., 1998; Valls & Vazquez, 2001). This variation in the influence of carbonation on Cu release might be attributable to the carbonation degree or the amphoteric phenomenon.

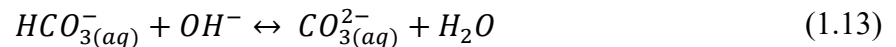
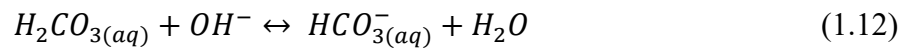
1.5 Carbonation

Exposure of S/S material to carbonation can result in physical and chemical exchanges between the material and the external environment, which can sometimes lead to long-term deterioration. Carbonation can lower the pH of the pore solution from 13 to 9, which increase the solubility of certain metals in the material (Rha, Kang & Kim, 2000). The carbonation process and its effects are summarized in the following sections.

1.5.1 Natural carbonation phenomenon

Under normal conditions, the carbon dioxide concentration in ambient air has an average concentration between 0.03 and 0.04%. (Thiery, Villain, Dangla & Platret, 2007). This concentration can reach 1% in urban areas, particularly locations subject to heavy traffic. Carbonation is a slow process governed by the source of CO₂ available for reaction and its diffusion through the material (Venhuis & Reardon, 2001). Indeed, the direct consequence of the consumption of portlandite by the carbonation reaction is a drop in the pH of the pore solution and the internal structure of the matrix. Carbonation can also cause shrinkage of the matrix, which could lead to long-term cracking of the structure, as presented in Section 1.6.2.1. (Chen, Thomas & Jennings, 2006). Experimental findings revealed that CO₂ can effectively immobilize certain metals in contaminated soils (Valls & Vazquez, 2001).

When concrete is exposed to air, atmospheric CO₂ diffuses into the pores and comes into contact with the pore water. Thiery et al. (2007) demonstrated that CO₂ (g) first dissolves in water according to reaction (1.10). The dissolved CO₂ (aq) converts to carbonic acid (H₂CO₃) (reaction 1.11). Then, carbonic acid changes to bicarbonate ion (HCO₃⁻), (reaction 1.12). Finally, the bicarbonate converts to carbonate ion (CO₃²⁻), (reaction 1.13).

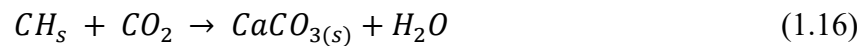


The pore solution in cementitious materials is highly alkaline prior to carbonation. Based on Equations (1.12) and (1.13), the dissolution of carbon dioxide in the pore solution leads to a lowering of the pH of the pore water. The pH value of the solution affects the speciation of the CO₂ in the pore solution (Valsaraj & Melvin, 2000).

1.5.1.1 Carbonation of portlandite

During the carbonation process, CO₂ reacts with the main products of hydrated cement such as the C-S-H gel, portlandite, and ettringite. The reactions produce calcium carbonate. Figure 1.5 summarizes the different chemical species involved in the carbonation of cement paste containing CH and C-S-H in the presence of water (Czarnecki & Woyciechowski, 2015). Figure 1.5 depicts that CO₂ (g) infiltrates the matrix, dissolves in the pore solution as CO₂ (aq), and reacts with cement hydrates, such as CH (g), resulting in the formation of CaCO₃ (s). Specifically, the diffusion of CO₂ causes the dissolution of Ca(OH)₂, owing to the decrease in pH of the pore water, as evidenced in reaction (1.14). Subsequently, the dissolved calcium ions engage in a reaction with carbonate ions, leading to the precipitation of calcium carbonate in

the pores (Venhuis & Reardon, 2001), as shown in reaction (1.15). Ultimately, the carbonation of portlandite can be expressed in reaction (1.16).



Šavija & Luković (2016) mentioned that a thin coating that forms when $CaCO_3$ precipitates in pores and around portlandite crystals slows the carbonation of $Ca(OH)_2$. The calcium carbonates formed during carbonation can exist in three polymorphic forms: vaterite, aragonite and calcite. Calcite is the most stable form under standard temperature and pressure conditions (Plummer & Busenberg, 1982).

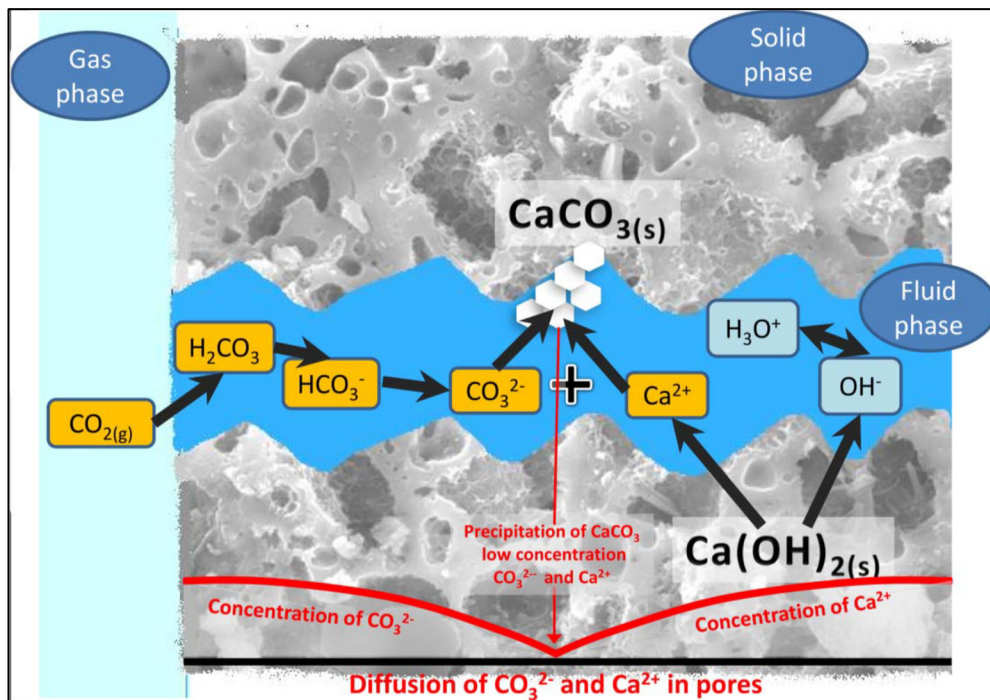


Figure 1.5 Main chemical species involved in the carbonation phenomenon
Taken from Czarnecki & Woyciechowski (2015, p. 43)

The precipitation of CaCO_3 caused by the carbonation of portlandite is accompanied by a release of water from the binder structure. Water is required for the dissolution of CO_2 , but the presence of excessive water can clog the pores, and impede CO_2 penetration and the carbonation process (Bertos, Simons, Hills, & Carey, 2004; Venhuis & Reardon, 2001). CO_2 diffuses more quickly into the pores via the gas phase than through the aqueous phase (Šavija & Luković, 2016). According to Šavija & Luković (2016) the presence of a large amount of water in the pores makes it more difficult for CO_2 to penetrate the sample, as presented in Figure 1.6.

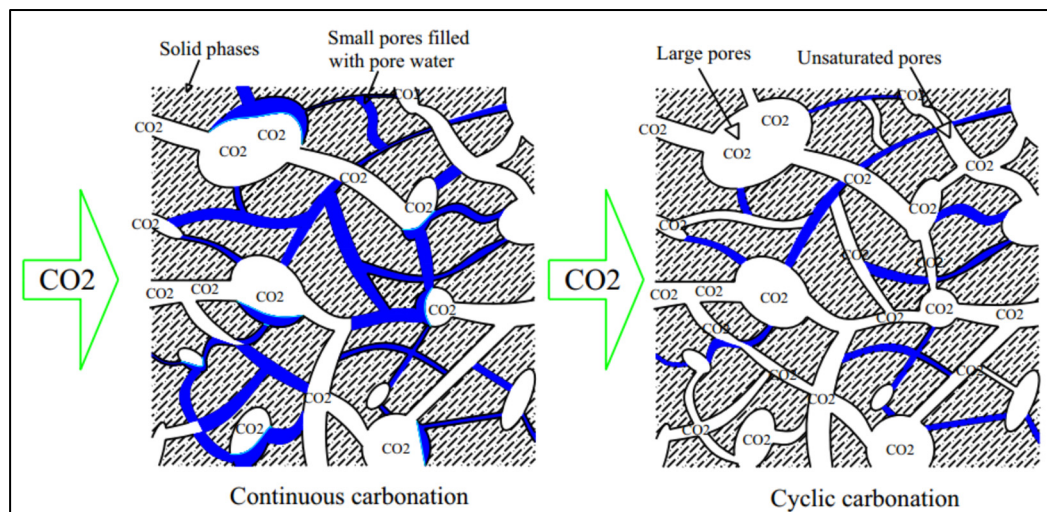


Figure 1.6 CO_2 distribution during the continuous and cyclic process
Taken from Šavija & Luković (2015, p. 25)

1.5.1.2 Carbonation of calcium silicate hydrate

The carbonation/decalcification of C-S-H has been studied by many authors who have presented the dissolution mechanisms (Bonen & Sarkar, 1995; Nishikawa & Suzuki, 1994; Šavija & Luković, 2016). Nishikawa & Suzuki (1994) concluded that the reaction between carbon dioxide and C-S-H leads to the formation of insoluble silica gel and calcium carbonate, and the release of water, as indicated in the following reaction:



The carbonation of C-S-H is influenced by its Ca/Si ratio. Black, Garbev & Gee (2008) used X-ray spectroscopy to investigate the impact of the Ca/Si ratio on the initial age of C-S-H. They observed that the amorphous calcium carbonate was the first carbonation product. Furthermore, the decalcification of the C-S-H was completed at high C/S ratios between 1.33 and 1.50 compared to low C/S ratios between 0.67 and 0.75. Šavija & Luković (2016) explained that when the Ca/Si ratio declines (during carbonation), the rate of C-S-H decomposition rises. They also showed that decreasing the Ca/Si ratio results in less CaCO₃ being produced since there is less calcium available to react with the CO₂. In addition, the effect of carbonation on the binders fades over time due to the gradual formation of calcium carbonates and the release of water, which clogs the pores, thus reducing the diffusion of atmospheric CO₂ (Tracz & Zdeb, 2019). According to Šavija & Luković (2016), the carbonation of C-S-H is slowed down by a thin coating that forms around it. This coating is comparable to that which forms around CH. Although the carbonation of CH and C-S-H seems to occur simultaneously, the carbonation of CH has priority over C-S-H (Groves, Rodway & Richardson, 1990; Šavija & Luković, 2016).

1.5.2 Factors influencing the carbonation process

1.5.2.1 Factors related to the surrounding environment

Relative humidity (RH) is an essential factor that can affect the process of carbonation. Figure 1.8 depicts the carbonation rate at 20°C as a function of RH measured for various concrete mixtures. The optimum value of relative humidity is between 60 and 70% (Ashraf, 2016), and the maximum depth reached by the carbonation occurs at RH of 65%. At low RH, the carbonation process is very lengthy because the volume of water is not sufficient to dissolve large amounts of CO₂ (Bertos et al., 2004; Elsalamawy, Mohamed & Kamal, 2019; Johannesson & Utgenannt, 2001; Šavija & Luković, 2016). In contrast, water condensation in the pores at high humidity prevents the penetration of CO₂ (Elsalamawy et al., 2019; Johannesson & Utgenannt, 2001; Loo, Chin, Tam & Ong, 1994; Morshed & Shao, 2013). The

differences in the results observed in Figure (1.7) are due to differences in W/C ratios and cement type.

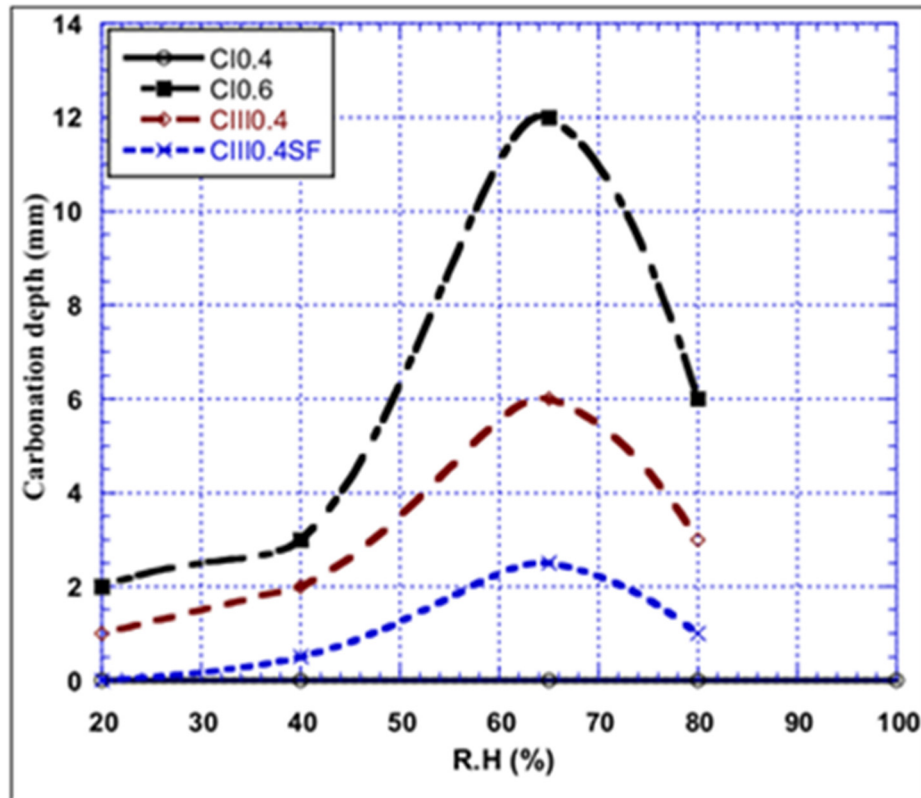


Figure 1.7 Relationship between the depth of carbonation and RH
Taken from Elsalamawy et al. (2019, p. 1262)

1.5.2.2 The influence of composition parameters

The composition of cementitious materials, such as type of cement, microstructure and aggregates, play a vital role in the carbonation process. For example, Carbonation reactions prefer materials containing calcium or silicon salts, such as Portland cement. The effectiveness of carbonation increases with the amount of Ca/Si ratio and calcium content in the materials. Additionally, adding pozzolanic materials enhances the degree of carbonation (Bertos et al., 2004; Ekolu, 2016; Hills, Sweeney & Buenfeld, 1999). Furthermore, the microstructure of the matrix depends on many factors such as the W/C ratio and compaction method. The higher water-cement ratio leads to an increase in porosity, thus prompting CO₂ penetration. In

contrast, high-compaction pressure leads to reduced porosity, which prevents CO₂ penetration (Bertos et al., 2004; Morandea, Thiéry & Dangla, 2015). Moreover, aggregates often do not affect chemical carbonation reactions. Their primary effect is a modification of the porous structure (i.e., tortuosity) and, therefore, the diffusion of CO₂ (Bertos et al., 2004; Johnson, MacLeod, Carey, & Hills, 2003; Wong, Zobel, Buenfeld & Zimmerman, 2009).

The degree of carbonation decreased when the cement content increased (Rao & Meena, 2017). This can be attributed to the fact that when there is more cement, more CH will form and more Ca²⁺ will be available for carbonate precipitation, which increases the consumption of CO₂. Moreover, the reduction of mixing water volume and an increase in cement dosage can decrease the porosity, thereby impeding the diffusion of CO₂ into the porous network (Song, Kwon, Byun & Park, 2006). Furthermore, extending the curing duration facilitates hydration, reduces porosity, and retards CO₂ diffusion within the pores (Fattuhi, 1988).

Therefore, a cementitious material with a high porosity will be carbonated more quickly than a material with a low porosity. Indeed, the presence of micro-cracks will significantly accelerate the diffusion of CO₂ (Isgor & Razaqpur, 2004; Song et al., 2006). Conversely, carbonation depth will decrease when the permeability decreases (Khan & Lynsdale, 2002).

1.5.2.3 Concentration of CO₂ and pore saturation

The degree of carbonation increases with CO₂ concentration (Ashraf, 2016; Castellote, Fernandez, Andrade & Alonso, 2009; Cui, Tang, Liu, Dong & Xing, 2015; Sanjuán, Andrade & Cheyrezy, 2003). Sanjuán et al. (2003) utilized 5% CO₂ and 100% CO₂ and discovered that a high CO₂ concentration induces a carbonation rate up to 40 times higher than for a low CO₂ concentration. Additionally, the authors concluded that subjecting concrete to laboratory accelerated carbonation for 5 days, whereby it is exposed to 100% CO₂, can yield an equivalent quantity of calcium carbonate to that generated through natural carbonation occurring over a year in the field. Subsequent to two years of natural carbonation, the average penetration depths were roughly 40 times lesser than those observed in accelerated carbonation under 100% CO₂ conditions. This suggests that the laboratory process can significantly hasten the carbonation

process while producing results that are comparable to those of natural carbonation. Nonetheless, it is crucial to note that laboratory conditions may not entirely simulate natural settings, and the effectiveness of carbonation may be influenced by various factors such as test method, CO₂ concentration, humidity, W/C ratio, and the presence of other chemical additives. Castellote et al. (2009) employed three different CO₂ concentrations in their study: 3%, 10%, and 100%. The researchers concluded that the decomposition of calcium silicate hydrate (C-S-H) increased as the concentration of carbon dioxide increased, leading to the complete disappearance of C-S-H.

In addition, a study by Cui et al. (2015) investigated the effects of carbonation on concrete, utilizing CO₂ concentrations ranging from 2% to 100%. The results of the study, depicted in Figure 1.8, demonstrate a clear correlation between CO₂ concentration and the depth of concrete carbonation at various test ages.

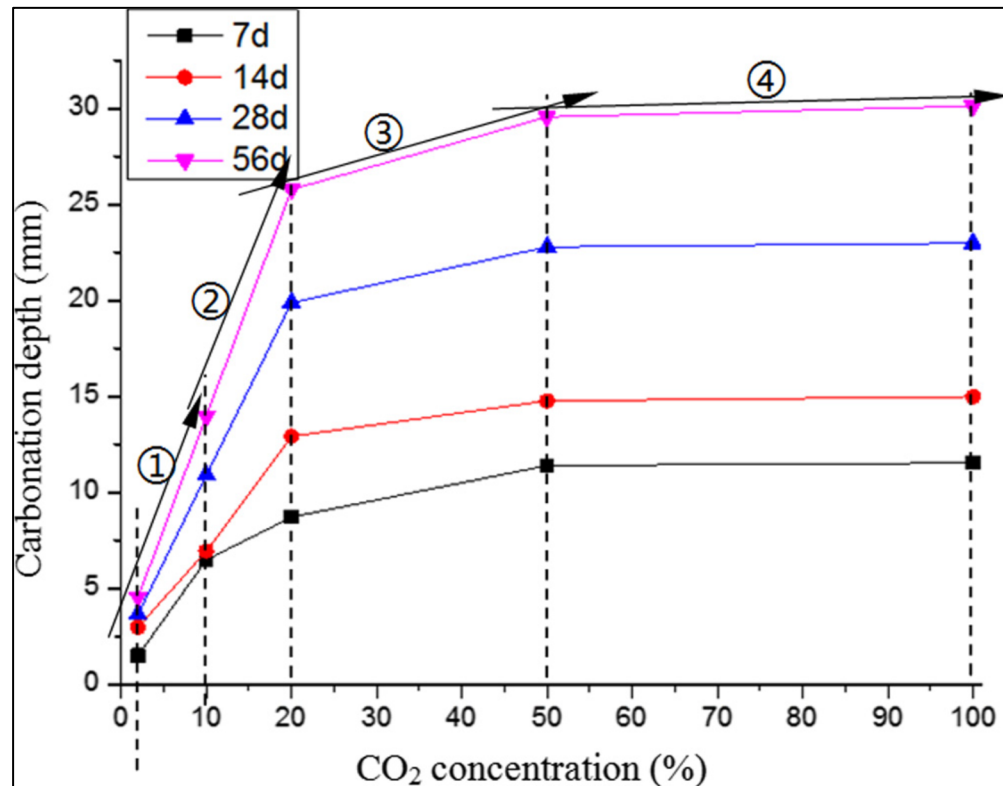


Figure 1.8 Relation between CO₂ concentration and carbonation depth
Taken from Cui et al. (2015, p. 524)

Four CO₂ concentration change zones were identified, and it was observed that concrete carbonation depth increased with higher CO₂ concentration levels, with the most significant increase occurring in zone 1 (2-10% CO₂ concentration) and the least significant increase in zone 4 (50-100% CO₂ concentration). Notably, the increase rates varied across the different concentration zones. Furthermore, the significance of the relationship between CO₂ concentration and carbonation depth decreased when CO₂ concentration exceeded 20%. In other words, when the CO₂ concentration is small, the influence of an increase in CO₂ concentration is more important than when the CO₂ concentration is large. However, Figure 1.8, shows that the penetration increases rapidly, and the relationship between CO₂ concentration and carbonation depth was non-linear and consistent across 7d, 14d, and 28d carbonation ages.

The impact of carbon dioxide pressure on the carbonation rate of cementitious materials is important to consider in the laboratory experiments of the S/S matrix. For example, when CO₂ is applied at high gas pressures, the CO₂ permeates the whole matrix before clogging the pore, resulting in good carbonation (Ashraf, 2016; Bukowski & Berger, 1979). Additionally, CO₂ applied under vacuum conditions can induce the carbonation process due to keeping the porous system open (Bertos et al., 2004).

1.5.3 Main consequences of carbonation on cement-based materials

1.5.3.1 Change in pH

As previously mentioned, the first consequence of carbonation is a drop in pH, which results from the dissolution of Portlandite in the pore solution and its reaction with dissolved CO₂ (El Bedoui, Duhaime & Dubé, 2018).

1.5.3.2 Modification of the microstructure

It is acknowledged that carbonation can modify the microstructure of cement-based materials as a result of the dissolution of CH, the decalcification of C-S-H, and the formation of CaCO_3 (Auroy et al., 2015; Morandea, Thiery & Dangla, 2014). The microstructural modifications observed in cementitious materials can be explained in the following way (Van Tittelboom & De Belie, 2013):

- Water enters the crack with a pH between 6 and 7.5. In the pore solution, the Ca^{2+} from portlandite and CSH increases the pH value ($\text{pH} > 8$). This pH value increases calcium concentration in the crack and converts bicarbonate into carbonate (formation of calcium carbonates).
- CO_2 dissolved in water reacts with unhydrated cement particles or hydrated products such as CH and C-S-H to form CaCO_3 (calcite), which precipitates in the pores (Li & Yang, 2007). According to Equations (1.14 and 1.15), these reactions are accompanied by a release of water from the binder structure generated by the carbonation of hydrated products.
- The volume of the calcium carbonate crystals increases to form a layer on the crack surfaces. The thickness of this layer continues to increase and leads to sealing the cracks.

The aforementioned reactions can effectively reduce the porosity and modify the pore size distribution in cementitious materials. These reactions are commonly referred to as self-healing mechanisms, and a detailed explanation of them is provided in Section 1.8. It is important to highlight that the continuation of these processes is dependent on the availability of calcium ions in the fractures (Dow & Glasser, 2003). These microstructure changes occur because of the lower molar volume of portlandite ($33 \text{ cm}^3/\text{mol}$) compared to calcite ($35 \text{ cm}^3/\text{mol}$) (Kangni-Foli et al., 2021). Ngala & Page (1997) showed that applying 5% CO_2 causes capillary pores to expand by up to 30 nm. Another investigation by Morandea et al. (2015) used 10% CO_2 . According to their findings, carbonation can create large capillary pores, lower overall

porosity, and modify the transport characteristics. Additionally, the reduction in pores is due not only to the difference in the molar volume of CH and CaCO_3 , but also to C-S-H that participates in reducing the solid volume of the matrix (Kangni-Foli et al., 2021; Ngala & Page, 1997; Pihlajavaara, 1968).

Table 1.3 shows examples of the influence of carbonation on porosity and pore size (Auroy et al., 2015). Results are presented for four cement pastes with different binders. Paste PI was prepared with Portland cement, whereas paste PIII, PV and PBP included varying proportions of pozzolanic additives (slag, fly ash and silica flume). For each binder, carbonation results in a CaCO_3 precipitate, which decreases the total porosity. The decrease in pore volume due to carbonation is more significant for the paste without pozzolanic additive (PI). They explained that the reduction in pore volume is directly associated with clinker substitution facilitated by the pozzolanic additive. Specifically, the higher the initial CH content, the greater the reduction in pore volume. Auroy et al., (2015) also show that the pore size distribution varies following carbonation due to calcite formation.

Table 1.3 Influence of carbonation on porosity
Taken from Auroy et al. (2015, p. 51)

Cement types		PI	PIII	PV	PBP
Porosity	Non-carbonated	36.3%	39.8%	36.9%	41.0%
	Carbonated	21.1%	29.3%	27.6%	35.5%

1.5.3.3 Modification of hydraulic conductivity

The carbonation phenomenon may have a favourable influence on the transport system of the S/S matrix. In the literature, many authors have studied the influence of carbonation on concrete permeability (Bertos et al., 2004; Metalssi, Ait-Mokhtar, Turcry & Ruot, 2012; Ngala & Page, 1997; Šavija & Luković, 2016). Their findings demonstrate that carbonation reduces the water permeability (k). The permeability results on cement samples revealed that after carbonation, the permeability was reduced by several orders of magnitude (Dewaele et al.,

1991). These results are consistent with the results obtained on Portland cement (CEM I) by Auroy et al. (2015). They show that carbonation clogs the porosity, thus decreasing the permeability.

These findings, however, contradicted another study. For example, De Ceukelaire & Van Nieuwenburg (1993) demonstrated that the permeability of the concrete matrix increased during accelerated carbonation (10% CO₂) compared to natural carbonation (0.03% CO₂). According to Lange, Hills & Poole (1996), the carbonation reaction produces thermal stresses that lead to microcracking in the matrix of solidified waste. Also, these micro-cracks are possible in the carbonated area owing to volume expansion during the carbonation process (Johannesson & Utgenannt, 2001). According to Šavija & Luković (2016), the carbonation process cannot continue to clog the pores over time since it eventually decalcifies C-S-H, increasing porosity. The change in porosity may cause a shift in the pore size distribution (PSD), for example, a slight increase in the proportion of capillary pores (pore size > 30 nm) (Ngala & Page, 1997).

1.5.3.4 Influence of carbonation on metals leachability

The pH decrease to values < 9.5 associated with carbonation renders the binder vulnerable to deterioration (acid attack) and can influence the release of metals (Bertos et al., 2004). Carbonation can either increase or decrease the release of contaminants. Moreover, the release of Ca decreases after carbonation (Garrabrants et al., 2004). Also, CO₂ can induce C-S-H decomposition, which increases the release of metal cations (i.e., Cu) (Valls & Vazquez, 2001).

As mentioned earlier, carbonation leads to consuming hydration products (e.g., C-S-H and CH) and lowers pH, which causes a degradation in the S/S matrix (Johannesson & Utgenannt, 2001). For example, carbonation can weaken the S/S matrix by increasing the release of metals such as calcium (Chen et al., 2009; Walton et al., 1997). Another study found that accelerated carbonation can improve the physical and chemical properties of the S/S matrix, such as lowering metal release (Lange, Hills & Poole, 1996). Perera et al. (2011) reported that the pH of the S/S matrix decreases as a consequence of carbonation, which can lead to an increase in

the solubility of metals in the pore solution. The extent of this increase in metal solubility is primarily dependent on the magnitude of the pH reduction. Therefore, understanding the factors influencing the extent of pH decrease is crucial in predicting the potential leaching of metals from S/S materials subjected to carbonation. However, Al Tabbaa & Stegemann (2011) showed that the contaminants may be encapsulated by carbonation products such as calcium carbonate. Antemir, Hills, Carey, Magnie & Poletini (2010) also investigated how carbonation affected S/S after four years of operation. The results demonstrated that Cu, Zn, and Pb were sufficiently immobilized. After 17 years of remediation, Wang, Wang & Al-Tabbaa (2014) investigate the performance of the solidification of contaminated soil. According to the results of the leaching test, the release of copper, lead, cadmium, zinc, and nickel is still below recommended values.

1.6 Mechanical Stresses

The cracking of cement-based materials plays a significant role in their durability (Van Breugel, 2007). Rupture typically takes place when the stress reaches the tensile or compressive strength of concrete. Cracks impact the hydraulic conductivity of cement-based materials and contaminant transport in their matrix (Akhavan & Rajabipour, 2012; Banthia, Biparva & Mindess, 2005; Picandet, Khelidj & Bellegou, 2009; Yi, Hyun & Kim, 2011). This section discusses the mechanics of crack formation and the causes of cracking.

1.6.1 Causes of cracks formation

Regardless of the mechanical stress which generates the deformation, crack evolution has three main stages. The first stage occurs in the first 24 hours of concrete hydration. During this stage, the moisture content gradually decreases until the capillary pressure causes micro-cracks in the concrete (Bisschop & Wittel, 2011; Wu, Farzadnia, Shi, Zhang & Wang, 2017). Water consumption dries the matrix and causes shrinkage (as explained in section 1.6.2.1), which increases the tensile stress. Because of the concrete young age, the tensile strength of the matrix is insufficient to prevent the growth of micro-cracks. At this stage, the micro-cracks are

distributed throughout the matrix and are hydraulically linked to the porosity network. Consequently, the first stage leads to an increase in connected porosity (Wu et al., 2017). In the second stage, the cracks grow as the stress increases along their edges. Crack growth is followed by the release of strain energy (Hillerborg, Mod er & Petersson, 1976; Hussain, Pu & Underwood, 1974; Sanchez, Drimalas, Fournier, Mitchell & Bastien, 2018). Hillerborg et al. (1976) proposed that cracks will continue to propagate as long as the energy released during crack growth exceeds the energy absorbed by the formation of new surfaces. Crack development ends when the difference between the released and absorbed energies is zero. The permeability increases noticeably during the second stage as the interconnection between the micro-cracks grows (Akhavan & Rajabipour, 2012). In the third stage, macro-cracks are fully formed, providing preferred pathways for fluid flow, while flow through capillary pores becomes negligible. It is more difficult to describe the flow in cement-based materials at this stage (Picandet et al., 2009).

There are three main causes for the formations of cracks in concrete: shrinkage, chemical reactions, and external loads.

1.6.1.1 Shrinkage

Wu et al. (2017) and Houst (1997) pointed out that carbonation can cause concrete to shrink. The shrinkage associated with carbonation is poorly understood and counterintuitive considering that carbonation leads to a decrease in porosity due to the higher molar volume of calcite compared to portlandite. The main hypotheses to explain carbonation shrinkage were proposed by Powers (1962) and Swenson and Sereda (1968). According to Swenson and Sereda (1968), the shrinkage would be due to the decalcification of C-S-H during carbonation. The latter results were confirmed by Chen, Thomas, & Jennings (2006). Figure 1.9 shows examples of micro-cracks produced by shrinkage.

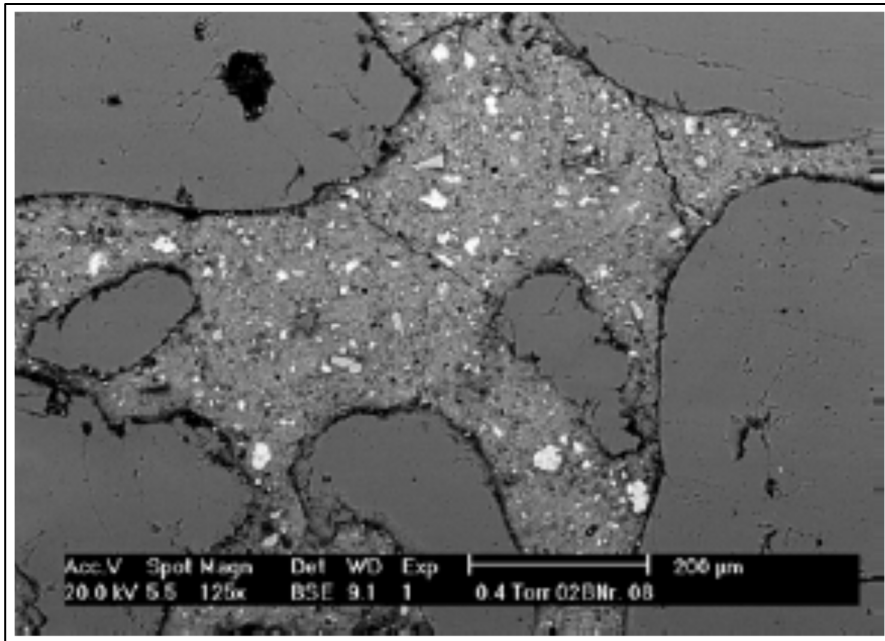


Figure 1.9 Micro-cracks due to shrinkage of paste
Taken from Van Breugel (2007, p. 3)

1.6.1.2 Chemical reactions

Internal swelling reactions (ISR) caused by the alkali-silica reaction (ASR) can degrade concrete structures in the long term due to the formation of expanding reaction products, leading to cracking and decreased compressive strength (Sanchez et al., 2018; Wang & Noguchi, 2020). Certain minerals in aggregates can provide alkalis that react with the silica in the aggregate to produce a hydrophilic gel, gradually filling the pores and causing expansion (Mohammadi, Ghiasvand & Nili, 2020).

1.6.1.3 External loads

External stresses, such as mechanical loads, can induce damage to the structure of cement-based materials, resulting in the creation of new cracks. Consequently, this leads to a decline in the material's strength and an increase in transport properties due to the propagation of micro-cracks (Hoseini, Bindiganavile, & Banthia, 2009; Picandet et al., 2009). The presence of pre-existing microcracks can intensify the impact of external stresses, leading to the

development and propagation of macrocracks. Upon exposure to external stresses, local deformations occur in the matrix, generating micro-cracks. These newly formed micro-cracks propagate throughout the material and intersect with primary pores, ultimately resulting in the formation of macro-cracks (Sanchez et al., 2018).

1.6.2 Influence of cracking on concrete permeability

Cracks create preferential pathways for the flow of fluids and other agents (Hoseini et al., 2009). The mechanical and hydraulic characteristics of the matrix are significantly affected by an increase in fractures and pores. Indeed, by increasing the deformation, the permeability of the material changes in a (more or less) progressive way (Hearn, 1999). In the presence of cracks, the permeability of the materials tends to increase more markedly as the degree of interconnection of the micro-cracks increases. In other words, fluids flow through the cracks and barely passes through the matrix porosity.

Furthermore, the crack opening displacement was observed during loading and unloading tests (Picandet et al., 2009; Wang, Jansen, Shah & Karr, 1997). Under loading, there is a relation between the crack widths and the water permeability of concrete (Wang et al., 1997). For example, the water permeability was not significantly affected when a crack opening displacement was smaller than 50 microns. However, when the crack opening displacement was between 50 and 200 microns, the permeability increased quickly. Finally, when the crack opening displacement was larger than 200 microns, the water permeability became steady (Wang et al., 1997).

Several authors have studied the influence of cracking due to external load on concrete properties. Picandet et al. (2009) exposed a cracked concrete matrix to gas, and then to water injection. They concluded that the water permeability increases with crack opening. However, they also observed that the water flow through the cracked matrix gradually decreased for a given crack opening. This decrease in permeability is the result of unhydrated materials dissolving and calcite precipitating (Picandet et al., 2009). Li & Yang (2007) discovered that

the fractures had been somewhat closed after unloading. Imran & Pantazopoulou (1996) concluded volumetric expansion and cracking are more pronounced during uniaxial loading than in the presence of confinement. In addition, the failure pattern under confining stress is less brittle than in the case of an unconfined system. This means the confinement stress reduces or slows the growth of the cracks (Imran & Pantazopoulou, 1996).

1.7 Leaching

In the literature, leaching refers to the process by which a liquid (e.g., water or solvent) induces the extraction of soluble components from the solidified matrix (e.g., mortar or concrete) (Catalan & Wetteskind, 2002; Poon et al., 1999; Zhang et al., 2009). Water is considered the primary environmental factor responsible for leaching and carrying the mineral materials and contaminants from and into the S/S matrix. For example, as the water penetrates the matrix, it interacts with the matrix components, leading to the dissolution of cement hydrate and changing the chemical equilibrium (Poon & Chen, 1999; Saito & Deguchi, 2000). In other words, when the solidified matrix is exposed to external conditions (such as rain and freeze-thaw cycles), its constituents, including major and trace elements, gradually leach into the soil and water (Zhang et al., 2009). Mainguy, Tognazzi, Torrenti & Adenot (2000) stated that water causes C-S-H to decalcify and CH to leach. Therefore, the consequences of these attacks on the matrix can increase the porosity and permeability, which would reduce its compressive strength (Mainguy et al., 2000; Saito & Deguchi, 2000). This phenomenon is particularly evident in scenarios where water continuously flows, causing the matrix to persistently strive for chemical equilibrium. Consequently, the elements in the matrix continually dissolve in the pore solution and leach out into the surrounding environment, ultimately leading to their release. The aggressiveness of water can also come from its acidity.

1.7.1 Selecting leaching test

The leaching of constituents from cementitious materials can be affected by several chemical and physical factors, which can change over time. Changes in pH, physical structure, and water

flow can all impact the leaching process. Even slight changes in these factors can significantly affect the equilibrium water concentration and the release of constituents into the environment (U.S. EPA, 2019). Predicting the long-term stability of the S/S matrix is generally based on its chemical performance, which is addressed by leaching tests in the laboratory (Catalan et al., 2002). For instance, laboratory leaching tests make it possible to estimate the immobilization of contaminants by testing several parameters simultaneously. In the literature, there are several protocols for leaching cementitious materials. The standard tests are the Toxicity Characteristic Leaching Procedure (TCLP), the sequential chemical extraction (SCE) test, column tests, and flow-through leaching. Several leaching test procedures have been utilized to evaluate environmental stability by accelerating the degradation of the S/S matrix. On the other hand, information on the long-term performance of S/S soils for real-field applications is limited (Al Tabbaa & Stegemann, 2011). Catalan et al. (2002) reported that these laboratory tests have several limitations for forecasting the long-term performance of S/S techniques in real-field applications. However, there is no leaching test available that simulates environmental conditions and estimates the stability of solidified materials in the long term (Butcher, Cheeseman, Perry & Sollars, 1996). For example, according to Zhang et al. (2009), leachant is not renewed under experimental conditions in the laboratory. In contrast, the situation is significantly different under natural field conditions because water is in contact with the S/S matrix, and leachant is continuously renewed (Catalan et al., 2002).

Furthermore, the TCLP test requires grinding the cementitious matrix into small particles (<9.5 mm) (U.S. EPA, 2019). The results are connected mainly to the tiny cementitious particles rather than to the entire sample (Butcher et al., 1993). In studies using columns and Sequential Chemical Extraction (SCE) tests, the material was also broken up into smaller particles (Jackson, Garrett, & Bishop, 1984; U.S. EPA, 2019). Despite the fact that the American National Standards Institute (ANSI) leaching tests overcame the particle size reduction issue, the solidified sample had been submerged in water for three months (Butcher et al., 1993). Many leaching test concepts are identical, and their findings are interpreted differently. The question is: which test is suitable for the intended goal? In this context, it is crucial to distinguish between the various leaching tests.

1.7.1.1 Flow-through leaching test

In general, two processes can govern matrix leaching. It is determined mainly by the matrix permeability and physical properties of the landfill. Figure (1.10a) illustrates the water flowing around the matrix; (1.10b) shows water flowing through the matrix.

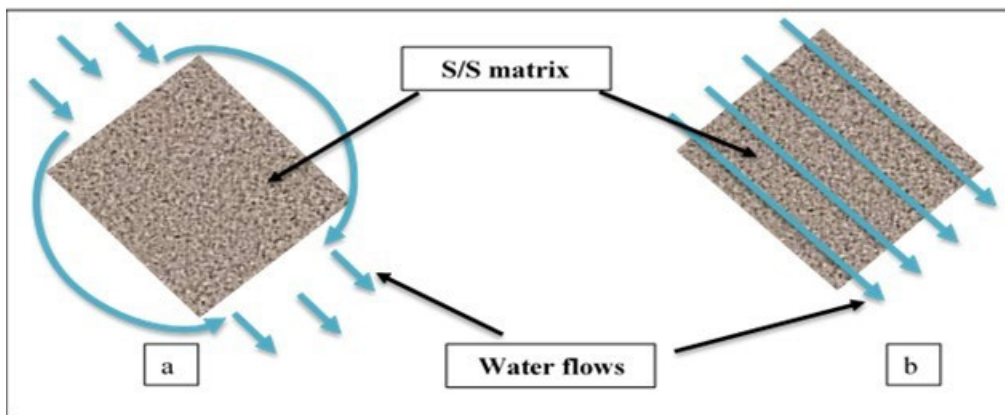


Figure 1.10 Water flowing (a) around the matrix; (b) through the matrix

Moreover, Poon et Chen (1999) mentioned that when the matrix is more permeable than the surrounding components, water flows through the matrix's pore structure. If the materials around the matrix are more permeable than the matrix, water flows around the matrix. Water can also flow as a result of a combination of the two processes (around and through the matrix). The flow-through leaching test is considered an essential tool for predicting the long-term behaviour of solidified waste. It enables the characterization of the stabilized/solidified waste and the identification of the crucial factors governing its release. In order to assess the long-term stability of S/S, a flow-through leaching test is required (Butcher et al., 1993; Poon & Chen, 1999; Zhang et al., 2009).

During a flow-through leaching test, water is allowed to flow through the pores of the sample rather than around it. When water flows through the pores, it comes into contact with the S/S materials, altering the dissolution of the more stable mineral phases and carrying the

contaminants (Poon, Chen, & Wai, 2001; U.S. EPA, 2019). In other words, it interacts with cement materials (which are the essential constituents of the matrix) and causes their dissolution, resulting in the leaching of constituents (such as calcium leaching) (U.S. EPA, 2019). The remaining contaminants and materials will continuously dissolve to re-establish equilibrium, thereby accelerating the contaminant gradient (Butcher et al., 1993; Mainguy et al., 2000). In addition, the quantity of leachable contaminants depends on their solubility and concentration in the matrix. It is also highly dependent on the permeability of the S/S matrix. A concrete matrix has a pore solution with a pH greater than 13, and any solution with a lower pH is deemed aggressive. Thus, natural water with a pH less than 7 might have an acidic character.

1.8 Self-healing Phenomenon

Numerous terms, including "self-healing," "self-sealing," and "autogenous healing," are used in the literature to explain the crack healing phenomenon (Ferrara et al., 2018; Hearn, 1998). Due to the similarities between these terms, the reader may occasionally confuse them. The term "healing" refers to the ability of cracks to close via external influences such as adding capsules that contain epoxy resin (Van Tittelboom & De Belie, 2013). On the other hand, the phrase "self-healing" describes the ability of the cementitious material to close concrete cracks without any healing agents that enhance the repair (Hearn, 1998; Van Tittelboom & De Belie, 2013). This phenomenon includes several processes and is dependent primarily on the chemistry of cement components and the accessibility of water. However, information regarding this phenomenon remains relatively rare. According to Zhong & Yao (2008), micro-cracks might be closing over time due to the phenomenon of self-healing.

1.8.1 Self-healing mechanisms

According to the literature, the primary causes of self-healing mechanisms can be classified into three groups: physical, chemical, and mechanical mechanisms (De Belie et al., 2018;

Hearn, 1998; Jacobsen & Sellevold, 1996; Heide & Schlangen, 2007). Figure 1.11 presents the primary mechanisms for enhancing self-healing (De Belie et al., 2018).

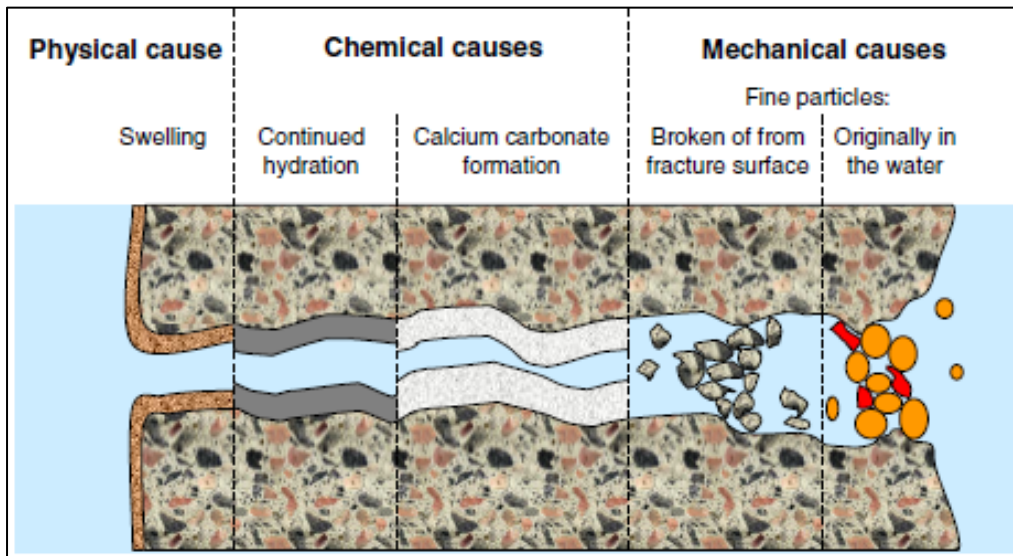


Figure 1.11 Self-healing mechanisms
Taken from De Belie (2018, p. 3)

These mechanisms do not occur sequentially, but rather separately or in combination. Furthermore, the presence of water is required for these processes to achieve autogenous healing.

Self-healing was noticed in concrete structures that were in contact with water. For example, healing occurs between the two surfaces of a crack in the presence of water and possibly with dissolved carbon dioxide (Herbert & Li, 2013). In other words, water is required since self-healing is reliant on chemical mechanisms such as interactions between water and unhydrated cement particles on the crack surface (Van Tittelboom & De Belie, 2013). Hearn (1998) mentioned that white crystals formed a layer on the crack surfaces. He stated that these crystals are formed by the carbonation of $\text{Ca}(\text{OH})_2$ or by reactions between $\text{Ca}(\text{HCO}_3)_2$ and $\text{Ca}(\text{OH})_2$. In addition, he carried out a study that focused on healing using water permeability measurements. He concluded that autogenous healing can significantly lower the water permeability of the matrix. According to Herbert & Li (2013), as the water passes into the

pores and fractures of the matrix, it causes minor micro-cracks to heal. Other complementary phenomena that induce cracks to close involve swelling of the cement paste or physical clogging by accumulating small particles after loading (De Belie et al., 2018; Van Tittelboom & De Belie, 2013). As stated by Heide & Schlangen (2007), compressive pressures induce the edges of a crack to close together and narrow, which facilitates healing.

1.8.1.1 Formation of calcium carbonate (CaCO_3)

The phenomenon of concrete carbonation causes the precipitation of calcium carbonate (CaCO_3) in cracks. Calcite precipitation is quite active in concrete that contains a substantial quantity of portlandite, particularly with a high W/C ratio. The self-healing phenomenon in cementitious materials occurs as a result of the increase in the volume of calcite precipitate, which is a consequence of portlandite and C-S-H carbonization (Van Tittelboom & De Belie, 2013). This precipitation leads to the formation of a layer on the crack surfaces, ultimately resulting in the sealing of cracks. A detailed explanation of this process has been provided in Section 1.5.

1.8.1.2 Continued hydration phenomenon

It is well known that unhydrated cement particles are disseminated throughout the concrete matrix when insufficient hydration exists. In addition, these particles will remain dehydrated for an extended period because the matrix does not recontact with water. Moreover, when the W/C ratio of concrete is lower than 0.42, the cement is not entirely consumed by the hydration reactions. According to Li & Yang (2007), up to 25% of the cement in the matrix may not be hydrated at low W/C ratios. This resulted from the lack of water, either difficulty accessing water to the non-hydrated grains of cement or from the lack of water (Van Der Zwaag, 2007).

When cracked concrete is exposed to water, the hydration reactions can resume according to the same equations as primary hydration (Li & Yang, 2007). The quantity of penetrated water that enters the matrix in the presence of micro-cracks may be greater than the amount of water that is added to the matrix during the mix. Furthermore, the percentage of hydration products

before and after continuous hydration may differ. Herbert & Li (2013) investigated the ability of the concrete matrix to restore rigidity after being exposed to natural environmental conditions. They discovered that as exposure time increases, matrix stiffness also increases, which can be attributed to self-healing created by ongoing hydration.

1.8.1.3 Accumulation of particles

Another hypothesis related to the mechanical phenomenon is particle accumulation. The appearance of cracks generates small particles (e.g., cement paste and aggregates), which can be carried by water to the narrowest areas of the fissure (Snoeck, Van Tittelboom, Steuperaert, Dubruel & De Belie, 2014). According to Banthia et Mindess (1989), tiny particles could become dislodged by the high-pressure gradient and block the pores, thereby progressively decreasing the permeability. The contribution of the particle accumulation mechanism to self-healing remains insignificant (De Belie et al., 2018). Although self-healing can close fractures and reduce the water permeability in the matrix, the matrix may not necessarily recover its original properties such as strength and stability (Herbert & Li, 2013).

1.8.2 Parameters influencing the self-healing

1.8.2.1 Influence of crack width on self-healing

Studies have shown that the capacity of a cracked matrix to heal itself is significantly linked to crack width (Herbert & Li, 2013; Ramm & Biscopig, 1998). According to various studies, even though the maximum permitted crack width for self-healing should be between 50 and 200 μm , this might be challenging depending on the environmental circumstances (Li & Yang, 2007; Snoeck et al., 2014; Van Der Zwaag, 2007). Yang (2008) concluded that a crack that is less than 50 μm wide heals entirely, while it heals only partially if the crack width is 150 μm or greater. Additionally, with crack widths ranging between 20 and 80 μm , Yang (2008) obtained positive results for crack healing. Figure 1.12 illustrates the evolution of the relative flow over time for crack openings at various widths of 0.05, 0.1, and 0.15 mm (Reinhardt &

Jooss, 2003). This figure explains that the flow decreases more quickly for a crack opening of 0.05 mm than for those of 0.1 and 0.15 mm.

1.8.2.2 Influence of matrix properties: pH, age, and W/C ratio

The matrix characteristics play a significant role in improving the ability of a matrix to self-heal and extend its lifetime. Ramm and Bischoff (1998) studied the healing phenomenon by continuously passing water of various acidity levels (pH = 5.2, 6, and 7) under pressure through cracks of 0.2, 0.3, and 0.4 mm. They concluded that healing is more significant in the case of a high pH value of 7. The influence of the age of the concrete and the W/C ratio are interrelated. Indeed, the age of the concrete is an important parameter. Zhong & Yao (2008) demonstrated that the healing mechanism produces favourable results when the damage occurs when concrete is fresher. For example, when newer concrete is cracked, the hydration of anhydrous cement could explain the healing process (Zhong & Yao, 2008). Schlangen, Heide & Breugel (2006) evaluated the matrix's capacity to recover stiffness at various ages (the matrix was kept submerged in water). They discovered that the rate of strength recovery slowed as the sample aged (cured), and the effect became less pronounced when cracking occurred in older concrete or mortar.

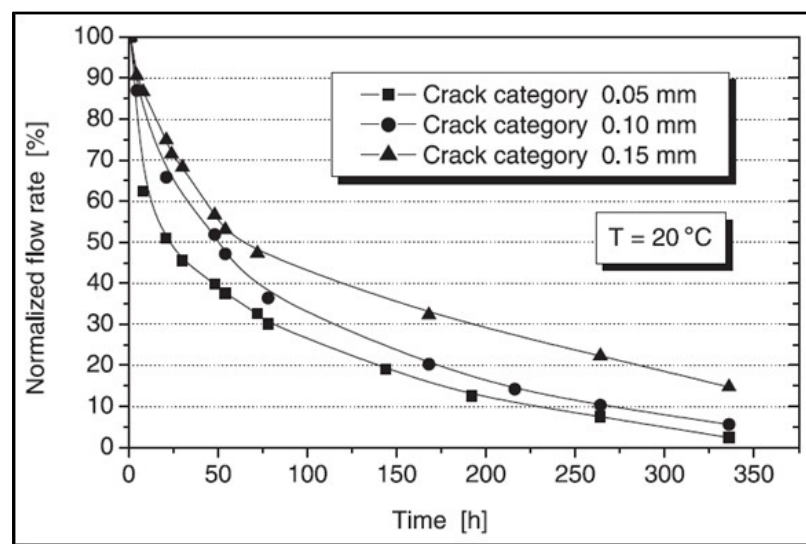


Figure 1.12 Water flow as a function of crack width
Taken from Reinhardt (2003, p. 984)

According to Li & Yang (2007), a low water-to-cement ratio combined with a large quantity of fly ash can stimulate self-healing thanks to ongoing hydration. Furthermore, the matrix with a low W/C ratio retains a significant amount of unhydrated cement grains (Ferrara et al., 2018). The continued hydration of cementitious materials produces C-S-H gels, thus inducing self-healing (De Belie et al., 2018). However, the capacity of a matrix to self-heal in a matrix with a high water-to-cement ratio is limited, and is dependent mostly on the amount of water added during mixing (Ahn & Kishi, 2010).

1.8.2.3 Influence of humidity

Healing can occur only in the presence of water since it is mainly the result of chemical reactions between water and certain compounds exposed to concrete near the crack (Clear, 1985). Therefore, water is essential; it can be stationary or flow through the crack (Ferrara et al., 2018; Li & Yang, 2007). According to Li & Yang (2007), in the case of sufficient water, $\text{Ca}(\text{OH})_2$ can react with dissolved CO_2 in water and migrate much quicker. If the matrix is less humid, there is less dissolved CO_2 for calcite formation (Ferrara et al., 2018). Schlangen et al. (2006) studied the change in healing when using two methods: submerging the sample in water, or leaving the sample in a room with a relative humidity of 95%. They concluded that the healing (in terms of recovered strength) was different depending on the level of humidity. In the case of water immersion, crack healing occurs exclusively under conditions of sufficient humidity. However, when the relative humidity (RH) is at 95%, this process occurs at a very slow rate, and there is no observable improvement in mechanical properties.

1.8.3 Effect of healing on concrete properties

Many mechanical tests were conducted to understand the effect of healing on the mechanical behaviour of concrete, such as tensile, compression and non-destructive techniques (De Belie et al., 2018; Granger, Loukili, Pijaudier-Cabot & Chanvillard, 2007; Herbert & Li, 2013; Snoeck et al., 2014; Van Tittelboom & De Belie, 2013). Their results showed that the matrix had been healed, and that its strength had slowly recovered. However, the stability of self-

healing products is debatable because they have lower resistance than the initial hydration products. For example, Li & Yang (2007) concluded that cracking occurs in the place where the crack had healed when the healed sample is subjected to a reloading cycle. Moreover, Jacobsen & Sellevold (1996) noted a slight increase in the compressive strength (up to 5 %) after three months of storage in water following damage due to freeze-thaw cycles.

1.9 X-Ray Micro-Tomography (CT Scans)

Understanding the S/S mechanisms and evaluating their long-term performance cannot be based solely on physical and chemical analyses (Klich et al., 1999). Micro-CT scan and high-resolution imaging are required (Carlson, Denison & Ketcham, 2000; Van Geet, Lagrou & Swennen, 2003).

1.9.1 Principle of tomography

The main concept behind tomography is to acquire several images of the object from various angles by measuring the transmission of X-rays through the object's internal structure. X-rays travel as straight lines and pass through an object. The object will absorb some of the X-rays, reducing the intensity of X-rays and then forming a shadow image (Ferrara et al., 2018). In this process, incoming X-rays will hit a fluorescent screen (detector), and the energy of the X-ray is absorbed and re-emitted as visible light. Thus, the fluorescent screen converts the energy of X-rays into the light to form images. These images will later be reconstructed by a computer program. Figure 1.13 illustrates the micro-CT scan process schematic and elements. A tomographic acquisition system is comprised of four elements: a source of X-rays, a detection system, a mechanical system for handling and rotating the object, and a computer for control (i.e., acquisition, reconstruction and analysis).

Micro-computed tomography is a useful technique with a wide range of benefits for researchers, such as high-resolution 3D images and the provision of quantitative data. The main advantage of an X-ray micro-CT scan is that a sample can be imaged many times without

destroying it, which allows other tests to be run on the same sample (Cnudde & Boone, 2013). X-ray CT can also provide a better analysis of the internal matrix's structure without the need for sample preparation or pre-treatment (Kaddhour et al., 2013; Kong, Wei, Wang, Chen, & Wang, 2020). However, the main drawback of imaging techniques using X-rays relates to the establishment and monitoring of radiation protection standards, which can be restrictive. Furthermore, the high image resolution is limited for small matrices (Snoeck, Dewanckele, Cnudde & De Belie, 2016; Wang et al., 2014).

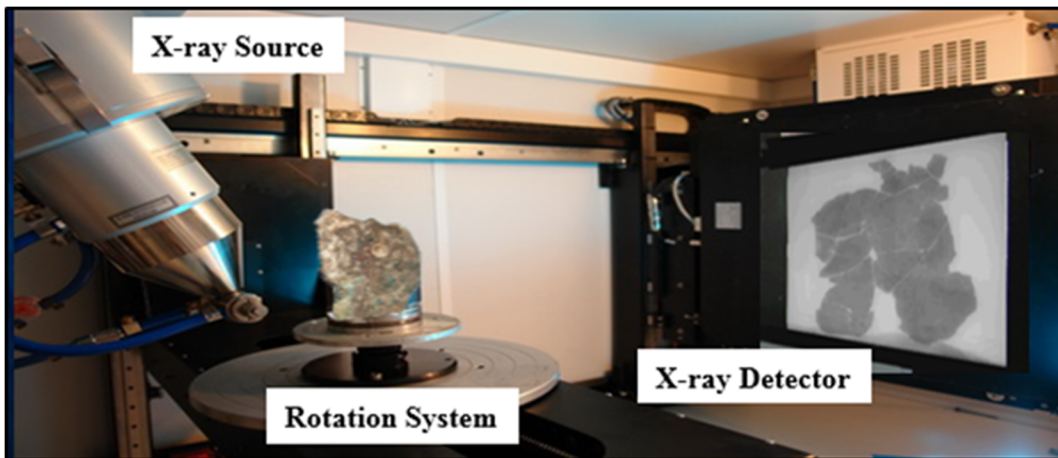


Figure 1.13 Schematic of the micro-CT and its elements

1.9.2 Micro-CT applications in geotechnical engineering

Many researchers have used image analysis with segmentation algorithms with appropriate threshold techniques for thorough damage analysis. Figure 1.14 illustrates the CT images before and after segmentation. Hazlett (1997) stated that prior to, the existence of tomography, displaying 3D pore structures was possible only through statistical or process-based models. Carlson, Denison & Ketcham (2000) reported that the effect of X-ray attenuation is more significant at low energy levels, and that the X-ray attenuation coefficient can be used to distinguish mineral phases with contrasting densities density. Vogel (2005) wrote that the attenuation of X-rays depends on X-ray energy and the density of the material under investigation.

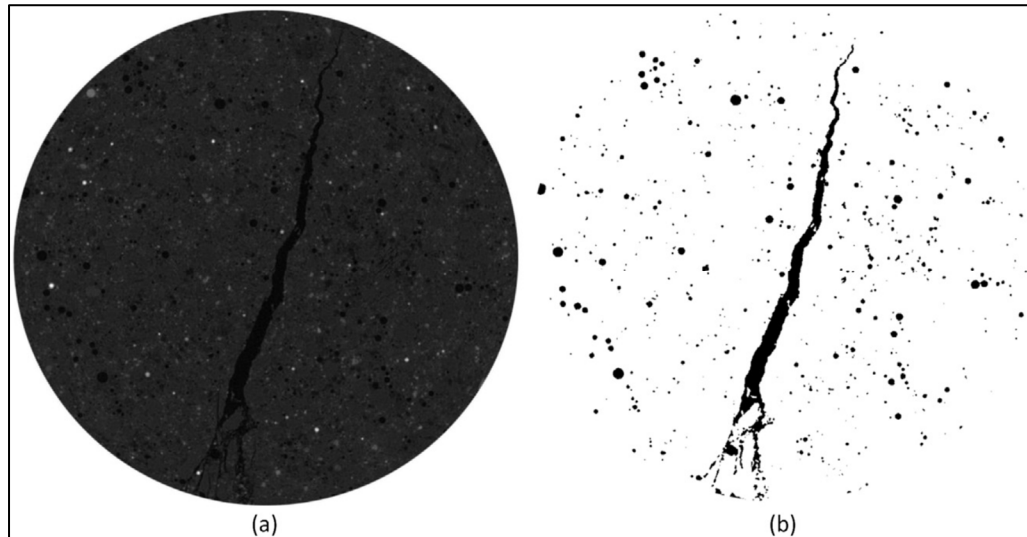


Figure 1.14 2D images (a) original image and (b) segmented image
Taken from Snoeck et al. (2016, p. 86)

X-ray CT can provide a better analysis of the internal structure of samples if there is a significant difference between the density and the atomic composition of materials under investigation. Van Geet et al. (2003) evaluated the porosity of limestone and compared the results with other techniques. They found that, micro-CT scans provide a precise 3D image of total porosity measurements and macro porosity distributions after the calibration. Moreover, they showed that the porosity images are better than the results obtained from optical microscopy measurements. Wang et al. (2014) investigated self-healing in mortar samples ($D = 8 \text{ mm}$, $h = 10 \text{ mm}$) using high-resolution X-ray μ CT. As observed in the second column of Figure 1.15, the 3D images indicated that the CaCO_3 precipitation (in yellow) was predominantly dispersed on the surface layer.

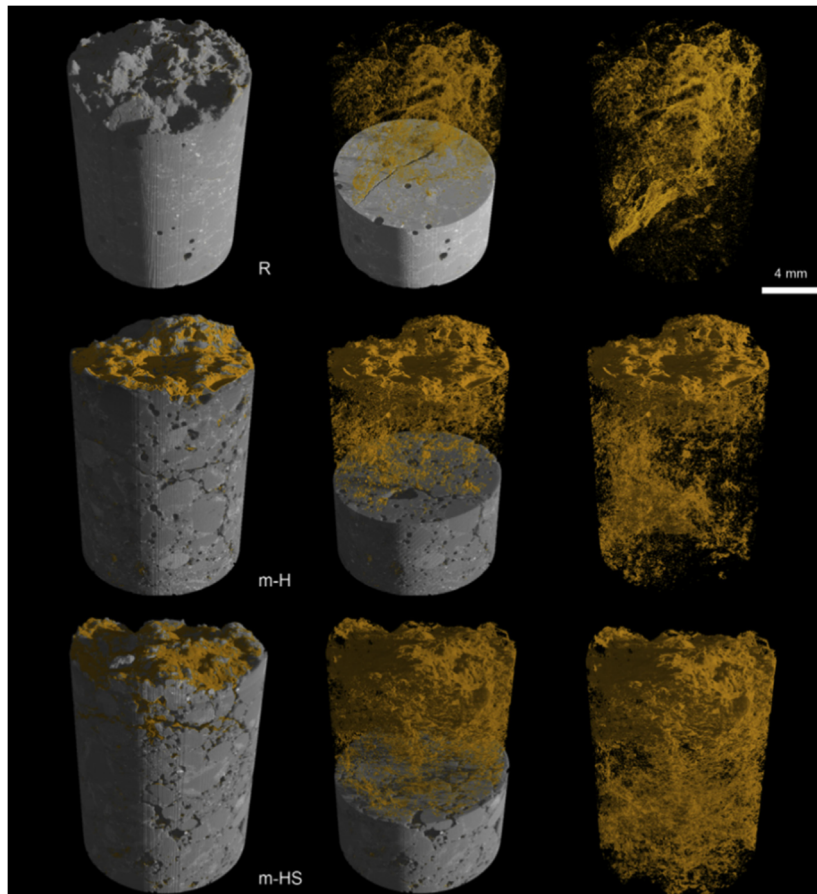


Figure 1.15 Distribution of healing products in 3D images
Taken from Wang et al. (2014, p. 301)

Lanzón et al. (2012) reported on their study of the crystallization of anhydrous and hydrated salts in the pores of limestone by using synchrotron X-ray micro-CT scanning. They concluded that synchrotron X-ray μ -CT is a promising technique for examining the pore space distribution of salts. De Argandona et al. (1999) evaluated pore structure using computed X-ray tomography during freeze/thaw cycles. They discovered that fissures formed, and observed that samples began crumbling after twelve freeze/thaw cycles. Ranachowski et al. (2014) used micro-CT to analyze the matrix's microstructure. Their findings demonstrated that a micro-CT scan was beneficial in characterizing porosity and pore size distribution. Snoeck et al. (2016) investigated a cementitious sample that measured 10 mm in height and 6 mm in diameter. They discovered that micro tomography is an effective method for evaluating porosity and self-healing products.

A series of operations such as image filtering, segmentation, and analysis methods can be used to identify fractures in images (Hornain, Marchand, Ammouche, Commene & Moranville, 1996; Iyer & Sinha, 2005; Vidal, Ostra, Imaz, García-Lecina & Ubide, 2016; Yiyang, 2014). Image segmentation is the process of partitioning an image into multiple regions of interest that are easier to further analyze. In the literature, details on segmentation methods used in X-ray CT images remain limited (Taina, Heck & Elliot, 2008). There are various methods that users can utilise for image segmentation, including simple thresholding, double thresholding, and machine-based algorithms (automatic thresholding). In general, histogram thresholding (binary image) is the most often used approach in image segmentation. Yang, Wu, Miao & Liu (2014) used pre-processing of images to increase the contrast between the solid phase and the pore phase. Finally, based on the gray-level histograms (visual examination), they select thresholding to discriminate between particles and pores. Figure 1.16 shows their procedure (image pre-processing) to distinguish between pores and solid phases.

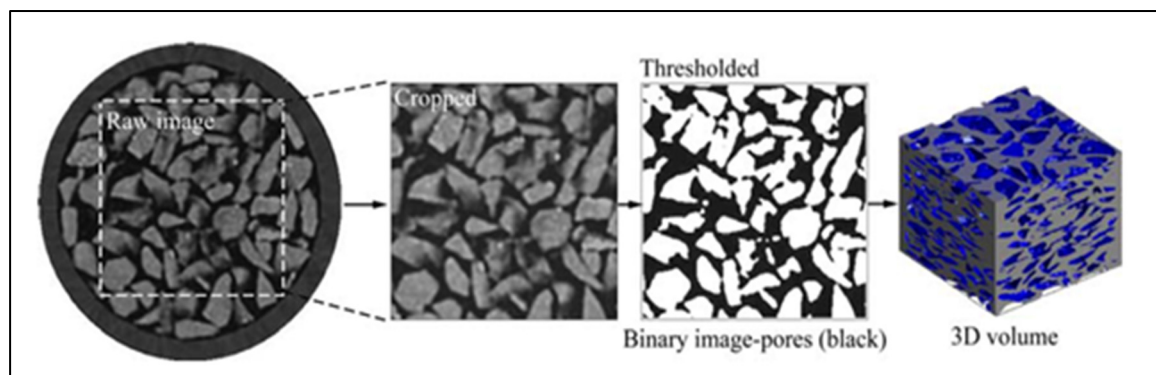


Figure 1.16 Image pre-processing procedure
Taken from Yang et al. (2014, p. 834)

Due to the low X-ray attenuation contrast in a cement matrix, image segmentation can be difficult, particularly when choosing the optimal threshold. For instance, in the presence of healing products, it might be difficult to distinguish between cracks, pores and healed cracks (Ferrara et al., 2018; Snoeck et al., 2016; Wang et al., 2014). Fukuda et al. (2012) used micro-

focus X-ray CT scans to study self-healing in concrete. Their findings in 2D images, as presented in Figure 1.17, indicate that cracks were sealed solely at the sample's surface.

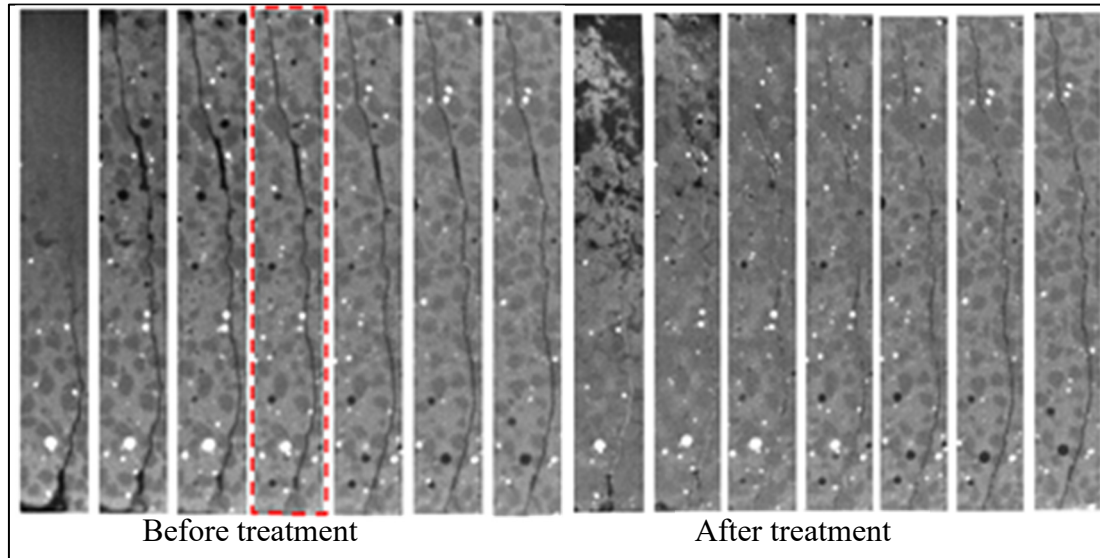


Figure 1.17 CT images of the crack healing
Taken from Fukuda et al. (2012, p. 1496)

Snoeck et al. (2016) investigated the autogenous healing of small cylindrical samples with dimensions of 10 mm in height and 6 mm in diameter using an X-ray μ CT scan. They concluded that μ CT is an effective method for examining self-healing products in a cementitious matrix, as shown in Figure 1.18.

Filtering techniques are also considered to be an effective image processing method. Salman, Mathavan, Kamal & Rahman (2013) proposed an approach to identify fractures in digital images with a detection precision of 95%. Talab, Huang, Xi & HaiMing (2016) proposed a new method to identify fractures in images of concrete structures obtained by optical fluorescent microscopy. Their methodology consists of three stages: 1) change the image from a colour to a greyscale image by using the edge of the image, and use Sobel's method to develop the image and to distinguish fractures; 2) categorize the image into foreground and background by using appropriate threshold binary images of the greyscale pixel; and 3) use

Sobel filtering for the elimination of residual noise once the images are classified. After this filtering procedure on the image, cracks are detected using Otsu's method.

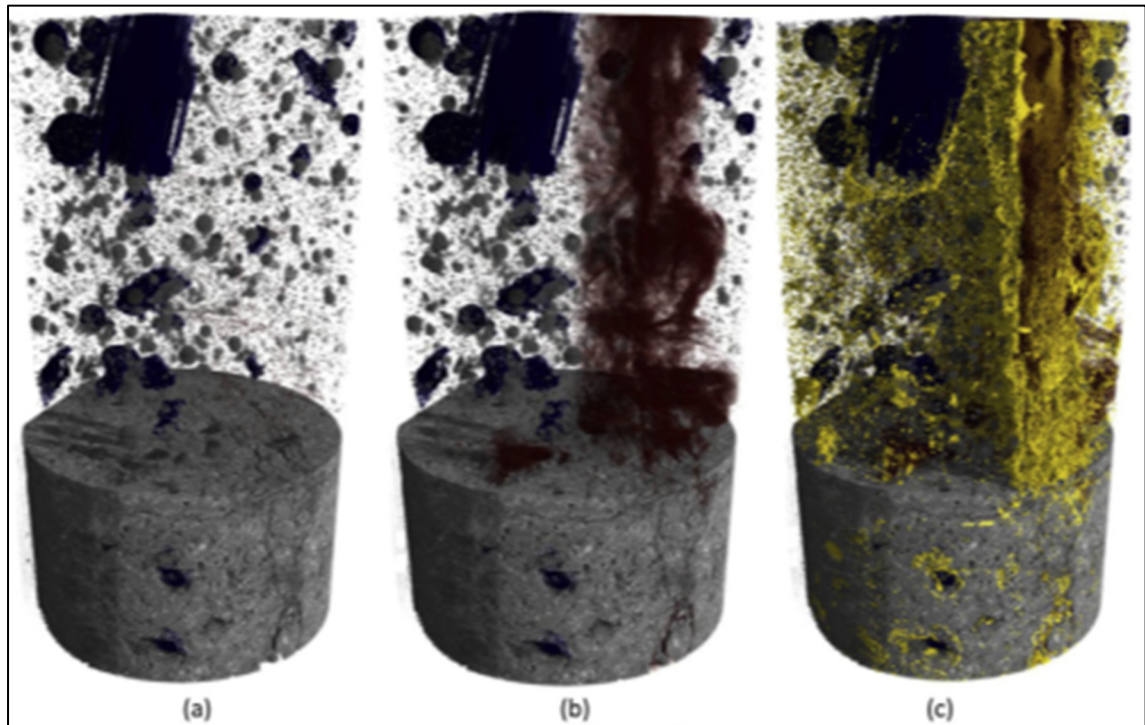


Figure 1.18 3D distribution of a) small pores (grey) and macropores (blue),
b) cracks (red), and c) healing products (yellow)
Taken from Snoeck et al. (2016, p. 90)

1.10 Summary and Research Objectives

Cement-based stabilization/solidification (S/S) techniques have been widely used to produce stable forms of contaminated soil (Perera et al., 2011). The S/S matrix is designed to immobilize contaminants (physically and chemically) in the matrix rather than treat them. However, this technique might lose its efficiency if the integrity of the S/S matrix is exposed to a chemical attack such as CO₂ penetration or physical damage such as microcracks formation, which is often a result of external stresses.

Numerous laboratory experiments have proven the effectiveness of the S/S technique in the remediation of polluted soil. In general, these experiments and methods facilitate the evaluation of the effectiveness of the S/S technique; however, they typically lack clear evidence of its long-term performance and rarely incorporate confining stress. Confining stresses are known to influence the S/S process performance in the long term (e.g., growth of cracks). Although various tests exist that focus on leaching cementitious materials in the literature, these laboratory experiments have several limitations in estimating the long-term performance of S/S binders (Catalan et al., 2002). Under confining stress conditions, the release of contaminants from the binders to the environment will differ. Moreover, the way water interacts with S/S binders in laboratory leaching tests remains unrealistic and does not represent field conditions. More specifically, in certain experiments, leaching is not renewed, and size reduction occurs by breaking a sample down into smaller particles. In field circumstances, on the other hand, the water in contact with the S/S matrix is constantly renewing. In addition, contaminants treated by S/S are not removed or destroyed; hence it is important to ensure that these contaminants will be immobilized in the long term. It is also notable that the long-term information regarding the physio-chemical performance of S/S remains sparse.

Given those considerations, this thesis aims to evaluate the effects of environmental conditions such as mechanical loading and carbonation on the physicochemical properties of the S/S matrix. It will consist of the following tasks:

1. Identify the influence of mechanical loading and carbonation on the hydraulic conductivity and unconfined compressive strength of a S/S matrix.
2. Determine the effect of mechanical loading and carbonation on the leaching of metals and the self-healing phenomenon.
3. Examine the stability of the S/S matrix in terms of change in microstructure, and define the parameters impacted by these conditions.

The experimental conditions and the materials studied created additional difficulties: relatively high gas pressures and high confinement pressures; in addition, specific axial loading rates were needed. Specific experimental devices, materials and protocols had to be developed in order to achieve the study's goal. The main experimental points that were considered to achieve the goal are as follows:

- Create a triaxial cell to combine the effects of micro-cracks and the acceleration of carbonation on the solidified sand. This method must be implemented to represent the impact of environmental conditions under the confining stresses.
- Establish five experimental scenarios to simulate the effects of carbonation and loading on the properties of the solidified sand. Two protocols were chosen for the water injection regime and total injection time. Each test protocol consists of five test scenarios.
- Develop a micro-Ct scan method to investigate the effect of these conditions on the internal microstructure of the solidified sand. The samples were subjected to a micro-CT scan before and after the application of the protocols.

CHAPTER 2

MATERIALS, METHODS, AND EXPERIMENTAL FRAMEWORK

In this project, a triaxial cell was used to determine the effect of strain and carbonation on S/S materials. The triaxial cell allowed carbonation and deformation to be applied under a confining stress. It also allowed leaching and permeability tests to be conducted on the S/S materials. Tests were also conducted to study the influence of carbonation and loading on mineralogy and microstructure with thermogravimetric analysis (TGA) and micro-CT. The objective of this chapter is to present the materials (samples and equipment) and the test program.

2.1 Leaching Protocols and Stressor Scenarios

Each test comprises a series of water injection stages defined by a leaching protocol and a stressor scenario. Figures 2.1 and 2.2 summarize the stressor scenarios for the continuous and intermittent leaching protocols. For each test, the solidified samples were subjected to micro-CT scan at the beginning and at the end of the stressor scenarios, a TGA analysis, a phenolphthalein test and a compressive strength test. The following sections define the main characteristics of the injection protocols and the stressor scenarios.

2.1.1 Leaching protocols

Two leaching protocols were used. In the continuous water injection protocol (Figure 2.1), deionized water was renewed and continuously injected into the S/S sample under a constant hydraulic head difference for three days during the flow-through leaching test (FTL). The FTL was accompanied by permeability tests and different combinations of carbonation (C) and loading (L) stages. In the intermittent water injection protocol (Figure 2.2), deionized water was renewed and injected into the S/S sample daily during four hours for ten days. Daily permeability tests were also carried out during this ten-day period. Both protocols involved

similar total leachate volumes, but the intermittent water injections allowed more time for equilibrium to be reached between the aqueous and solid phases.

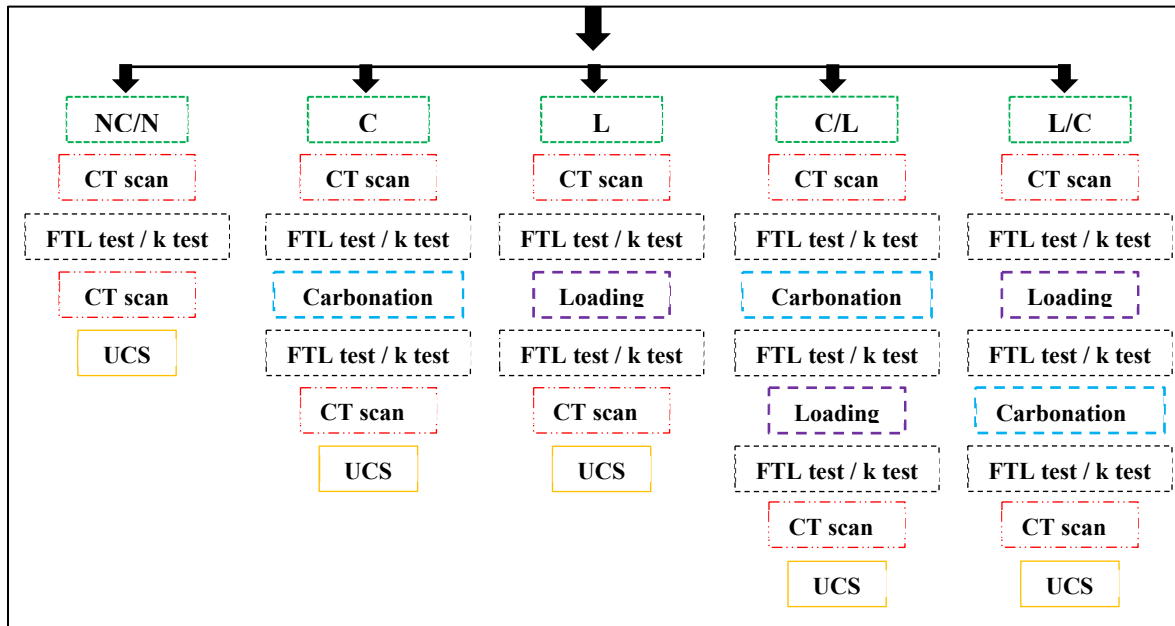


Figure 2.1 Stressor scenarios for the continuous water injection protocol

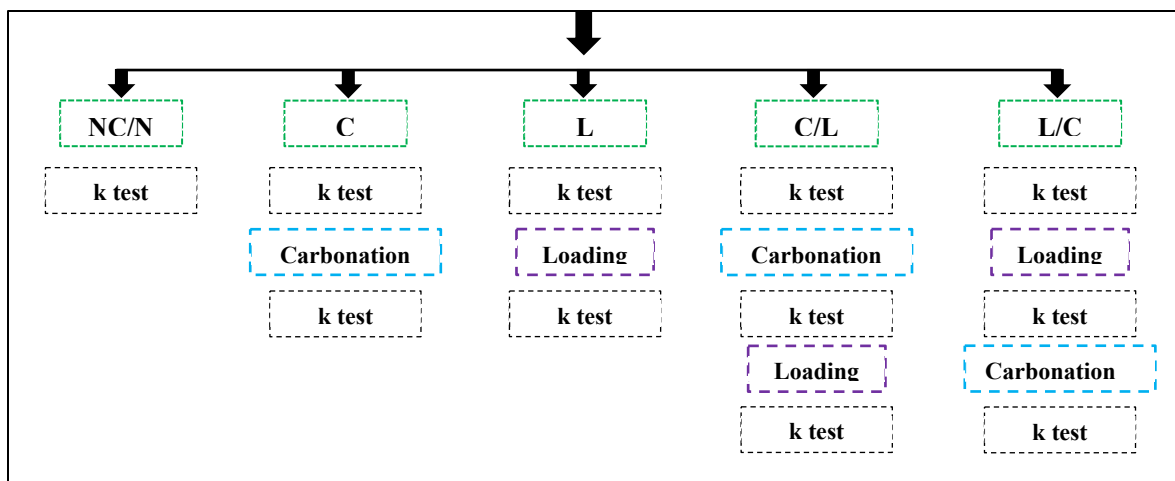


Figure 2.2 Stressor scenarios for the intermittent water injection protocol

2.1.2 Stressor scenarios

Figures 2.1 and 2.2 show that each injection protocol consists of five stressor scenarios: no carbonation/no loading (NC/NL), carbonation only (C), mechanical loading only (L), carbonation followed by mechanical loading (C/L), and mechanical loading followed by carbonation (L/C).

The NC/NL scenario acts as a reference scenario. During this scenario, the solidified sand sample did not undergo accelerated carbonation or external loading. After the saturation stage, the sample was only subjected to permeability and FTL tests.

For scenario C, the sample was subjected to the hydraulic conductivity/flow-through leaching tests after a 24-hour saturation period. Then, carbon dioxide was injected into the sample for 72 hours. After the carbonation stage, permeability and FTL tests were carried out based on the appropriate leaching protocol in section 2.1.1.

Scenario L was similar to scenario C, but the carbonation stage was replaced with a loading stage. During this stage, an axial load was applied and removed gradually over 14 hours to cause an axial strain of approximately 1.96 %.

With the C/L scenario, the first hydraulic conductivity and flow-through leaching tests were completed within 24 hours. Next, the sample was subjected to a carbon dioxide injection for 72 hours, followed by a water injection. After 24 hours of permeability and FTL tests, an axial strain of approximately 1.96 % was applied. The sample was loaded and unloaded over a period of 14 hours, in accordance with the procedure outlined in Section 2.2.2.2. The loading was followed by permeability and FTL tests. The L/C scenario was similar but the order of the loading and carbonation scenarios was reversed.

2.2 Experimental Setup and Devices

2.2.1 The modified triaxial cell

The primary purpose of a triaxial cell is to measure the mechanical and hydrodynamic properties of soils, such as the shear strength and hydraulic conductivity. In this project, a triaxial cell was modified to allow the carbonation and leaching of solidified sand.

Figure 2.3 shows a cylindrical sample placed inside the modified triaxial cell. All parts of the triaxial cell in contact with water were made of stainless steel to avoid copper leaching from brass components. The cylindrical samples were inserted between two porous stones (discs) and two circular filter papers. The sample was enclosed in a latex membrane with a thickness of 0.3 mm (Figure 2.4). The membrane prevents the hydraulic fluid from penetrating the S/S sample. Four O-rings were used to hold the membrane in place. The porous stone allowed an equal pressure distribution on the sample section. The saturation step began after the cell was installed and all connections were made.

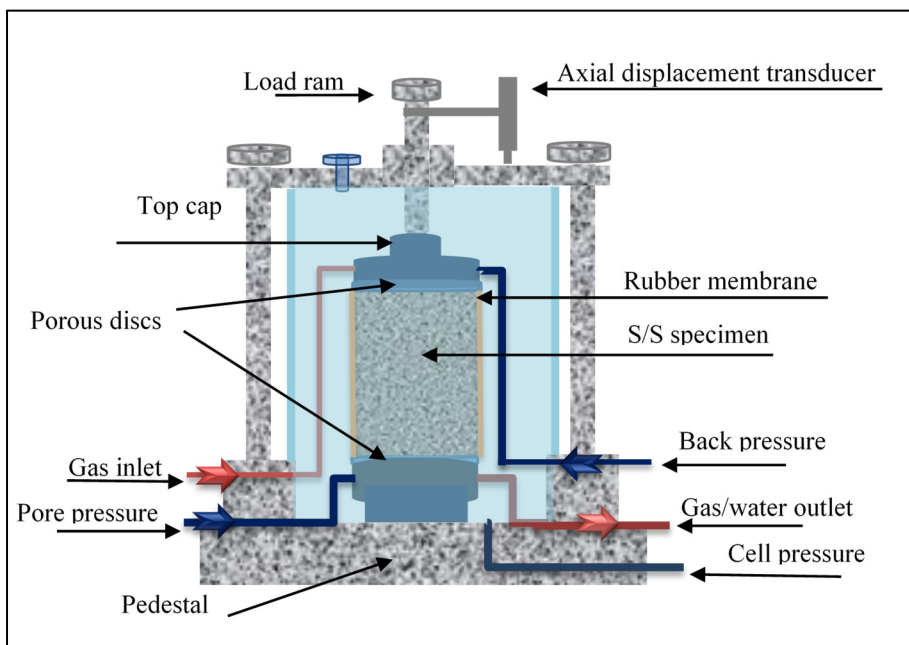


Figure 2.3 Cross-section of the modified triaxial cell

The objective of the saturation stage was to fill the sample voids with water. The water was de-aired before being used in the test. To facilitate saturation, water was injected into the top and base caps of the sample at the same time. A confining pressure of 50 kPa was applied at the beginning of the saturation stage. The Skempton B coefficient was used to verify saturation. This coefficient represents the ratio between the difference in pore pressure and the difference in cell pressure. Cell pressure increments of 50 kPa were applied successively to determine the B coefficient. The sample was considered saturated when $B \geq 0.95$ or when the B value was constant for successive pressure increments. Maximum B values between 0.85 and 0.95 were obtained. It is common to observe maximum B values lower than 0.95 for rigid materials such as solidified sand.

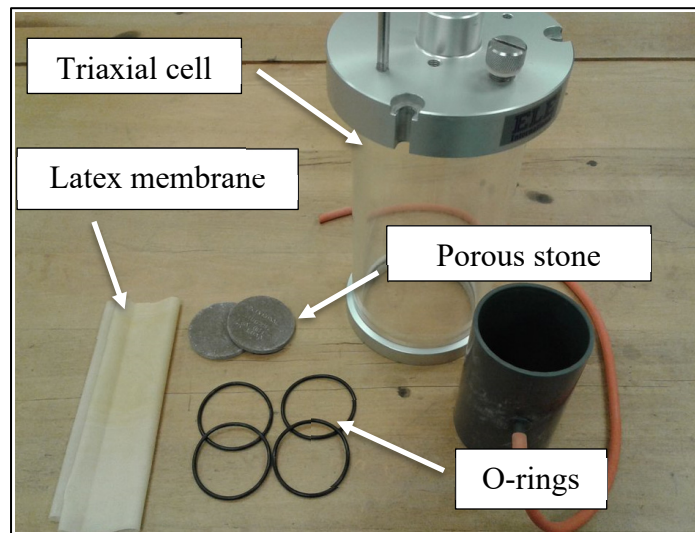


Figure 2.4 Equipment required for the test sample

It should also be mentioned that it is essential to maintain a cell pressure greater than the pore pressure (i.e., the backpressure). When the pore pressure exceeds the cell pressure, swelling of the sample will occur as the water flow is always from the high hydraulic head to the low hydraulic head. Two pressure transducers were used to monitor the pressure. Most tests were conducted with a cell pressure of 750 kPa and a backpressure of 700 kPa.

2.2.2 Test system for stressor scenarios

2.2.2.1 Accelerated carbonation

Figure 2.5 shows the accelerated carbonation system. The main components of the system are the compressed gas cylinder that provides CO₂ and the leachate collection reservoir. Two pressure transducers are used to monitor the gas pressure at the inlet and the leachate pressure at the outlet. An electric solenoid valve was used to control the gas injection.

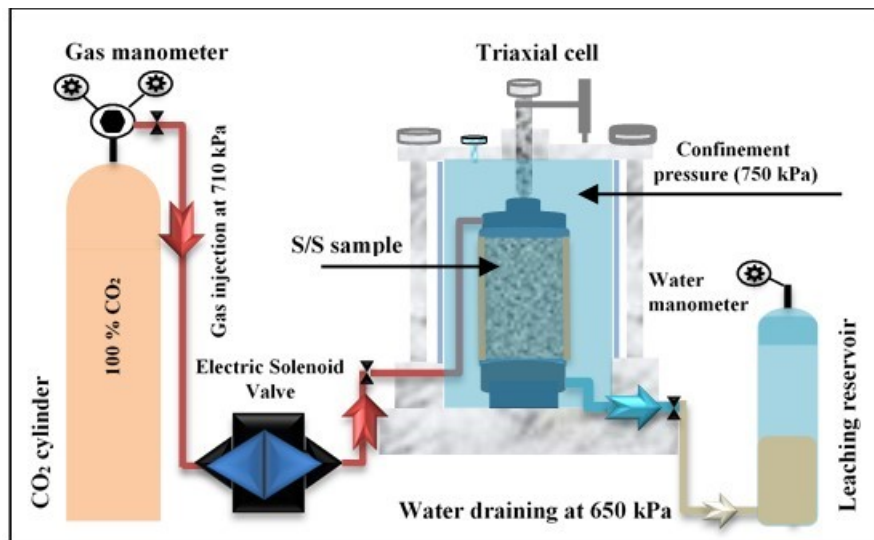


Figure 2.5 The system of CO₂ injection into the sample

The modified triaxial cell injected 100 % dry CO₂ gas into the sample. As mentioned in section 1.5, the extent of carbonation and CaCO₃ precipitation in the S/S sample is influenced by the CO₂ pressure. The precipitation of CaCO₃ closes the pores before completion of carbonation at low gas pressure. Also, a low gas pressure decreases the carbonation rate and decreases the CO₂ diffusion during the injection (Bertos et al., 2004). During the carbonation stage, a pressure of 710 kPa was maintained in the injection pipe connected to the top of the sample. A pressure of 650 kPa was maintained in the water drainage pipe connected to the bottom of the sample. The confining stress was kept constant at 750 kPa. The total length of the carbonation stage was 72 hours.

The CO₂ gas injection during the carbonation stage was cyclic. Every 30 minutes, CO₂ was injected for 30 seconds by opening the electric solenoid valve and by applying a CO₂ pressure of 710 kPa. The total injection time in the S/S sample over the 72-hour carbonation stage was 1.2 hours. According to Phung et al. (2015), cyclic injection increases the degree of carbonation by flushing the excess water during the gas injection phase. When a large amount of water remains in the pores, it prevents CO₂ from penetrating the S/S sample as mentioned in Section 1.5.

2.2.2.2 Mechanical Loading

The objective of the loading stage was to create microcracks in the sample. Microcracks were created by applying a load on the sample in the triaxial cell. The displacement was controlled during the loading stage. A displacement of 2 mm was applied with a displacement rate of 0.02 mm per minute. The target displacement corresponds to an axial strain of 1.96 %. The displacement of 2 mm was kept constant for 5 hours and 20 minutes. The sample was then unloaded until the displacement measurement returned to its initial value with a displacement rate of 0.02 mm per minute. The displacement was again kept constant for 5 hours and 20 minutes before the next test stage. Drained conditions were maintained throughout the loading and unloading. The total duration of the loading stage was 14 hours. After the loading stage, water permeability and FTL tests were conducted.

The two main parts of the loading system are the loading frame and loading control. The loading frame was designed to provide up to 50 kN of axial force. An axial displacement transducer (LVDT) attached to the top of the sample was used to measure the deformation. The displacement rate was controlled by a computer using the software PuTTY.

2.2.2.3 Flow-through leaching test (FTL)

The main objective of this step is to force the deionized water to flow through the solidified sample based on the method presented by Butcher, Cheeseman, Sollars, & Perry, (1996). Figure 2.6 shows a schematic diagram of the flow-through leaching test of the solidified

sample. After the test sample was placed in the triaxial cell, the equipment (cell and water tubes) was filled with deaerated /deionized water. The sample was then saturated for 28 hours (ASTM International D5084, 2016). The hydraulic conductivity test was analysed based on Darcy's Law using test method C in the standard. The cell pressure and backpressure were respectively set to 750 kPa and 700 kPa. This corresponds to an effective stress of 50 kPa.

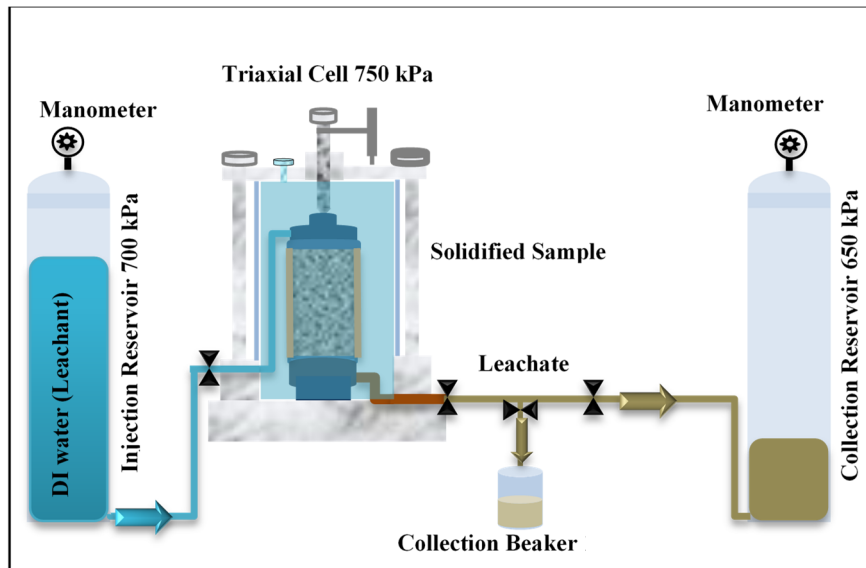


Figure 2.6 Schematic diagram of flow-through leaching test

In this series of leaching tests, the water continued to flow one way for three consecutive days based on protocol 2.1.1. Every 30 minutes, approximately 30 mL of leachate was expelled into the collection tube during the day (Figure 2.7a). At night, a separate reservoir was used to collect the leachate (Figure 2.7b). The average total DI water injected into the cylindrical sample was approximately 2000 cm³ for each FTL. It is noteworthy that subsequent to the loading test, the valve opening, which regulates the rate of leaching exit, was reduced in order to maintain the identical volume of DI water that was injected into the samples in the other scenarios. Copper and calcium leaching was measured, and temperature and electrical conductivity tests under five experimental condition scenarios (control, C, L, C/L, and L/C). In these test scenarios, approximately 188 samples of leachate were collected. The collected leachate samples were filtered using 0.45 µm polypropylene membrane syringe filters (Figure

2.7c.). The sample pH, electrical conductivity (EC), and temperature (T) were measured after filtration (Figure 2.7d). The leachate sample pH was then lowered to less than two by adding concentrated nitric acid to keep the metals dissolved. Finally, the collected leachate samples were preserved in the refrigerator at 4 °C for ICP-OES analysis.

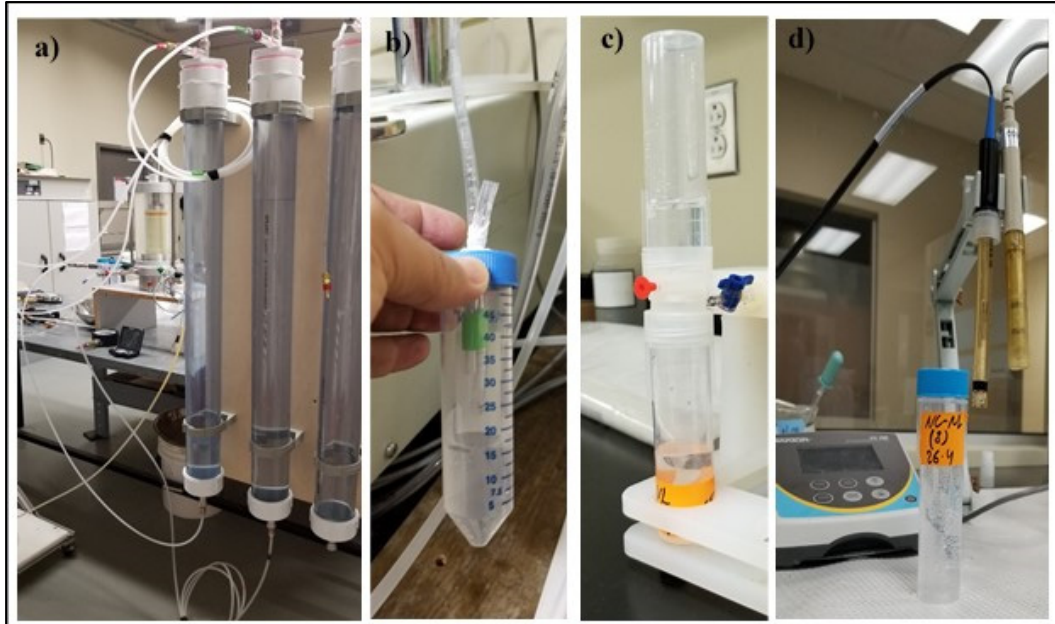


Figure 2.7 Accelerated leaching test: a) collection reservoir during the night, b) collection tube during the day, c) membrane syringe filters, and d) the initial set of leachate tests

2.3 Materials

Solidified sand samples were produced by mixing Portland cement (GU), tap water, and silica sand and fine gravel.

2.3.1 Silica Sand

Silica sand comprises over 99% silicon dioxide (SiO_2) and traces of other minerals, most commonly in the oxide form. The solidified sand samples for this testing program were prepared using silica sand from supplier Atlantic Silica Inc (Poodiac, NB, Canada). The sand

was prepared by mixing a series of products corresponding to different particle sizes (#00, #0, #1, #2, #3, and #1/4 sand, Figure 2.8). In order to obtain representative samples of these products, a mechanical splitter was used to separate the material. The silica sand mixtures were stored in plastic bags to prevent an increase in moisture content in the sand.

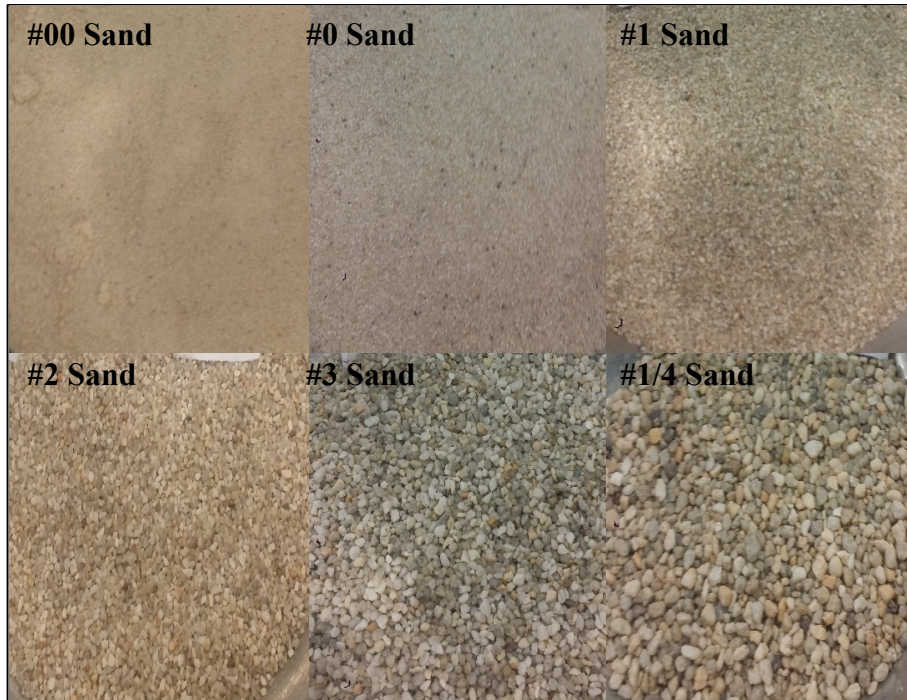


Figure 2.8 Silica sand from Atlantic Silica Inc

The sand grains have a sub-angular shape. The chemical composition of the silica sand and its particle size distribution (PSD) are given in Table 2.1 and in figure 2.9, respectively. The PSD was obtained through sieving following ASTM standard C136 (ASTM International, 2019). It presents the cumulative particle size distribution in terms of particle mass. Other size characteristics of the silica sand are given in Table 2.2. The coefficient of uniformity (C_u) and coefficient of curvature (C_c) values imply that the sand is well-graded (SW with $1 < C_c < 3$ and $C_u > 6$) based on ASTM standard D2487 (ASTM International, 2017).

Table 2.1 Chemical composition of silica sand
(Atlantic Silica Inc)

Element Compound	Weight %
SiO ₂	99.6
Al ₂ O ₃	0.2
Fe ₂ O ₃	0.06
TiO ₂	0.02
CaO	<0.01
MgO	<0.01
K ₂ O	<0.01
Na ₂ O	<0.01
LOI	<0.1
Acid Demand	<1
Specific Gravity	2.64

Table 2.2 Geometric characteristics of silica sand

D₆₀ (mm)	D₃₀ (mm)	D₁₀ (mm)	C_u	C_c	Classification
1.94	0.85	0.31	6.3	1.2	SW

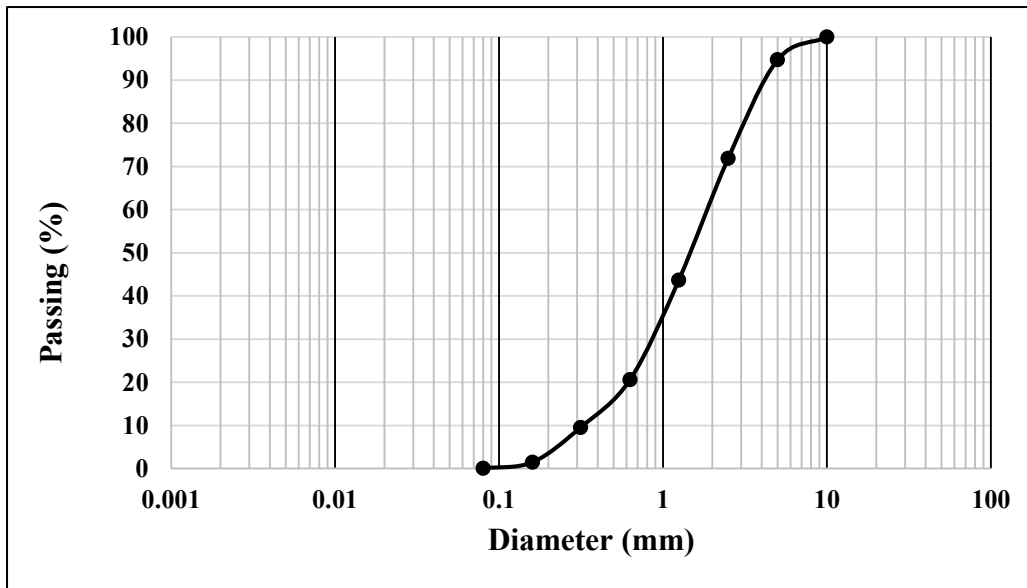


Figure 2.9 Grain size distribution of the tested silica sand

2.3.2 Cement (GU)

General use (GU) Portland cement was used as the binder. According to ASTM standard C1157 (ASTM International, 2008), the chemical composition and physical properties of Portland cement (GU) type 10 are given in Tables 2.3 and 2.4, respectively.

Table 2.3 Chemical composition of Portland cement (GU)

Chemical Composition	Weight %
SiO ₂	20
Al ₂ O ₃	4.9
Fe ₃ O ₃	2.2
CaO	63.2
MgO	1.9
Na ₂ O	0.86
Loss on ignition at 1000°C (LOI)	6.5
Total	99.56

2.3.3 Contaminant

The contaminant employed in this study was copper (II) oxide (CuO), with a concentration of 3000 mg/kg of copper oxide added to each mixture, as outlined in section 2.3.4.

Table 2.4 Physical properties of Portland cement (GU)

Physical Properties		
Setting time	Initial	130 min
	Final	235 min
Compressive strength	At three days	29.8 MPa
	At seven days	32.3 MPa
	At 28 days	41.5 MPa

2.3.4 Preparation of solidified/stabilized samples

In this study, Portland cement GU was used as a cementing material. Horpibulsuk, Katkan, Sirilerdwattana, et Rachan (2006) observed that the unconfined compressive strength increases rapidly in soil stabilized with 7 % OPC. Therefore, in this experiment, 7.5 % Portland cement was used. The physical properties of the matrix, such as pore structure, are mainly related to the water/cement ratio (W/C). Generally, by increasing the W/C ratio, the linked pores and voids are also increased. A W/C ratio of 2 was used to maximize the capillary porosity. The corresponding ratio of water to solids (W/S) is 0.13. Cylindrical solidified sand samples were produced by mixing General Use Portland cement (139.68 g), silica sand (1862.4 g), copper oxide (6.8441 g), and tap water (279.36 g). The samples were mixed based on ASTM standard C192 (ASTM International 2019). To obtain a homogeneous solidified matrix, dry cement and dry silica sand were mixed using an electric mixer for five minutes at 140 revolutions/minute. We first added tap water to the copper oxide to ensure the uniform distribution of the contaminants in the matrix. It was then gradually added to the mix in the mixer. Then, all the

components were mixed for five minutes at 140 RPM. Finally, the components were manually mixed with a trowel for a further ten minutes. Figure 2.10 shows the stages of the solidified sample preparation.



Figure 2.10 Stages of solidified sample preparation:
a) copper oxide and tap water mixed,
b) electric mixer, c) manual mixing,
d) samples in a plastic bag in a humidity room

According to ASTM C192 (ASTM 2019), the samples with a 50 mm diameter and a 100 mm length were cast in a cylindrical mould and set in three layers. Oil was spread over the internal surface of the mould to reduce friction between the sample and mould during the demolding process. To prevent bubbles in the layers, the first two layers were tamped eight times with a hammer similar to the proctor hammer, while the last layer was tamped nine times. Figure 2.11 shows the compacting tools used to prepare samples.

The top surface of each layer was scarified after compaction to obtain good adhesion for the next layer. After 24 hours, the samples were placed in the humidity room at a relative humidity of 96 %. All the samples were demolded after seven days. To reduce the reaction with atmospheric CO₂, all S/S samples were kept in a sealed plastic bag and stored in a humidity room to cure for 28 days. Following the completion of the curing process, the samples were mounted in the triaxial cell to initiate the experiments.



Figure 2.11 Compacting tools used to prepare S/S samples

2.4 Experimental Characterization Tests

2.4.1 Mechanical and hydraulic characterization

2.4.1.1 Unconfined compressive strength (UCS)

The unconfined compressive strength (UCS) was determined for all cylindrical samples. The UCS was carried out after 28 days of curing and at the end of the test protocol. The UCS was conducted according to ASTM standard C39M (ASTM International 2021). The results were compared between samples with different exposure scenarios. The maximum compressive stress was evaluated with cylindrical samples with a length of 100 mm and a diameter of 50 mm (Figure 2.13). A 1000-kN loading frame was used to apply the axial force with a loading rate of 0.5 kN/s. A sulphur-based compound was used to prepare the cylinder cap as recommended in the ASTM C617M procedure (Gerges, Issa, & Fawaz, 2015). Two caps (at the top and bottom of the sample) were used to distribute the loading during the compression test. Also, these caps were used to overcome the material's fragility and avoid any gaps between the sample and the press device.

2.4.1.2 Hydraulic conductivity test

The hydraulic conductivity test was carried out with the modified triaxial cells available at the soil mechanics laboratory of ÉTS. The tests were conducted according to ASTM standard D5084 (ASTM 2016), following method C, which applies variable upstream and downstream water levels. Figure 2.13 shows the control panel, the membrane (thickness of 0.3 mm) around the sample and a sample placed in the triaxial cell.



Figure 2.12 Uniaxial compression test on a cylindrical sample



Figure 2.13 Equipment of triaxial cell: a) control panel, b) sample placed on the base of the cell, c) the sample under the test, and d) the hydraulic conductivity panel (burettes)

The interpretation of water flow through the sample was made according to Darcy's law. The hydraulic conductivity test begins after the sample is entirely saturated. Then, the water levels in the burettes of the permeability panel were adjusted to obtain an initial hydraulic gradient equal to 20. Afterward, the valves of the triaxial cell are open, and a stopwatch is started. Water level readings are taken on the two burettes until the water level stabilizes. The hydraulic conductivity was calculated as follows:

$$K = \frac{a_{in} a_{out} L}{(a_{in} + a_{out})A(t_2 - t_1)} \ln \frac{h_2}{h_1} \quad (2.1)$$

where K is the hydraulic conductivity (m/s), a_{in} and a_{out} are the sections of the upstream and downstream burettes; A is the section of the test sample ($\pi D^2/4$, where D is the sample diameter); L is the length of the test sample; h_1 and h_2 are the head differences between upstream and downstream at time t_1 and t_2 , respectively. To facilitate the test calculation, equation (2.1) can be converted into a linear relationship between t and $\ln(h)$. The hydraulic conductivity is then determined from the slope (M) of this linear relationship.

$$K = \frac{M a_{in} a_{out} L}{(a_{in} + a_{out})A} \quad (2.2)$$

It is important to note that a sample hydraulic conductivity depends on its pore characteristics (e.g., shape, connected/not connected, orientation, and pore volume).

2.4.2 Chemical analysis of pore solution

The concentrations of copper, calcium, aluminium, and silicon in the leachate samples were obtained using inductively coupled plasma-optical emission spectrometry (Agilent 5100 ICP-OES). Each sample was acidified at pH 2 with concentrated nitric acid. After that, the sample was injected into the plasma as a fine aerosol by a pneumatic device (nebulizer). The

concentrations of major and trace elements in leachate samples were obtained following the ISO 11885 standard (ISO, 2007). In order to obtain good results, the ICP was calibrated using standard solutions. Calibration was verified by running check standards and blanks at the beginning and the end of each analysis session, as well as after every ten samples in an analysis run.

The pH, temperature, and electrical conductivity (EC) of the leachate water were measured right after it came into contact with the solid matrix (U.S. EPA, 2019). A tabletop pH meter (Oakton, 510 series) was used for these measurements.

2.4.3 Techniques for carbonation detection

2.4.3.1 Colour Indicator (Phenolphthalein)

The colour indicator allows visualizing the transition zone between carbonated and non-carbonated areas. Several colour indicators exist, such as cresol red, thymolphthalein, and Nile blue. However, the most commonly used colour indicator is Phenolphthalein spray. This indicator makes it possible to visually identify the presence of carbon dioxide in the cement-soil mixture (Poursaee, 2016). At high pH (above 9), the phenolphthalein becomes an intense purple colour; at a low pH (below 9), phenolphthalein is colourless (Morandea et al., 2014). Figure 2.14 presents an example of phenolphthalein on concrete with and without carbonation. The phenolphthalein test is a qualitative indicator of the presence of carbonation below the pH of 9, but it does not provide a quantitative measure of carbonation depth inside the sample.

2.4.3.2 Thermogravimetric analysis (TGA)

Thermogravimetric analysis (TGA) is a technique used to measure the kinetics of decompositions of solids and is carried out using thermobalance. The TGA continuously records the mass variations of a sample subjected to ramped temperature, going from 30 °C (maximum ambient temperature) to 1150 °C. Thus, we quantify species that lose water vapour

for different temperature ranges (C-S-H, CH) and calcium carbonates that decarbonate and lose their CO₂ gaseous for higher temperatures.

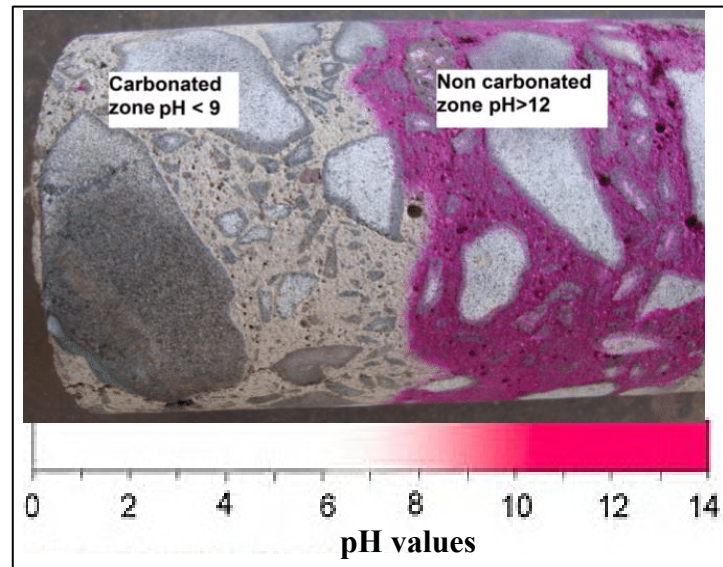


Figure 2.14 Example of phenolphthalein on concrete

In the present study, a PerkinElmer SII TGA device was used to determine the degree of CO₂ penetration. The instrument has an accuracy of $\pm 2^\circ\text{C}$ for measuring the temperature and $< 5 \mu\text{g}$ for measuring weight. The dried sample was ground by a ring roll mill to carry out this test and distributed into four homogeneous powder samples. The TGA was started by placing the empty platinum crucible in the device and resetting the mass of the crucible to zero. Then, approximately 5 g of powder from each sample were taken and placed in the platinum crucible. The initial mass (M_i) was recorded. Next, the powder sample was subjected to an inert gas (argon) at 100.0 mL/min and held for 2 minutes at 50 °C. The temperature was increased at a rate of 10 °C/min over a temperature range of 50 °C to 1000 °C. In the last 10 minutes, the sample was subjected to air at 1000 °C. During the operation, the resulting mass loss was recorded continuously as a function of temperature.

The easiest way to identify the decomposition of minerals is to derive and smooth the TGA curve from the original data to obtain the DTG curve. The DTG curve shows peaks

corresponding to the decomposition of specific phases. The percent masses of CO₂ and CaCO₃ were determined based on equations 2.3 and 2.4, respectively (Barnard et al., 2005). In other words, the percent masses of CO₂ and CaCO₃ were assessed based on the degradation temperature ranging from relatively low (450 °C) to high (900 °C).

$$\% \text{ MassCO}_2 = \left(\frac{M_{450} - M_{900}}{M_i} \right) \times 100 \quad (2.3)$$

$$\% \text{ MassCaCO}_3 = \% \text{ Mass CO}_2 \times \left(\frac{100}{44} \right) \quad (2.4)$$

where M_i = initial mass; M_{450} = mass loss at 450 °C; and M_{900} = mass loss at 900 °C. According to Barnard et al. (2005), this test method is very accurate. The proportion of CaCO₃ determined from TGA corresponds to between 94-96% of the real CaCO₃ concentration. Generally, several transformations occur in the temperature range between 100°C and 1000°C (Ma, Pan, Cai, Zhang, & Han, 2021). Table 2.5 shows the decomposition of cementitious materials obtained from thermogravimetry curves.

Table 2.5 Decomposition of hydration products
Taken from Collier (2016, p. 340)

Phase	Temperature
Decomposition of CSH	100 - 450°C
Decomposition of Ca(OH) ₂	450 - 520°C
Decomposition of CaCO ₃	600 - 800°C

2.4.4 Observation by X-ray CT

Computed tomography (CT) was used for the observation of S/S samples. In this experiment, XT H225 X-ray μ CT system (Nikon, MI, USA) was used to characterize the porosity, as presented in Figure 2.15. Categorization of the fractures and internal pores is based on 2D/3D images and statistical data collected from the sample. These images allow the internal pore

structure of the scanned sample to be viewed. The primary procedures for fracture detection in image processing are shown in Figure 2.16.

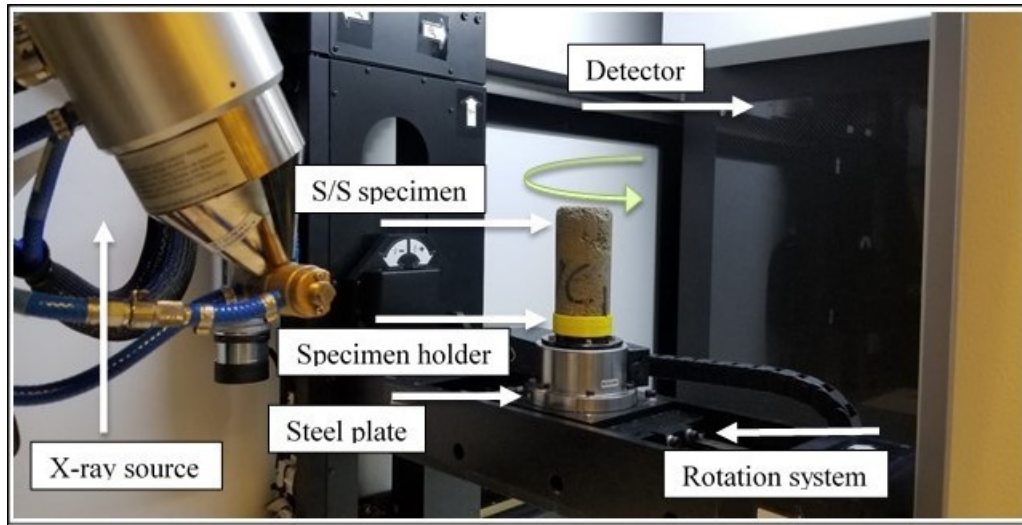


Figure 2.15 S/S sample placed on CT system at École de technologie supérieure

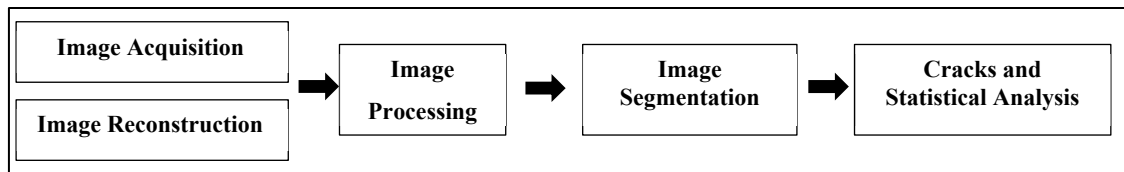


Figure 2.16 Stages of image observation and pores detection

2.4.4.1 Image configuration and acquisition

The first stage requires the acquisition of X-ray images. The samples were scanned using a transmission scan (micro-focus source with 3 μm focal spot size) configured with a beam energy of 190 kV voltage and beam current of 85 μA with a digital detector. The sample location inside the micro-CT machine allowed a minimum voxel size of 65 μm . For each experiment, the field of view of the scan is obtained with detector pixel ($X=1677$, $Y=2000$) and projections (2634).

To reduce beam hardening, a copper filter with a thickness of 0.25 mm was placed over the X-ray source. The filter thickness was chosen based on the attenuation needed to allow full X-ray penetration. The exposure time was set to 2 ms. There are essential rules to follow during the acquisition stage. For example, the object should be fully in the field of view (image window) during 360° rotation. In some cases, there is an issue related to the center of rotation when the sample is not on the center axis, and it is impossible to get a clear image. This error can be compensated by using the reconstruction algorithm to extract a clear image with manual or automatic calculations. Filtration, and calibration are used to overcome some artifacts that occur during scanning (e.g., beam hardening, image noise, and ring artifacts). If beam hardening arises, the CT Pro (Nikon, MI, USA) algorithm can correct it automatically or manually.

The second stage requires image reconstruction (volume reconstruction). Volume reconstruction was done using the CT Pro 3D software and the raw X-ray images. The fundamental principle behind image reconstruction is transforming the 2D X-ray images acquired by a computed tomography (CT) scanner into a 3D image. The CT Pro 3D software uses algorithms to align the images (2D slices) and combine them on top of each other to generate a 3D model of the object scanned. Once the 3D images have been acquired, the operator can rotate the object (3D model) and examine the interior structure of the object from different angles.

2.4.4.2 Image processing

The third stage requires image processing. In this step, Dragonfly software, version 4.1 (Object Research Systems, Montreal, Canada) was used to process the image (Głowacki, Bouin, Ethier, Dubé, & Duhaime, 2018). Additionally, the 2D reconstructed images were enhanced using the Dragonfly software to show the contrast between voids and solids. The CLAHE filter (Contrast Limited Adaptive Histogram Equalization) was used in this study to adjust the contrast in images before image segmentation was undertaken, as shown in Figure 2.17 (B). Certain filters have a tendency to overamplify noise in very homogenous regions, but the CLAHE filter avoids this issue by limiting amplification. It should be emphasized that the Dragonfly tool

simply improves the visual appearance of the image and does not modify the original data in any way.

After image processing, the segmentation procedure is the first step applied to the reconstructed images to define the voids network and distribution of pores. The segmentation is a crucial step because it depends on the clarity of images and the skill and accuracy of the experimenter. The fundamental principle behind image segmentation using the Dragonfly software is to show the contrast between dark objects, i.e., voids, and grey objects, i.e., solids. However, the contrast between the objects is relatively poor, so post-processing (image filters) is essential to estimate the contrast and isolate between the objects (pores and solids). The segmentation process was based on the grey-level histogram, where the operator can select an adequate threshold value to isolate between two objects, such as dark and grey. This step can change the results by increasing or decreasing the estimated void space percentage. For example, if the contrast value between light and dark areas of the image is not well adjusted, it will cause a misestimation of the void percentage. We used two different thresholds in the grey value diagram to overcome this issue: low and high levels (Otsu, 1979; Talab et al., 2016). Furthermore, the threshold values were chosen specifically for each scanned sample. The total voids were calculated based on image segmentation. The last step was based on the grey-level histogram. In order to identify the percentage of voids and their relevant statistics, the main sequence is depicted in Figure 2.17. It involves the following steps:

1. In order to obtain the optimum threshold, image filters offered by Dragonfly software were used to improve image quality and enhance the contrast between the objects (pores and solids), as shown in Figures 2.17 (A and B).
2. Threshold grey values were selected from the histogram to distinguish the pores and the solid phases. The threshold value was chosen by analyzing visually the segmented regions and by judging if the segmentation is appropriate. As the threshold choice is slightly subjective, two threshold values were used (maximum and minimum thresholds) to get an appreciation of the method accuracy.

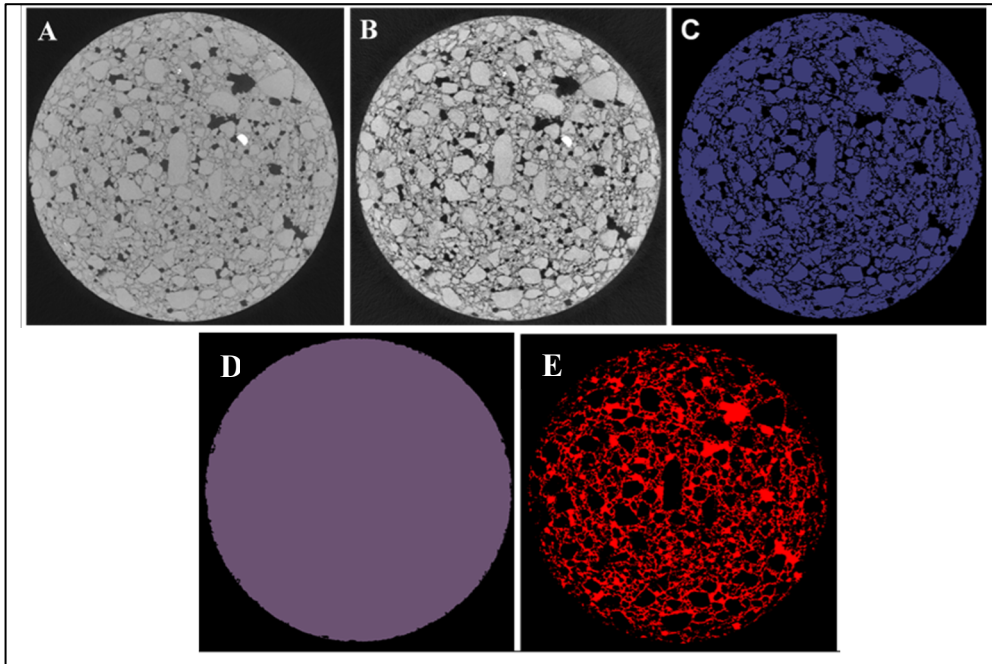


Figure 2.17 2D images processing and segmentation: A) original image;
 B) image filtering; C) Material with pores;
 D) pores filled; E) pores obtained

3. The defined threshold was used to create a new image (representing material with pores), as shown in Figure 2.17 C.
4. A copy of the same image was made and then used with Dragonfly's fill built-in function to close all the pores, as shown in Figure 2.17 D.
5. At this point, step 3 displays an image with material and pores, while step 4 displays a similar image but without the pores.
6. To obtain the pores, a logical subtraction operation was applied between the two images (steps 3-4), as shown in Figure 2.17 F.

7. Finally, several relevant statistical calculations (e.g., the aspect ratio, pore size, and pore percentage) were rendered with Dragonfly software.

CHAPTER 3

EXPERIMENTAL RESULTS

The objective of this chapter is to present the experimental results for the five scenarios that were introduced in the previous chapter. Each scenario included hydraulic conductivity and compressive strength measurements. Flow-through leaching tests were utilized to evaluate the leaching of copper and other elements. The electrical conductivity and the pH of the leachate were also measured. The effects of carbonation and loading on porosity was also evaluated using an X-ray CT scan.

3.1 Hydraulic conductivity

Figure 3.1 presents the hydraulic conductivity values for the five scenarios of the intermittent injection protocol. With this protocol, water was injected into the sample for 4.2 hours every day for the permeability and leaching tests. The initial hydraulic conductivity for all scenarios varied between 2.1×10^{-7} m/s and 7.8×10^{-7} m/s. Each loading stage (scenarios L, C/L and L/C) was followed by an increase in hydraulic conductivity varying between 156 and 519 %. Carbonation stages (scenarios C, C/L and L/C) were followed by a decrease in hydraulic conductivity varying between 19 and 67 %. A slow decrease in hydraulic conductivity was observed after the loading and carbonation stages varying between 9 and 19 % with respect to the first permeability test after the carbonation and loading stages. The slow decrease in hydraulic conductivity was more significant for the scenarios involving both loading and carbonation stages (35 and 62 % for scenarios L/C and C/L, respectively).

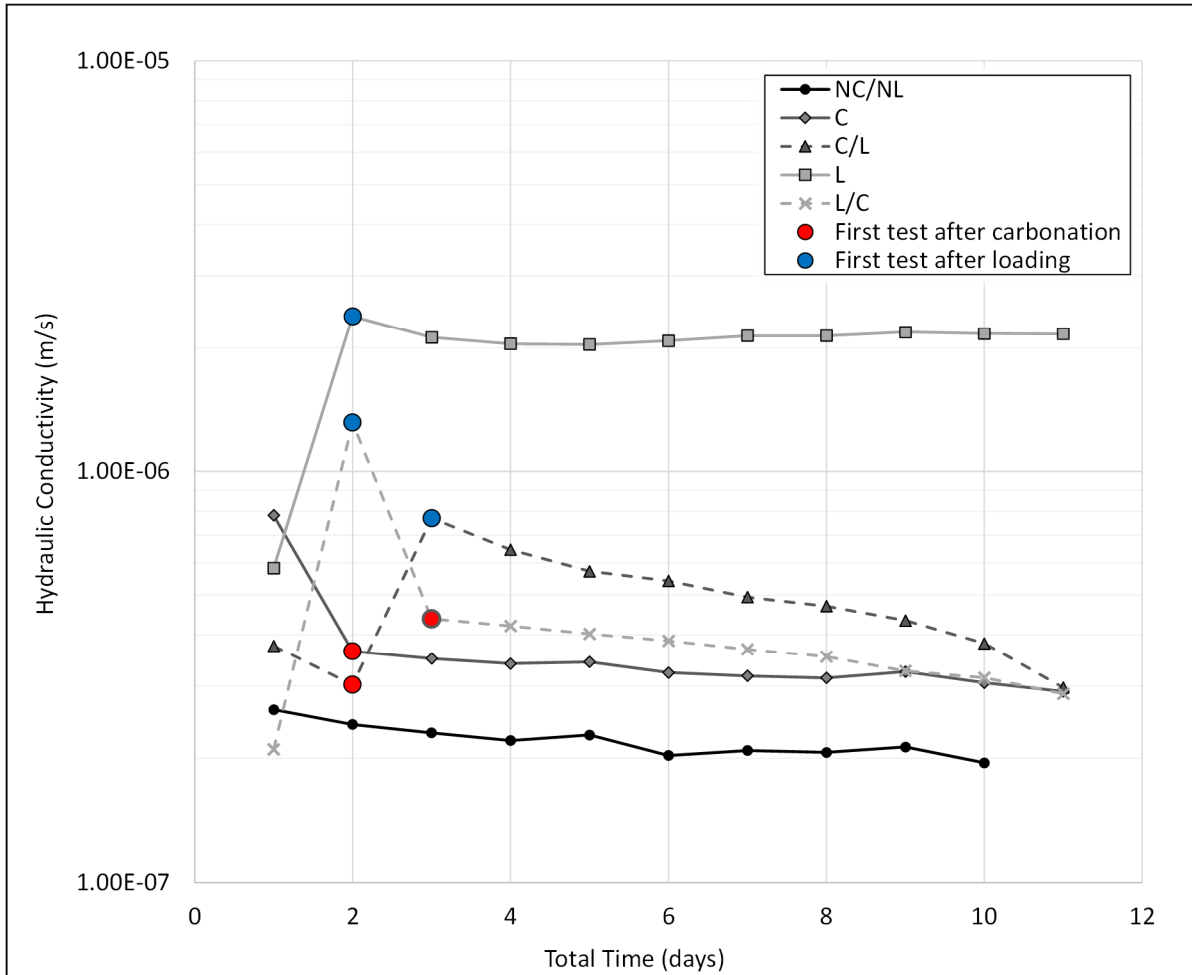


Figure 3.1 Hydraulic conductivity for the intermittent water injection protocol

Figure 3.2 shows the hydraulic conductivity values for the continuous water injection protocol. With this protocol, the deaerated and deionized water was injected continuously into the cylindrical sample for three days. The initial value of hydraulic conductivity varied between 7.3×10^{-8} m/s and 9.6×10^{-8} m/s. These hydraulic conductivity values are lower than the values that were obtained for the intermittent injection protocol. The hydraulic conductivity changes that were observed following the loading and carbonation stages were of the same order of magnitude as for the intermittent water injection protocol.

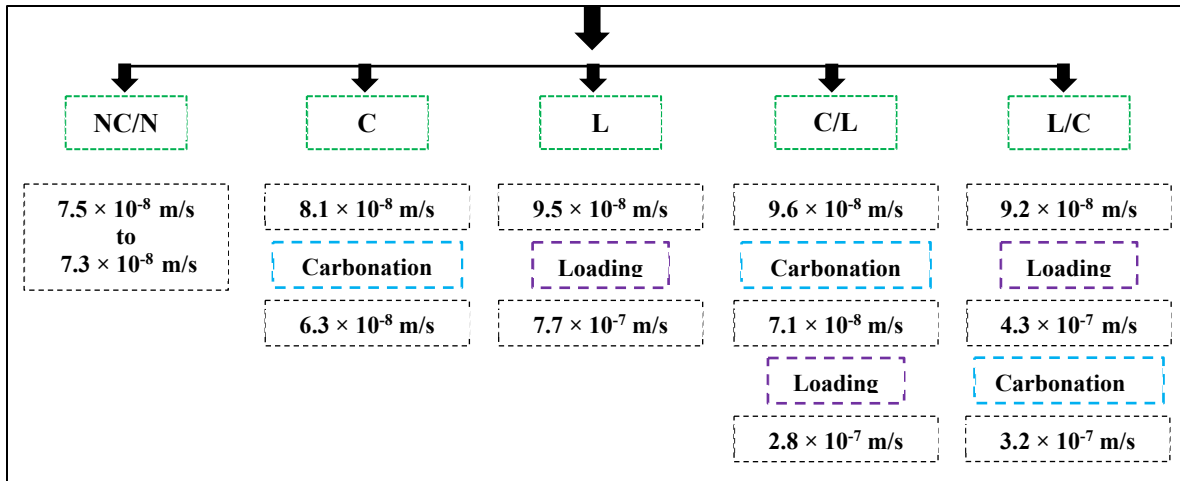


Figure 3.2 Hydraulic conductivity values for the continuous water injection protocol

3.2 Compressive strength

The unconfined compressive strength (UCS) of the S/S samples was evaluated at two different time points for each scenario. The first test was performed after 28 days of curing, before the sample was installed in the triaxial cell. The second test was conducted at the end of the experimental period on separate samples.

Table 3.1 shows the USC for the five scenarios concerning the effects of leaching, carbonation and loading. The initial compressive strength was calculated as the average of the five samples that were tested after 28 days (one for each test scenario). A reduction in compressive strength between 21 and 56 % was observed after each scenario. The decrease was more pronounced for the two scenarios combining loading and carbonation stages (C/L and L/C).

Tableau 3.1 Results of unconfined compressive strength test

Test Scenario	Compressive Strength (UCS) (MPa)		% Reduction in UCS
	Initial	Final	
No Carbonation /No Loading (NC/NL)	2.77	2.20	20.6
Carbonation Only (C)		1.98	28.5
Loading Only (L)		1.78	35.7
Carbonation/ Loading (C/L)		1.23	55.6
Loading/Carbonation (L/C)		1.45	47.7

3.3 Evaluation of chemical properties

This section presents the results for the flow-through leaching test of the S/S matrices. For the five test scenarios, approximately 188 samples of leachate were collected. Results are presented for pH, electrical conductivity, copper, aluminium, and silicon.

3.3.1 pH

The pH was determined every day for 10 days with the intermittent water injection protocol. As expected for a cementitious material, the initial pH was high. For the five scenarios, the initial pH ranged between 13.1 and 13.7. Each carbonation stage was followed by a sharp drop in pH (scenarios C, C/L, and L/C). The pH after carbonation varied between 6.4 and 6.7. This range is of the same order as the pH of the deionized water that was used as a leachant (pH between 6 and 7). In contrast, the pH was relatively stable for the control sample and the scenario involving only loading (scenarios NC/NL and L), with values between 12.2 and 13.7.

With the continuous water injection protocol, the initial pH ranged between 13.1 and 13.4. As expected, the scenarios involving carbonation (C, C/L, and L/C) resulted in a decrease in pH. The pH after carbonation ranged between 6.0 and 6.9. During the control and loading stages, the pH was relatively stable for scenarios NC/NL and L, with values between 13.0 and 13.2

units. This is expected because the control and loading stages do not involve chemical reactions that would impact the pH of the solution.

3.3.2 Electrical conductivity

The electrical conductivity (EC) values of the leachate are given in Figures 3.2 and 3.3. The initial EC values recorded at the beginning of the leaching test fall between 10.9 and 11.3 mS/cm. Figure 3.2 shows that during the first day of the leaching test, the EC gradually decreased below 10 mS/cm. This pattern was also observed in scenarios C, C/L, and L/C, as shown in Figures 3.3 and 3.4.

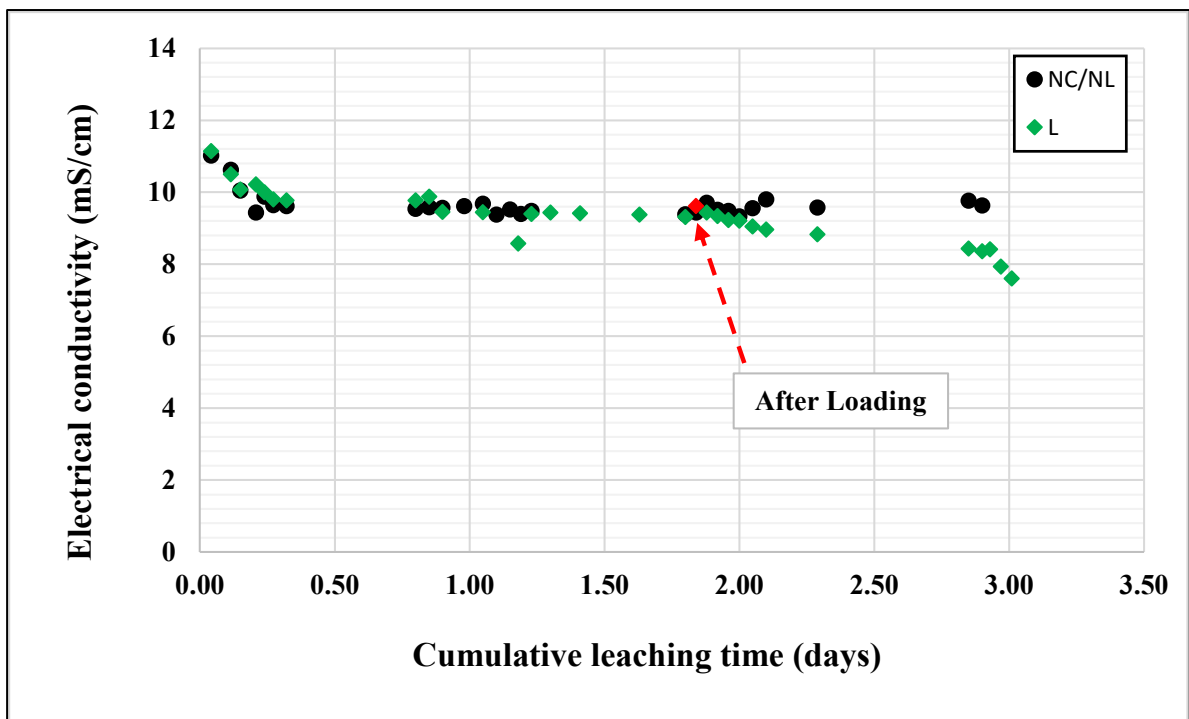


Figure 3.2 Variation of electrical conductivity values (scenarios NC/NL and L)

As water flowed through the sample, the EC values for the NC/NL scenario were relatively stable between 9.4 and 9.7 mS/cm. The L scenario led to a slightly more pronounced decrease in EC at 7.6 mS/cm.

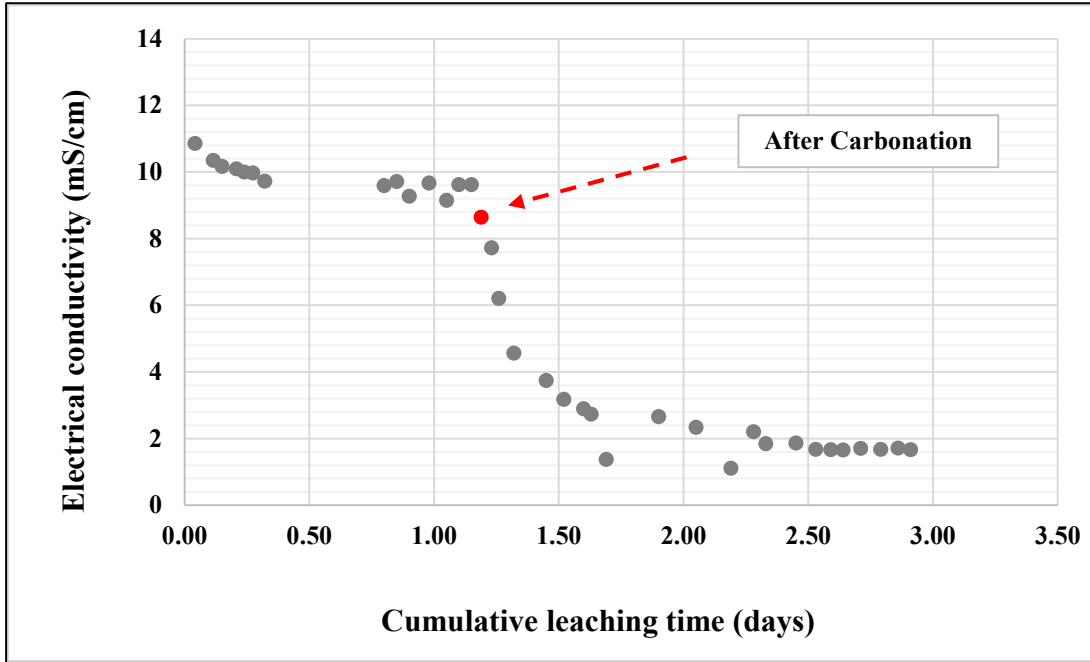


Figure 3.3 Variation of electrical conductivity values (scenarios C)

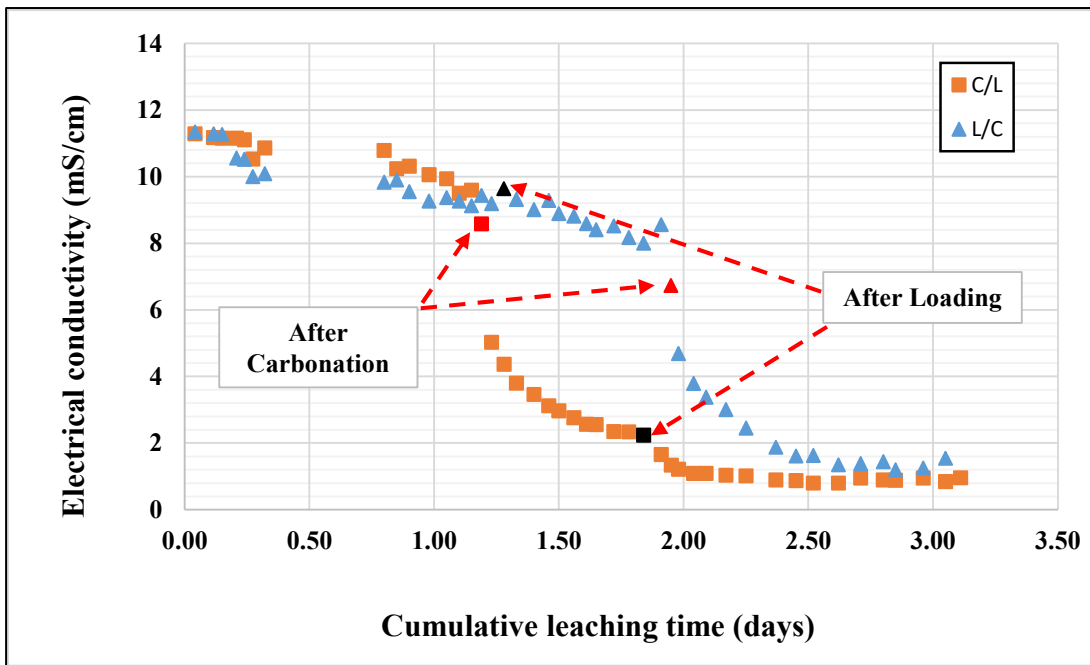


Figure 3.4 Variation of electrical conductivity values (scenarios C/L, and L/C)

The carbonation stages were all followed by a significant decline in EC as shown in Figures 3.3 and 3.4. For example, EC was reduced by 89.7 %, 92.5 %, and 89.5 % for scenarios C, C/L, and L/C, respectively.

3.3.3 Aluminium leaching

Figure 3.5 shows the variation of aluminum (Al) concentration as a function of cumulative leaching time. A high release of aluminium was recorded for all scenarios at the beginning of the leaching test. The initial Al concentrations varied between 2.8 and 3.5 mg/L. After a few hours, the Al concentrations decreased by approximately 60 % for each scenario. Figure 3.5 illustrates that the release of aluminum from the control sample (scenario NC/NL) remained relatively stable, ranging between 1.07 mg/L and 0.7 mg/L after the first few hours of leaching.

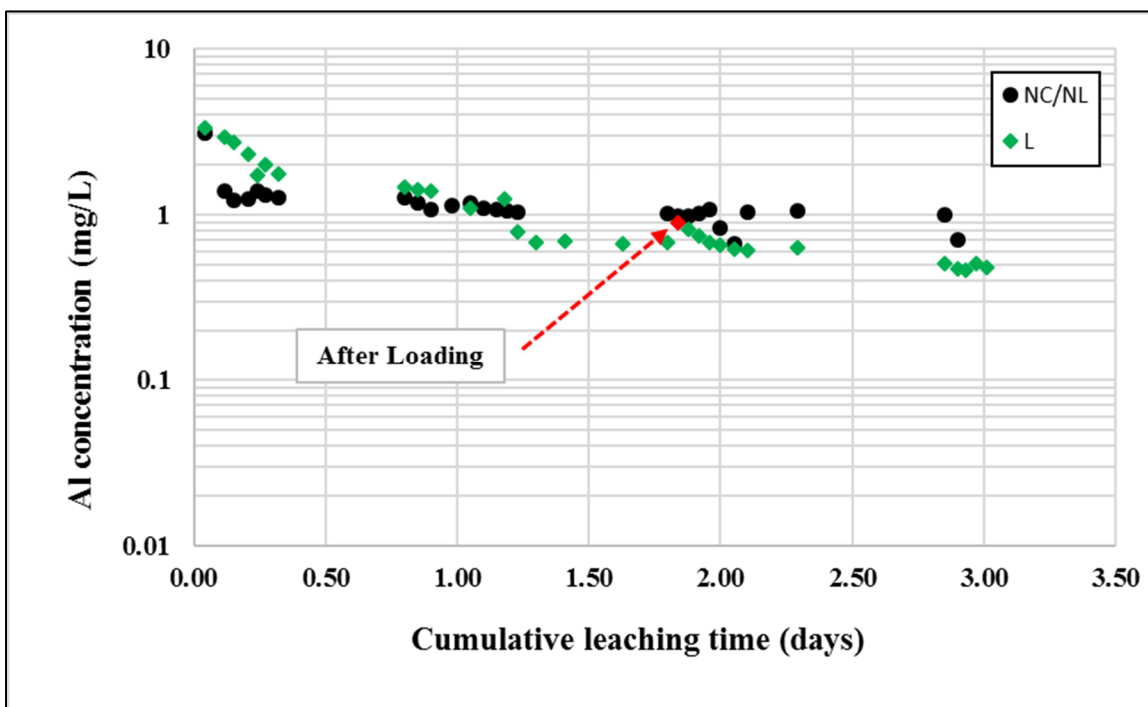


Figure 3.5 Variation of Al values (scenarios NC/NL and L)

As shown in Figures 3.6 and 3.7, there was a immediate reduction in the release of aluminum after carbonation for scenarios C and C/L. The Al concentration for scenarios C and C/L,

decreased by 69 % and 47 %, respectively. This decrease occurred immediately after the carbonation stage. After the immediate decrease, the Al concentration remained approximately constant for scenarios C and C/L. For scenario L/C, the loading stage that preceded the carbonation stage produced a more significant decrease in Al. Carbonation was not followed by a significant decrease in Al.

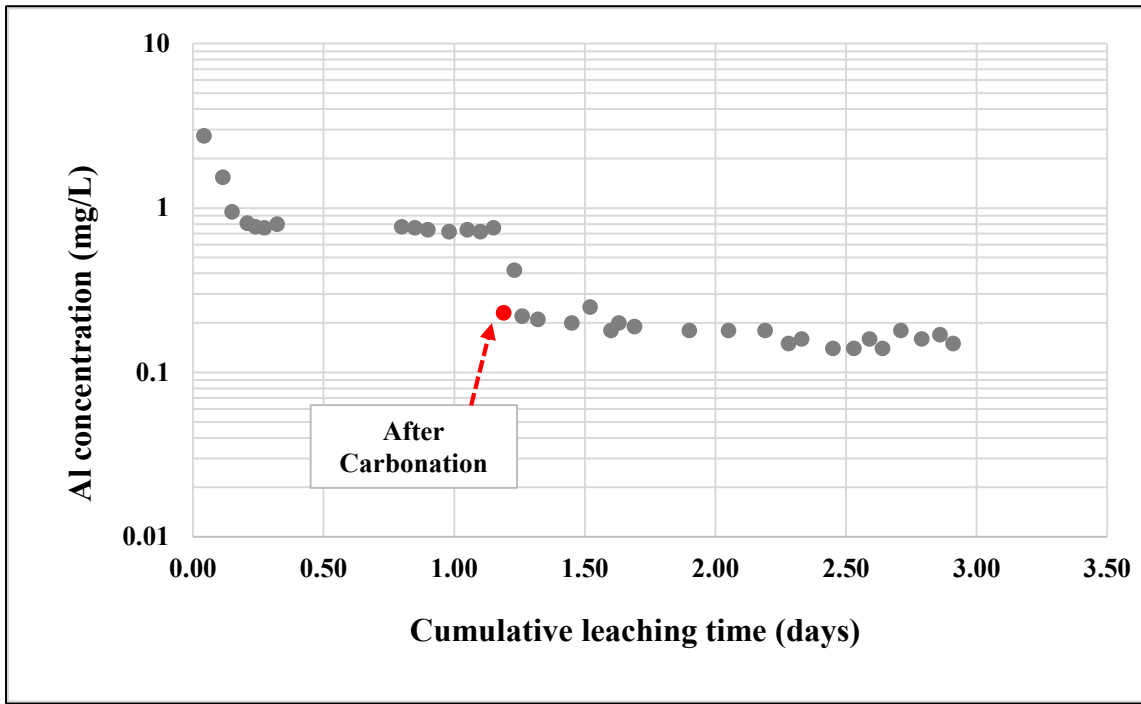


Figure 3.6 Variation of Al values (scenario C)

The influence of loading on Al concentration is less clear. The loading stage for the L scenario was associated with a rapid increase in Al and a slower decrease (Figure 3.5). The loading stages for scenarios C/L and L/C were respectively followed by gradual decrease and increase in Al, respectively (Figures 3.7).

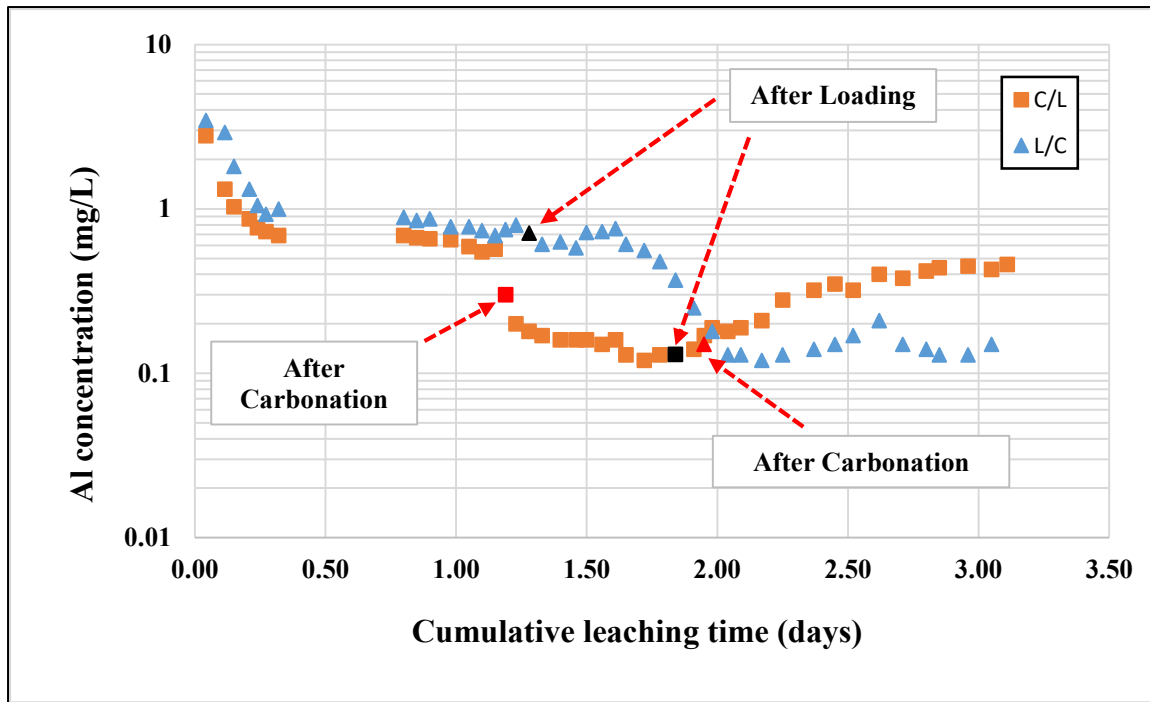


Figure 3.7 Variation of Al values (scenarios C/L and L/C)

3.3.4 Silicon leaching

Figures 3.8 and 3.9 present the Si concentration in the leachate for the five test scenarios. The initial Si concentrations for all scenarios ranged from 0.76 to 1 mg/L.

The NC/NL and L scenarios resulted in a gradual reduction in Si concentration. The NC/NL scenario led to a 34.8% decrease in Si concentration from the initial testing phase to the final leachate sample. Similarly, the L scenario yielded a 39% decrease in Si concentration prior to the mechanical loading and at the end of the leaching test.

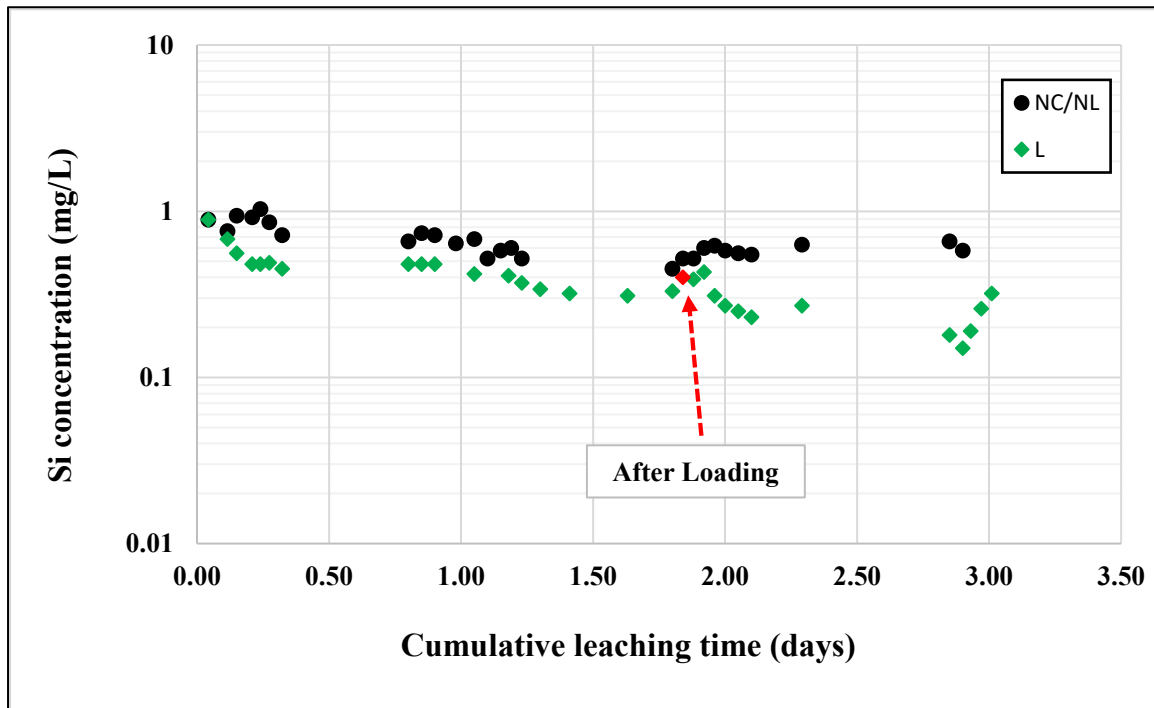


Figure 3.8 Variation of Si concentrations (scenarios NC/NL and L)

Figure 3.9 illustrates that the carbonation for scenarios C, C/L, and L/C was associated with a sudden increase in Si. In scenarios C, C/L, and L/C, the Si concentration increased from 0.63 to 23.6 mg/L, from 0.45 to 38.2 mg/L, and from 0.37 to 25.8 mg/L, respectively. In contrast, during the loading stage, there is a tendency for a decrease in the release of silicon, with levels dropping from 21.77 mg/L to 0.13 mg/L for scenario C/L and from 0.87 mg/L to 0.37 mg/L for scenarios L/C, between the beginning and the end of the loading stages. The variation in silicon concentrations exhibited oscillations after the loading stage in scenario L/C. The Si concentration decline was more pronounced but delayed when carbonation preceded loading in scenario C/L. This delay may be attributed to the extended effect of carbonation, which occurs over a longer period. In particular, the effect of carbonation persisted throughout the carbonation period and approximately half of the loading period in the C/L scenario, where carbonation occurred prior to loading.

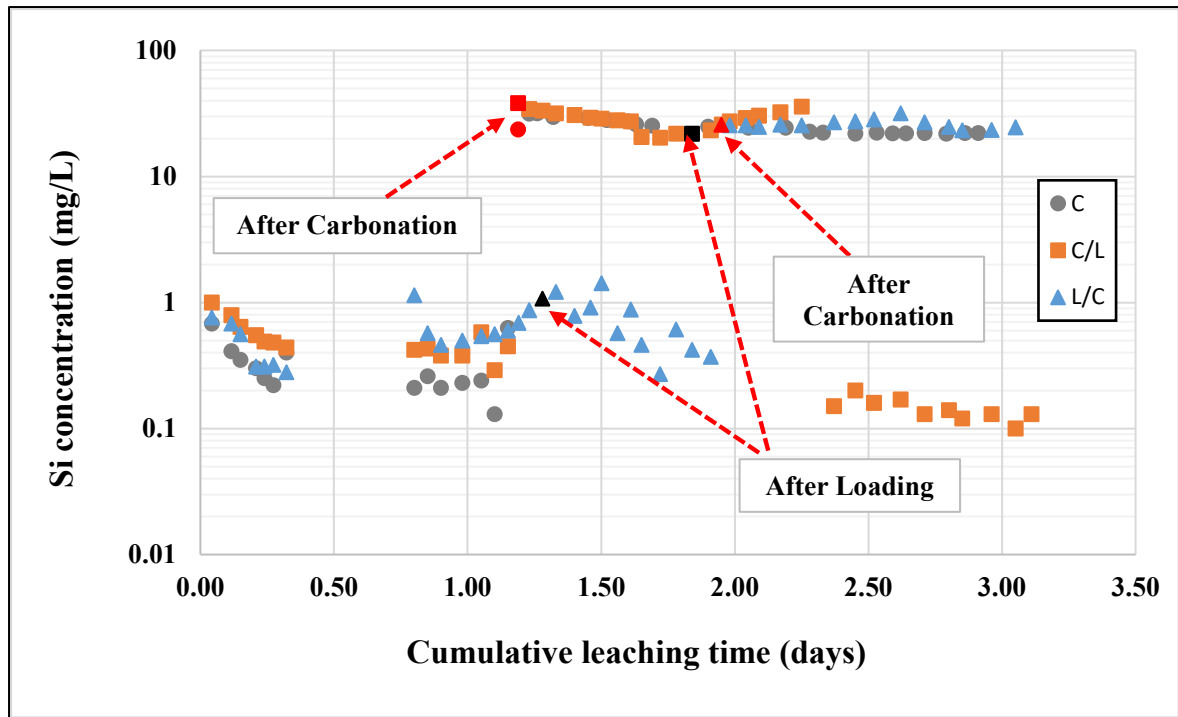


Figure 3.9 Variation of Si concentrations (scenarios C, C/L, and L/C)

3.3.5 Calcium leaching

The concentration of Ca in the leachate during the NC/NL, C, and L scenarios is illustrated in Figure 3.10. The initial Ca concentration released during these scenarios varied between 734 mg/L and 781 mg/L. As water flowed through the sample, the release of Ca remained fairly constant prior to carbonation or loading for all scenarios, with concentrations ranging from 700 to 843 mg/L. In Figure 3.10, it can be observed that the carbonation stage caused a peak release of Ca, which reached 1303 mg/L. Following the carbonation stage, there was a gradual reduction in the release of Ca, and by the end of the experiment, it had decreased to 75% of its peak value. The loading stage for scenario L did not cause a significant reduction in the release of Ca compared to the NC/NL scenario.

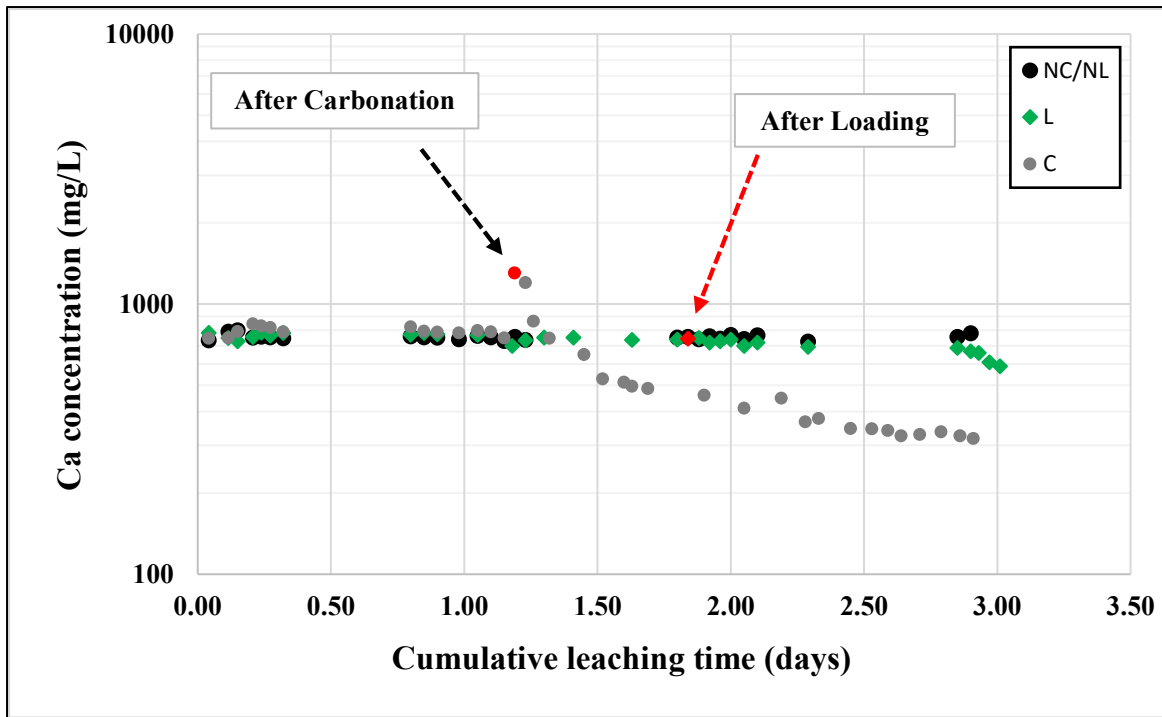


Figure 3.10 Variation of Ca concentrations (scenarios NC/NL, C and L)

Figure 3.11 presents the release of Ca for scenarios C/L and L/C. The release of Ca was initially similar in both scenarios, with initial concentrations of 741 mg/L and 737 mg/L, respectively. Carbonation resulted in a 108% increase in Ca release for the C/L scenario and an 82% increase for the L/C scenario. Figure 3.11 indicates that the release of Ca gradually decreased after this increase. In combined loading and carbonation stages (C/L and L/C), the release of Ca can be influenced by the order in which the stages occur. Specifically, in the C/L scenario where the carbonation stage precedes the loading stage, loading has a more severe impact on Ca release. Conversely, in the L/C scenario where the loading stage precedes the carbonation stage, the influence of loading on Ca release is less severe. Furthermore, as deionized water was continuously injected into the sample, it carried out calcium at decreasing concentrations. At the end of the experiment, the calcium release in the leachate was recorded at 154 mg/L and 294 mg/L for C/L and L/C scenarios, respectively.

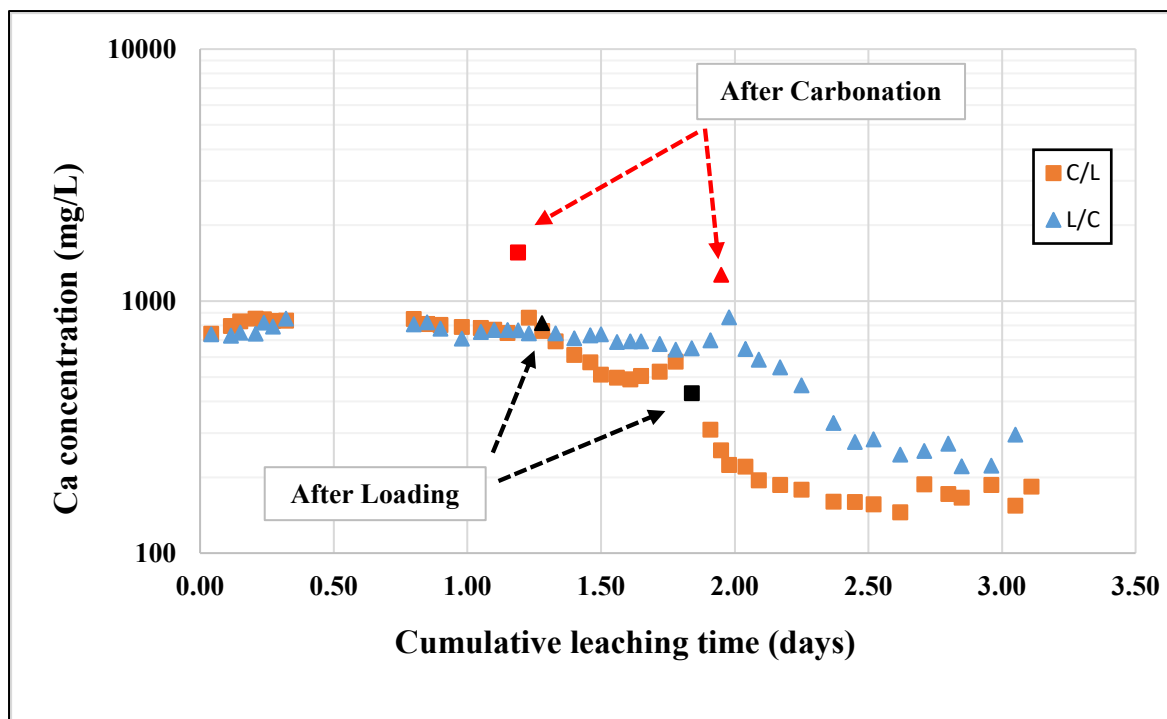


Figure 3.11 Variation of Ca concentrations (scenarios C/L and L/C)

3.3.6 Leaching behaviour of Copper (Cu)

In Figure 3.12, the leaching of copper is presented as a function of cumulative leaching time for the NC/NL and L scenarios. Following the injection of water for one hour, the initial release of Cu peaked at 0.54 and 0.74 mg/L for the NC/NL and L scenarios, respectively. In the NC/NL scenario, as water continued to be injected into the solidified sample, the concentration of Cu gradually decreased to 0.04 mg/L by the end of the test.

The release of Cu before and after carbonation is shown in Figure 3.13. Initially, the concentration of copper decreased from 0.53 mg/L to 0.06 mg/L. Then, immediately after the carbonation, the release of Cu increased rapidly and peaked at 1.14 mg/L. As the water continued to be injected into the solidified sample, the release of Cu gradually decreased to 0.3 mg/L.

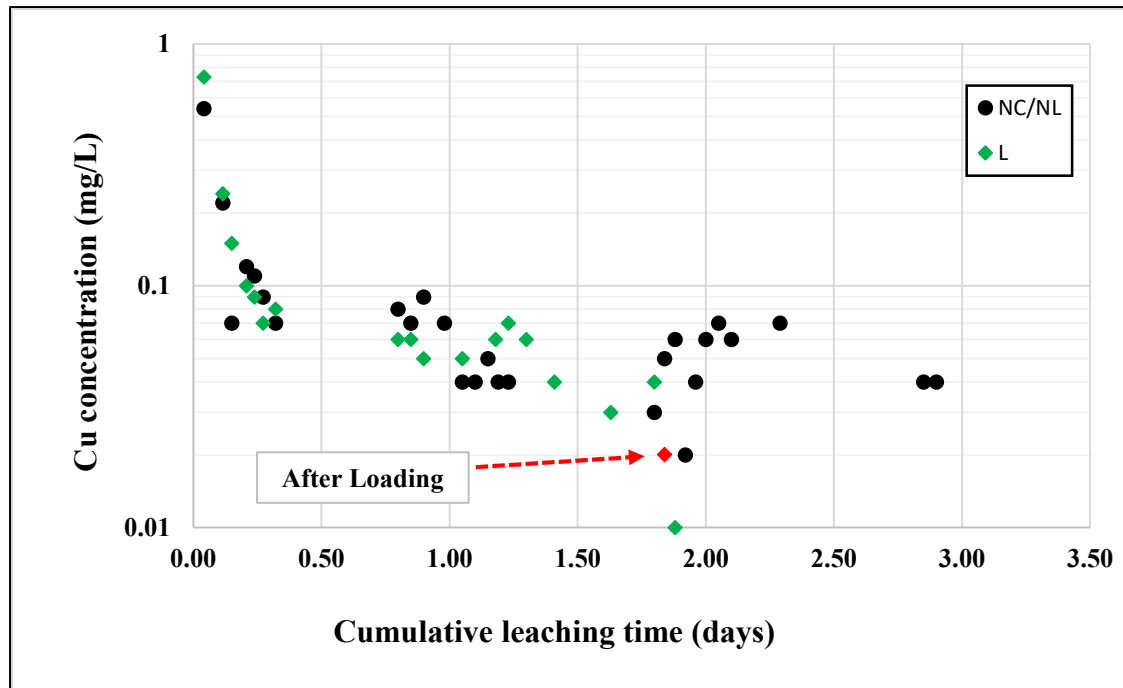


Figure 3.12 Variation of copper as a function of cumulative time for NC/NL and L scenarios

Figure 3.14 shows the influence of carbonation on the Cu concentration for the combined loading and carbonation scenarios. The initial Cu concentrations in the leachate were 0.68 mg/L and 0.46 mg/L for scenarios C/L and L/C, respectively. As water was injected into the solidified sample, the release of copper from the sample gradually decreased over time. For scenarios C/L and L/C, carbonation is always followed by a marked increase in Cu followed by a gradual decrease, as it was the case in Figure 3.13 for scenario C. All carbonation stages led to a peak Cu concentration above 1 mg/L.

For scenarios L, C/L, and L/C, loading is always followed by a gradual decrease in the Cu concentration. The three loading stages led to a Cu concentration of 0.02 mg/L or less after this gradual decrease. For scenario C/L, the decrease in Cu was preceded by an increase of Cu concentration to 0.41 mg/L.

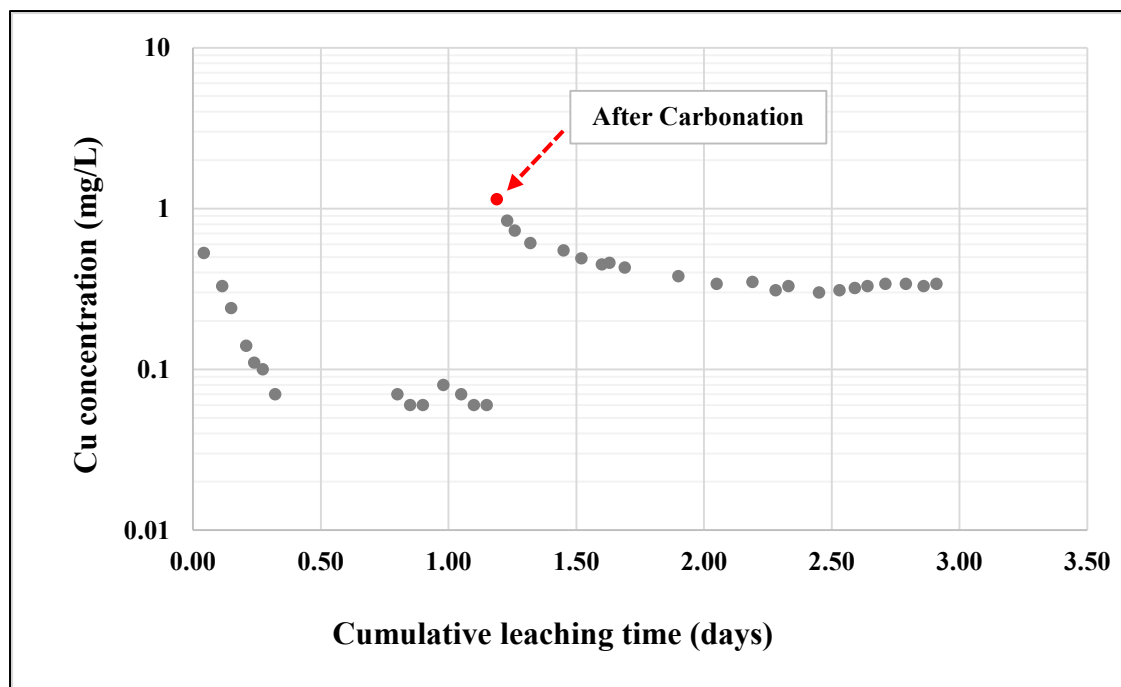


Figure 3.13 Variation of copper as a function of cumulative time for C scenario

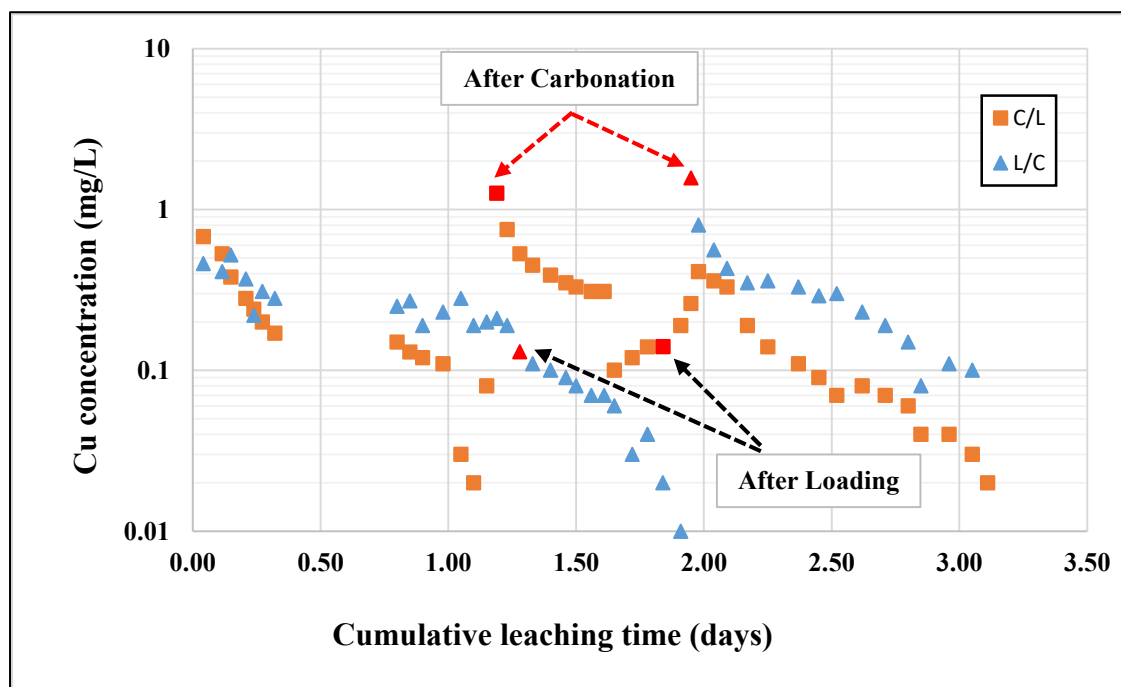


Figure 3.14 Variation of copper as a function of cumulative time for C/L and L/C scenarios

3.4 Carbonation detection

The extent of carbonation was determined using a phenolphthalein solution and TGA analysis before and after the leaching test.

3.4.1 Phenolphthalein test

Phenolphthalein is colourless for a pH below 8.2 and deep pink for a pH above 9.9. The deep pink colour is observed for the parts of the samples that have not been carbonated. The phenolphthalein solution is colourless when applied on surfaces that have been carbonated. The phenolphthalein solution was applied immediately after the leaching test to avoid surface carbonation.

The samples for the NC/NL and L scenarios did not show significant carbonation at the end of the leaching tests. For the NC/NL and L scenarios, the samples were split into two parts after the leaching test. The phenolphthalein solution was sprayed on one part. Figures 3.15 and 3.16 show that the sprayed surfaces were deep pink as a result of the limited extent of carbonation (pH exceeds 9.9). It is important to note that these two test scenarios only involved natural carbonation and did not include accelerated carbonation. For the scenarios with carbonation, (C, C/L, and L/C), after the experiment, the cylindrical sample was split into three discs with a thickness of 3 cm (Figure 3.17).



Figure 3.15 S/S sample stained with the phenolphthalein solution (NC/NL scenario)



Figure 3.16 S/S sample stained with the phenolphthalein solution (L scenario)

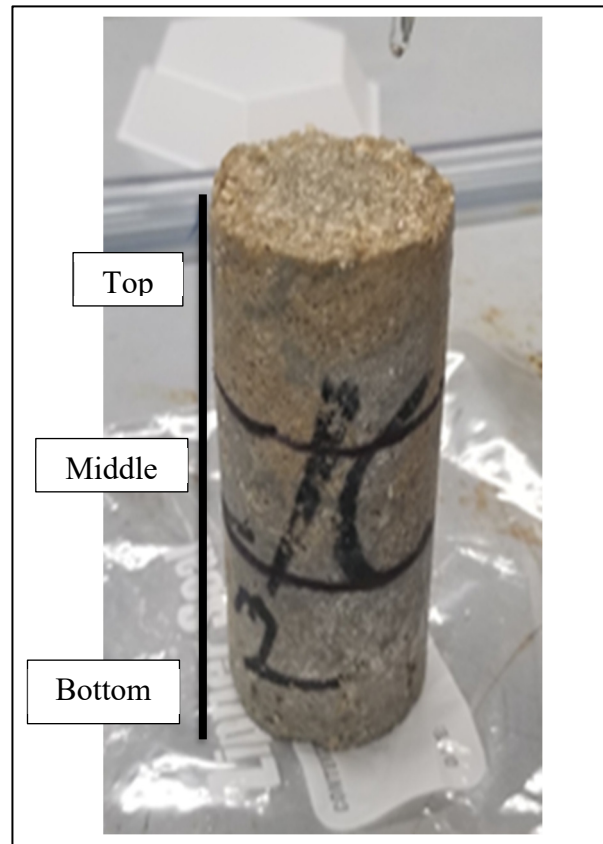


Figure 3.17 Sample before being cut into three discs, each with a thickness of 3 cm

At the end of the experiments, carbonation was assessed by spraying phenolphthalein on the surface of each disc, namely, the top cylinder, the middle cylinder, and the bottom cylinder. Colour changes were observed with the naked eye. The results of the phenolphthalein tests for scenarios C, C/L, and L/C are presented in Figures 3.18, 3.19, and 3.20, respectively. These figures show two different characteristic zones of Phenolphthalein from top to bottom, as follows:

- The carbonated zone refers to the top part of the sample, which is colorless.

- The mixed zone, where the middle and bottom parts of the sample appear light pink, indicates partial carbonation.

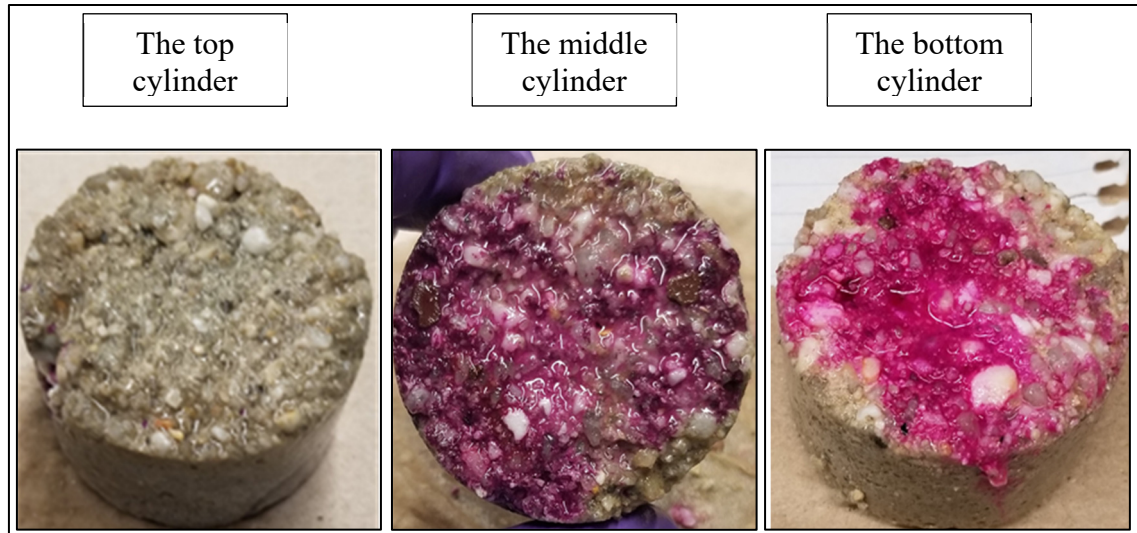


Figure 3.18 Solidified sample stained with the phenolphthalein solution (C scenario)

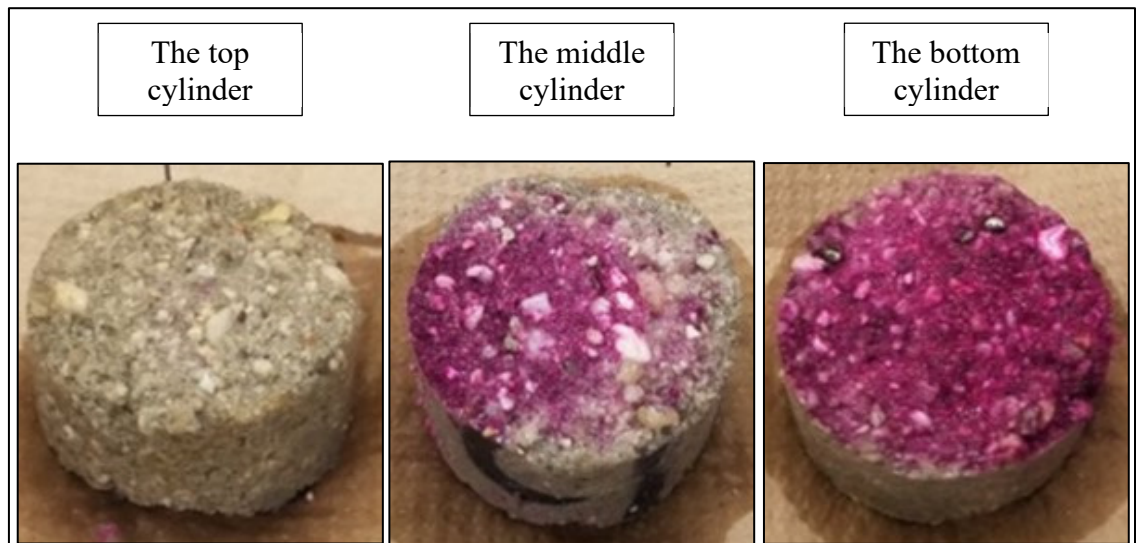


Figure 3.19 Solidified sample stained with the phenolphthalein solution (C/L scenario)

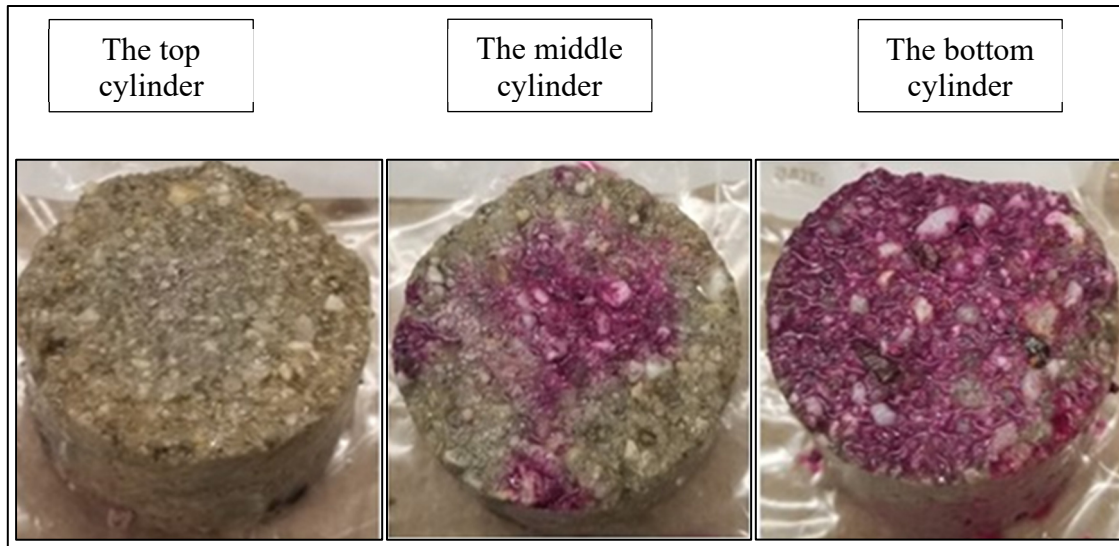


Figure 3.20 Solidified sample stained with the phenolphthalein solution (L/C scenario)

In general, the colourless area that was revealed by Phenolphthalein represents the fully carbonated zone. Furthermore, it is noteworthy that complete carbonation is not observed in the middle portion of the sample.

3.4.2 Thermogravimetric analysis (TGA)

Figure 3.21 presents the initial results of the DTG curve, showing three main peaks of mass loss due to mineral decomposition before the leaching test.

The decomposition peaks for all scenarios were similar. For example, in scenarios NC/NL, C, C/L, and L/C, the first peak was observed between 30°C and 200°C, except for the loading scenario where it occurred later and ranged from 60°C to 200°C. The second peak was recorded between 400 °C and 500 °C for all scenarios, except for the NC/NL scenario which ranged from 400 °C to 460 °C. The third prominent peak occurred between 500°C and 700°C, as shown in the DTG diagram in Figure 3.21. The diagram revealed that the third peak typically begins with a large shoulder and ends in a steep incline.

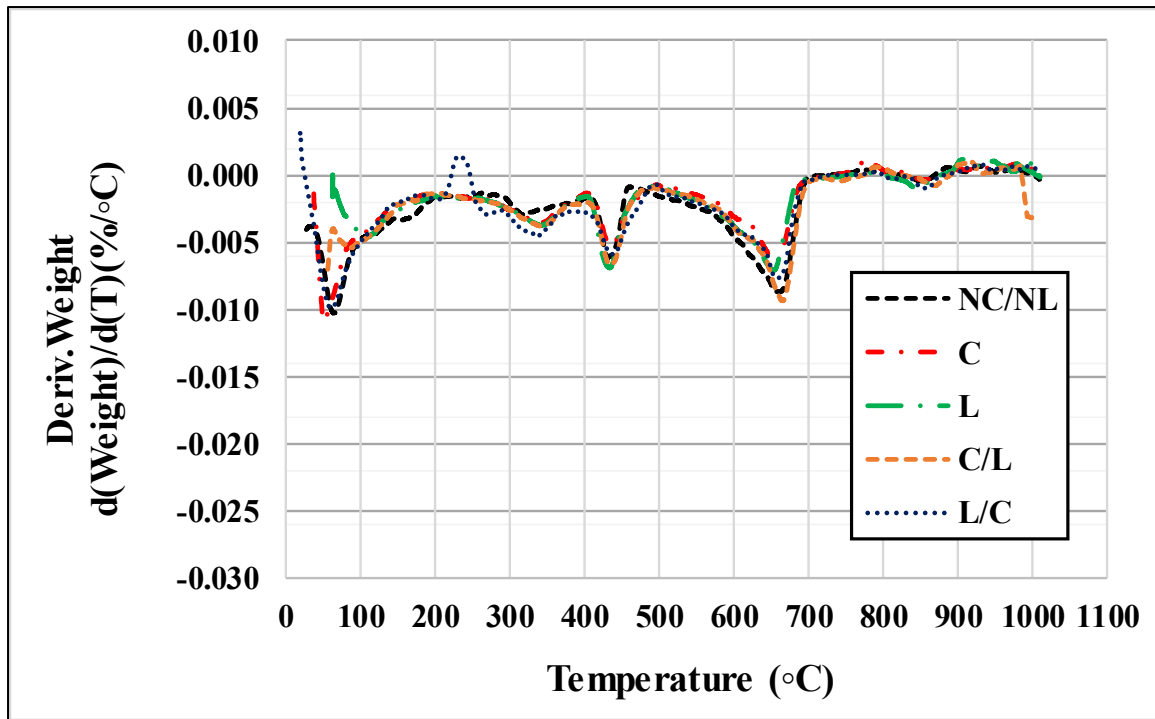


Figure 3.21 DTG curves of all scenarios before any tests (initial stage)

After conducting a series of leaching, loading, and carbonation tests, another thermogravimetric analysis was performed. In the NC/NL scenario, the DTG curve exhibited slight deviations in the decomposition peaks compared to those observed before testing. Particularly, the third peak showed a notable change in its shape, beginning with a prominent shoulder prior to testing and a less prominent one after the testing, as illustrated in Figure 3.22.

Furthermore, the loading scenario manifested comparable numbers of peaks, i.e., three major peaks, to those observed prior to the leaching test, albeit with different values, as evidenced in Figure 3.23. Specifically, the first peak was detected within the temperature range of 60°C to 200°C before the leaching test, while it manifested at a lower temperature range of 26°C to 200°C after the leaching test. Additionally, the third peak was observed in the temperature range of 500°C to 690°C before the leaching test, which shifted to a higher temperature range of 590°C to 700°C after the leaching test.

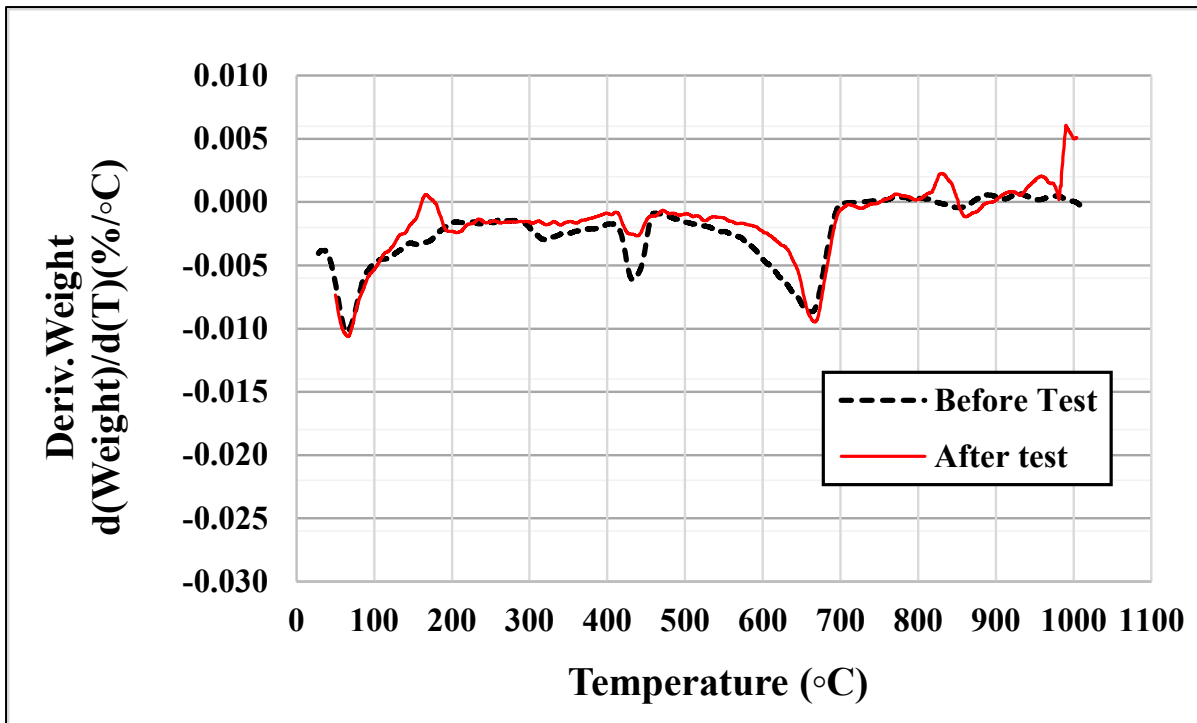


Figure 3.22 DTG curves of the NC/NL before and after the leaching test

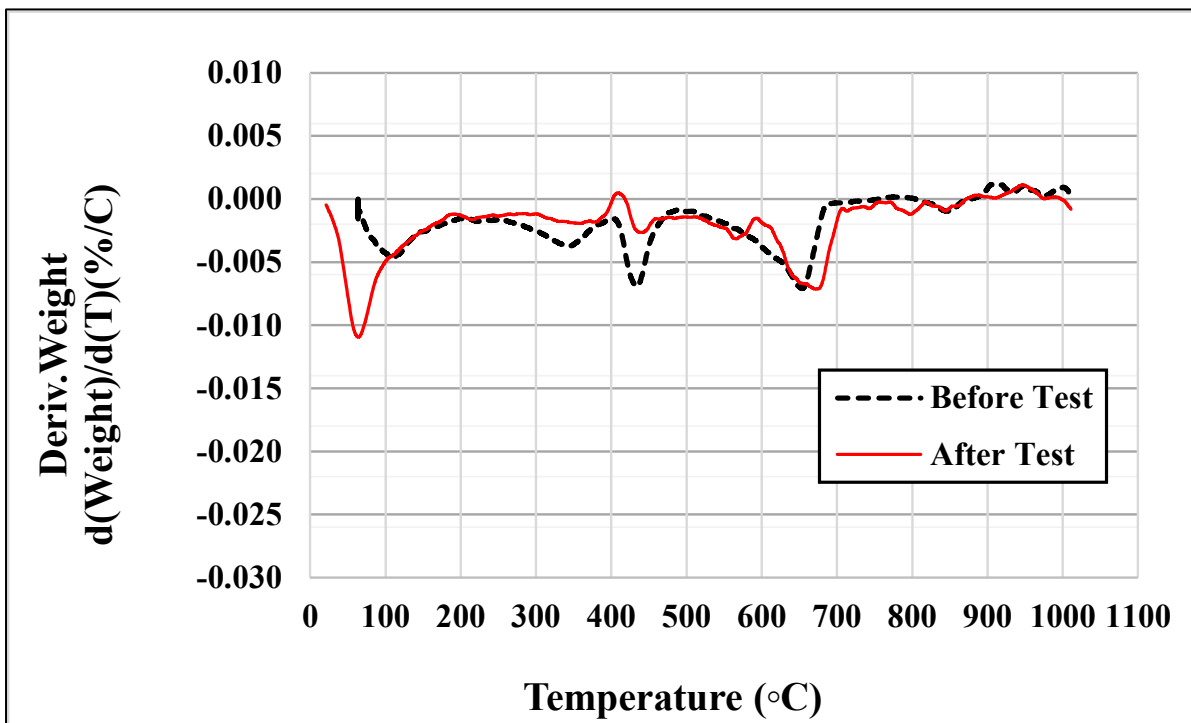


Figure 3.23 DTG curves for the loading (L) scenario before and after the leaching test

The results of the DTG curve following the leaching/carbonation test are presented in Figure 3.24. During the carbonation stages (scenarios C, C/L, and L/C), there was a reduction in the number of decomposition peaks observed. Furthermore, the decomposition peaks for all scenarios after carbonation exhibited a similar pattern. As illustrated in Figure 3.24, the DTG curve showed a single, prominent peak of mass loss occurring over a temperature range of 580°C to 740°C. This peak in mass loss is attributed to the decomposition of calcite (as CO₂ is released during the decarbonization of calcite).

The degree of carbonation was measured based on equations 2-3 and 2-4 (Barnard et al., 2005), as presented in section 2.4.3.2. The percent values of CO₂ and CaCO₃ before the leaching test were calculated as the average values of all test scenarios.

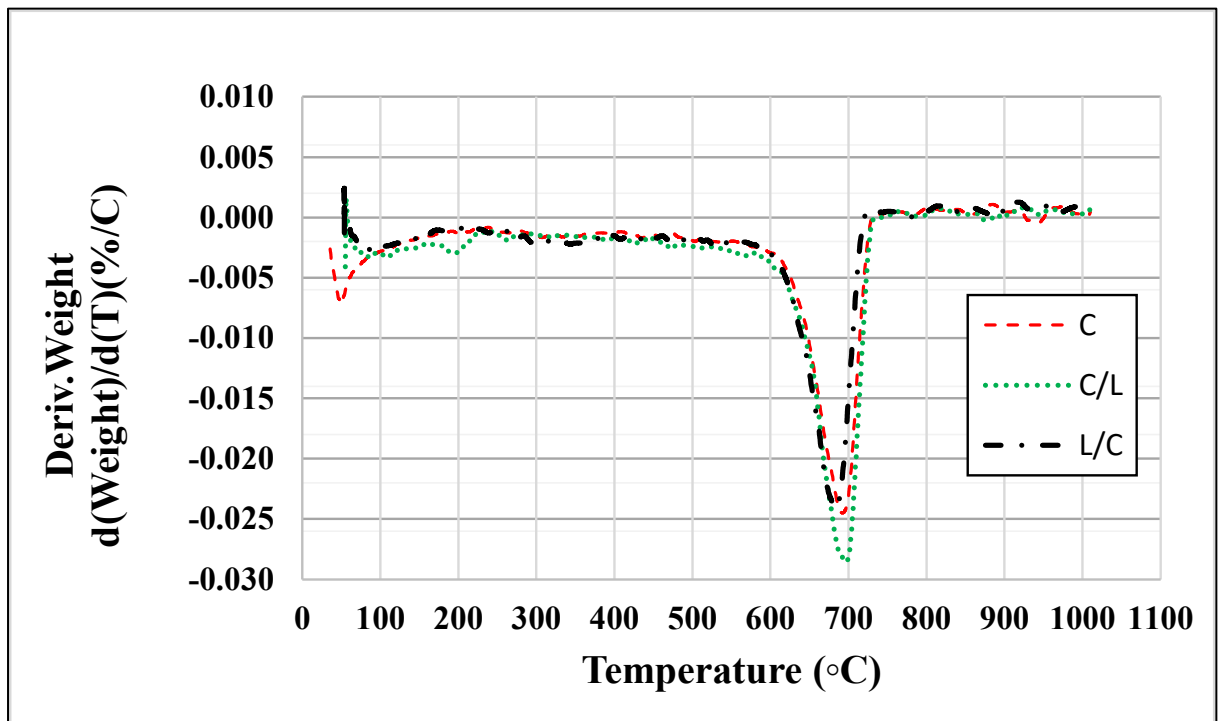


Figure 3.24 DTG curves for C, C/L, and L/C scenarios after the leaching test

The results for CO₂ and CaCO₃ before and after the leaching test for scenarios NC/NL and L are presented in Table 3.1. The results are similar, with slight changes observed following the leaching test. For instance, a decrease of 6.3 % and 9.2 % was recorded for the percentage of carbon dioxide and calcium carbonate, respectively, after the leaching test. In the loading scenario, on the other hand, an increase of 20.6 % and 13.8 % was observed for the percentage of CO₂ and CaCO₃, respectively.

Table 3.1 Percentage of CO₂ and CaCO₃ before and after leaching test (NC/NL and L scenarios)

Test scenarios	Carbon dioxide (CO ₂)		Calcium carbonate (CaCO ₃)	
	Before	After	Before	After
NC/NL	0.63 %	0.59 %	1.52 %	1.39 %
L		0.76 %		1.73 %

During the carbonation stages (scenarios C, C/L, and L/C), measurements of the percentages of CO₂ % and CaCO₃ % were done using two distinct procedures. The first procedure involved measuring each disc (top, middle, and bottom) individually. In other words, each disc was ground separately, and 25 g of powder was taken from each and placed in a platinum crucible for measuring. The second procedure involved taking 8 g of powder from each disc and mixing them together to represent the entire cylindrical sample. Table 3.2 displays the percentages of CO₂ and CaCO₃ for the three parts.

Table 3.2 reveals that the percentages of both CO₂ and CaCO₃ decrease as they pass through the top, middle, and bottom of the entire sample. The lowest percentages of CO₂ and CaCO₃ were observed in the middle and bottom sections of the sample. In scenarios C, C/L, and L/C, the percentages of CO₂ decreased by 0.77 %, 21 %, and 42 %, respectively. Additionally, the percentages of CaCO₃ decreased by 0.34 %, 19 %, and 40 % for scenarios C, C/L, and L/C, respectively, in comparison to the initial percentage.

Table 3.2 Percentage of CO₂ and CaCO₃ after leaching test (first procedure)

Test scenarios	Carbon dioxide (CO ₂)			Calcium carbonate (CaCO ₃)		
	Top disc	Middle disc	Bottom disc	Top disc	Middle disc	Bottom disc
C	1.3 %	1.1 %	1.3 %	2.9 %	2.5 %	2.9 %
C/L	1.4 %	1.3 %	1.1 %	3.1 %	2.9 %	2.5 %
L/C	1.4 %	1.4 %	0.8 %	3.1 %	3.1 %	1.9 %

Table 3.3 presents the results of the second procedure (the entire sample) for scenarios C, C/L, and L/C. The percentages of CO₂ and CaCO₃ increased following accelerated carbonation. Furthermore, it appears that the loading stage, specifically scenarios C/L and L/C, has a notable influence on enhancing the carbonation effects when compared to the C scenario, which involves solely carbonation. The L/C scenario, for example, creates micro-cracks during loading that facilitate carbonation penetration. Similarly, in the C/L scenario, loading might induce an increase in the rates of chemical reactions between the dissolved carbonic acid and uncarbonated materials, thus enhancing the carbonation effect.

Table 3.3 Percentage of CO₂ and CaCO₃ before and after leaching test (C, C/L and L/C scenarios)

Test scenarios	Carbon dioxide (CO ₂)		Calcium carbonate (CaCO ₃)	
	Before	After	Before	After
C	0.6 %	1.4 %	1.5 %	3.1 %
C/L		1.9 %		4.4 %
L/C		1.5 %		3.4 %

Moreover, Table 3.3 illustrates that the percentage of carbonation significantly increased by 133 %, 216.6 %, and 150 % for scenarios C, C/L, and L/C, respectively. Correspondingly, the

percentages of CaCO_3 augmented by 106.6 %, 193 %, and 126.6 % for scenarios C, C/L, and L/C, respectively.

3.5 Evolution of the microstructure observed in X-ray tomography

In order to comprehend the impact of the FTL test on the entire solidified matrix, a comparison was made between changes in matrix microstructure and findings from laboratory experiments, encompassing chemical and mechanical characteristics. The porous system in all samples investigated in this study consists of capillary pores (Narayanan & Ramamurthy, 2000), which are categorized as macropores (Paria & Yuet, 2006; Zdravkov, Čermák, Šefara, & Janků, 2007).

It should be noted that during the preliminary stages of experimental methodology selection, such as determining the water-to-cement ratio, carbonation and loading techniques, and CT scan parameters, the matrix porosity varied depending on the exposure scenarios. For instance, following successive cycles of carbonation and loading, higher porosity was observed after loading, whereas reduced porosity was recorded after carbonation (Al Tabbaa & Stegemann, 2011; Morandeau et al., 2015). Figure 3.25 illustrates that after multiple successive cycles of loading and carbonation, interconnected open pores (highlighted in red) were formed, extending to the external surface and causing fractures at the top of the sample.

Table 3.4 presents the percentage of total pores (i.e., pores or cracks) before and after the leaching test for all scenarios of the continuous injection protocol. Among the different scenarios, the NC/NL scenario exhibited a slight increase in porosity of 3% after the leaching test.

Table 3.4 Percentage of total pores before and after the leaching tests

Test scenarios	Porosity range (%)		Average porosity (%)	
	Before	After	Before	After
NC/NL	19.7 - 26.1	20.2 - 27.0	22.9	23.6
L	23.2 - 27.8	28.4 - 32.8	25.5	30.6
C	23.9 - 26.9	19.2 - 23.5	25.4	21.4
C/L	19.9 - 24.9	21.7 - 25.7	22.4	23.7
L/C	21.2 - 25.3	22.9 - 26.8	23.2	24.9

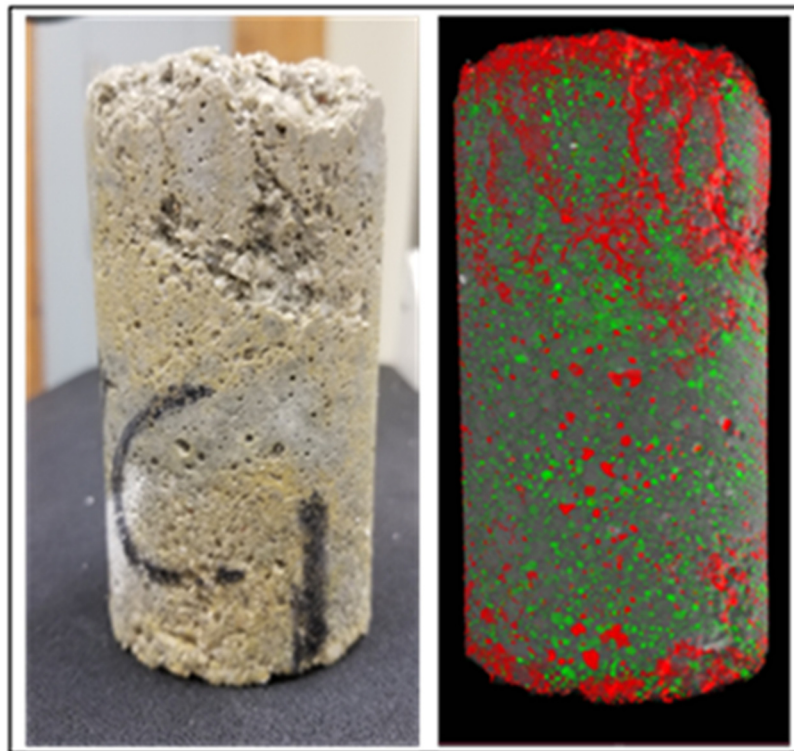


Figure 3.25 Pores and cracks on the S/S matrix after multiple cycles of loading and carbonation

It is worth noting that loading seems to increase porosity, with scenario L showing the highest average porosity after the leaching test in these experiments. In contrast, the carbonation phase led to a reduction in pores, with scenario C having the lowest average porosity after the leaching test, showing a decrease in porosity to a value of 21.4 %. When considering the

combined effects of loading and carbonation in scenarios C/L and L/C, a slight increase in porosity was observed, with values of 23.7 % and 24.9 %, respectively. Overall, the data in Table 3.4 highlights the complex interplay between the different scenarios that influence the porosity of the tested samples.

Figure 3.26 presents the changes in pore size distribution for the NC/NL scenario. After the leaching test, slight changes in pore size were observed. Specifically, the volume proportion of small pores below 270 μm increased, while the volume proportion of large pores between 318 μm and 914 μm decreased.

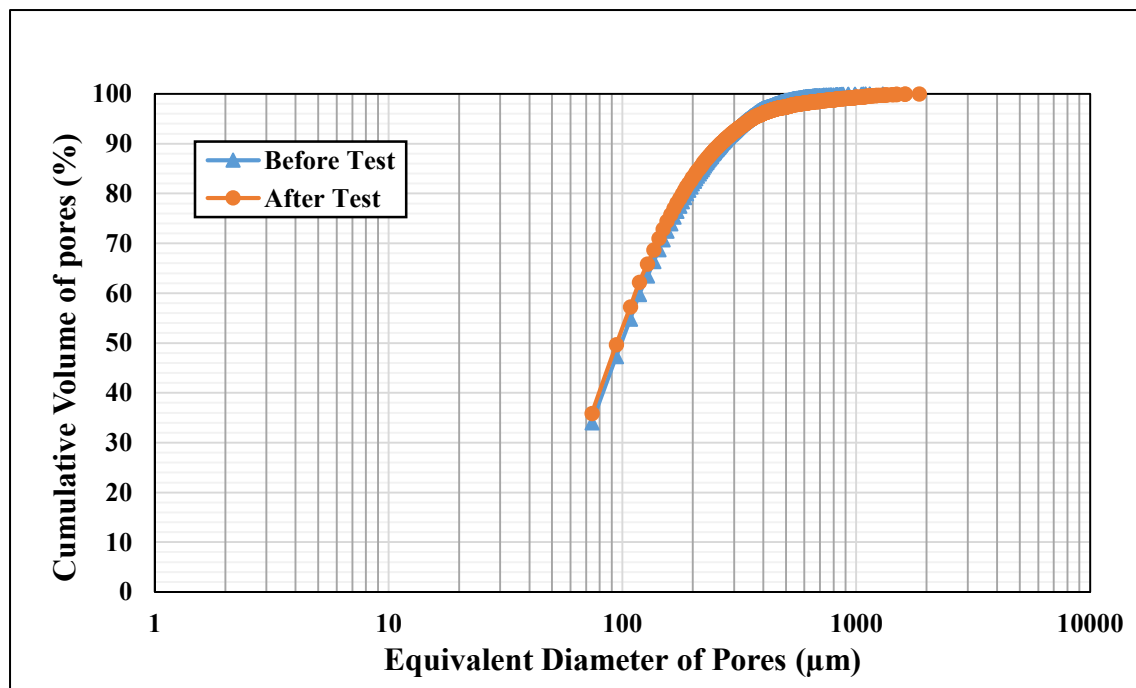


Figure 3.26 Pore size distribution before and after the leaching test (NC/NL scenario)

The loading scenario induces the formation of new cracks, resulting in an increase in the volume proportion of pores within the matrix. As a result, the amount of empty space in the matrix increases. Figure 3.27 exhibits a remarkable rise in the volume proportion of pores post-loading. These pores can exist as isolated or connected voids. It is noteworthy that an elevation

in the volume proportion of pores can exert a detrimental effect on the long-term performance of the matrix.

The decrease in the volume proportion of pores has been observed to be associated with the carbonation stages in scenarios involving C, C/L, and L/C. This decline in pore volume during the carbonation stage can be attributed to the formation of carbonation products that can fill the empty spaces (i.e., pores) within the S/S matrix. As depicted in Figure 3.28, the carbonation process caused a reduction in both large and small pores. Consequently, the reduction in pore volume can lead to an improvement in the properties of the S/S matrix. This improvement can render the matrix more resistant to various environmental conditions, as will be detailed in the subsequent chapter.

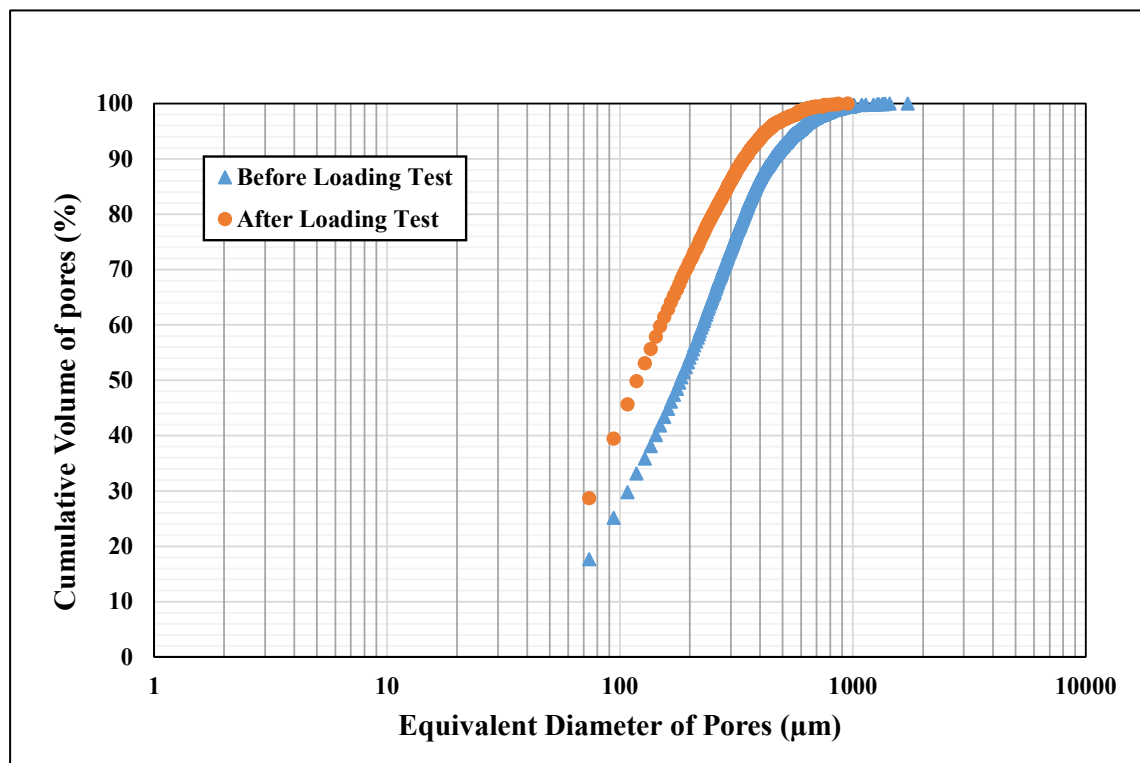


Figure 3.27 Pore size distribution before and after the leaching test (L scenario)

Figure 3.29 illustrates the pore size distribution for scenario C/L before and after the leaching test. Combining loading and carbonation resulted in a reduction of the volume proportion of pores with diameters ranging from 200 μm to 1600 μm , and an increase in the volume proportion of pores smaller than 200 μm .

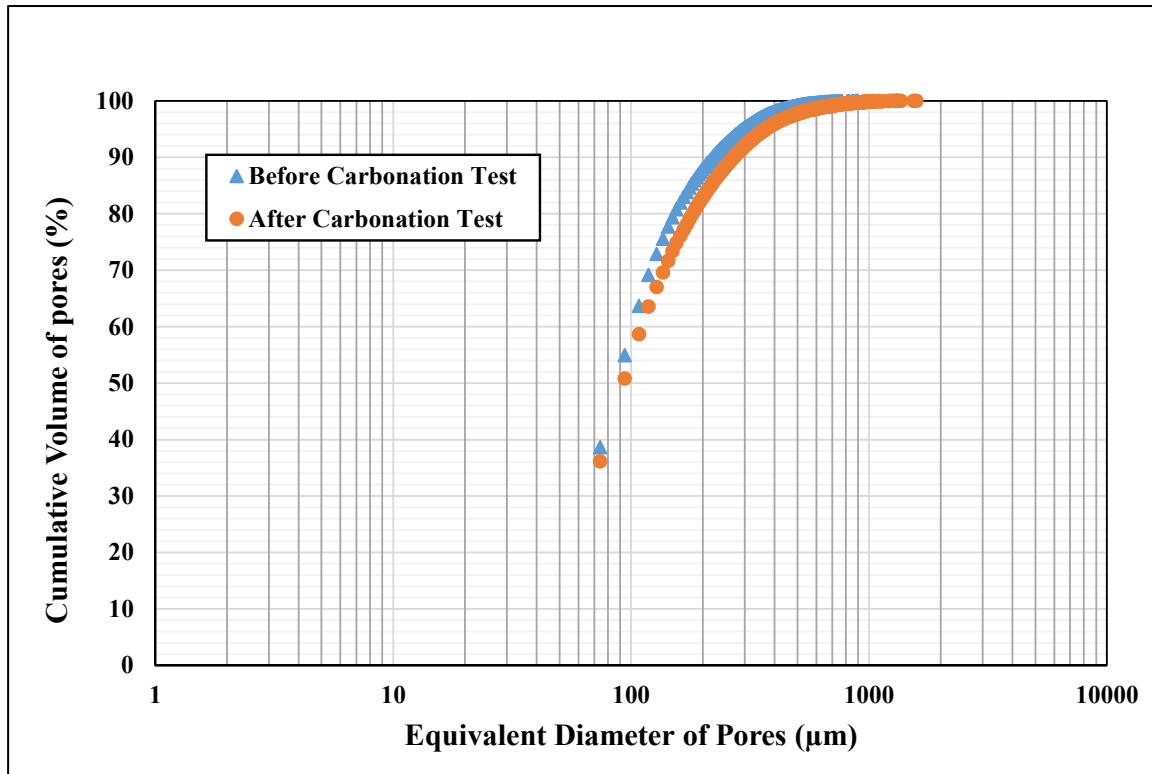


Figure 3.28 Pore size distribution before and after the leaching test (C scenario)

The alterations in the distribution of pore size, in terms of equivalent diameters, within the L/C scenario are illustrated in Figure 3.30. Specifically, a marginal increase in volume proportion of pores was observed in the diameter range of 94 to 108 μm , followed by a period of no alteration in pore size within the range of 109 and 128 μm . Subsequently, there was a further increase in volume proportion of pores for diameters ranging from 128 to 358 μm . However, no modifications were detected in volume proportion of pores sizes larger than 358 μm in diameter.

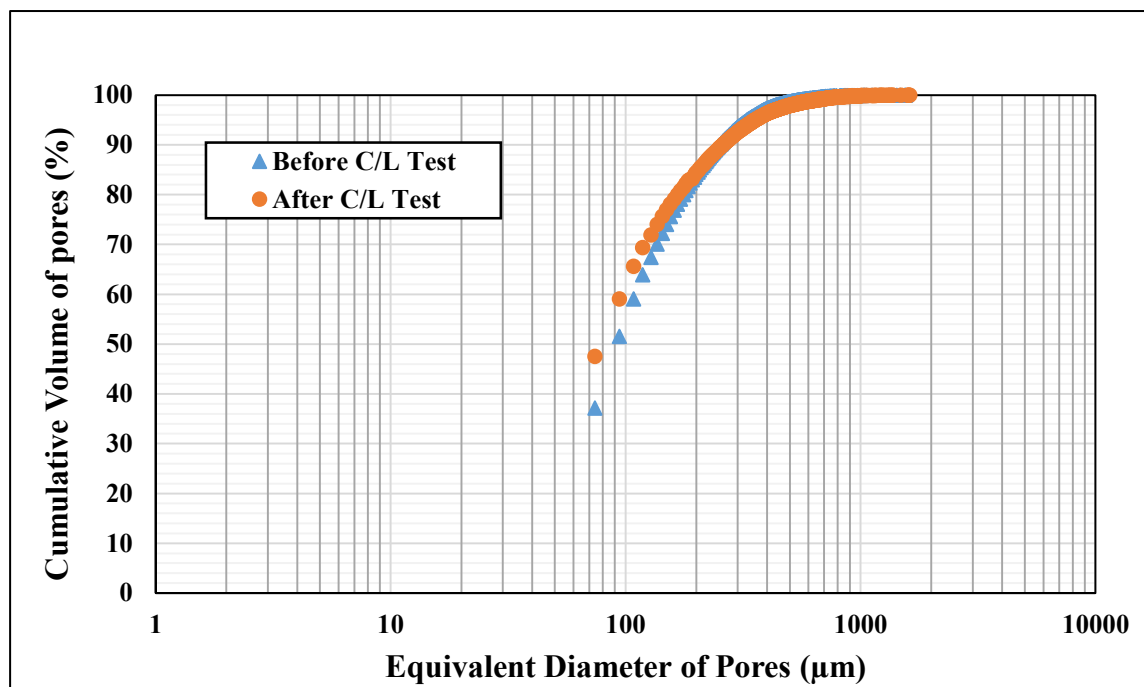


Figure 3.29 Pore size distribution before and after the leaching test (C/L scenario)

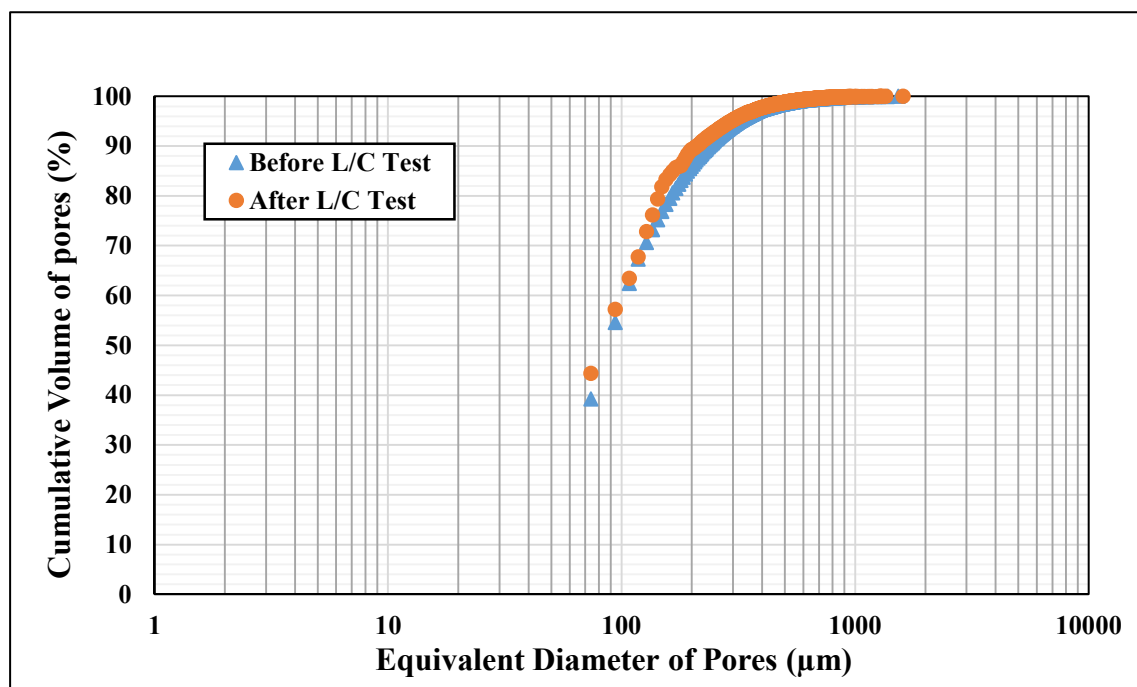


Figure 3.30 Pore size distribution before and after the leaching test (L/C scenario)

3.6 Influence of carbonation and loading on the sample appearance

The difference in size between un-leached and leached samples was calculated for each scenario, and the values are provided in Table 3.5. Visual examination of leached samples showed a slight increase in volume in most scenarios except the C scenario. These results were duplicated using two different protocols.

Table 3.5 Variations of a sample volume before and after the leaching test

Scenario / Test protocol	NC/NL	C	L	C/L	L/C
Constant water flow	0.13 %	0.00 %	0.69 %	0.84 %	2.05 %
Intermittent water flow	0.28 %	-0.65 %	0.51 %	0.85 %	2.05 %

The volume change might be attributable to a variety of factors, including the W/C ratio, matrix permeability, and pore size. Furthermore, the leaching of CH and C-S-H may alter the pore volume of sample (Haga et al., 2005). These results are consistent with the effects of each scenario, in which carbonation decreases the pore volume and mechanical loading, on the other hand, increases it.

In general, the colour of all samples before the test was light grey (Butcher et al., 1996). However, after leaching, it changed based on each test scenario, as shown in Figure 3.30. For example, carbonation can change the sample's colour to dark brown (Butcher et al., 1996; Venhuis & Reardon, 2001). These changes in colour could be caused by the raised retention of iron (Butcher et al., 1996). However, no colour change was observed after the loading scenario.

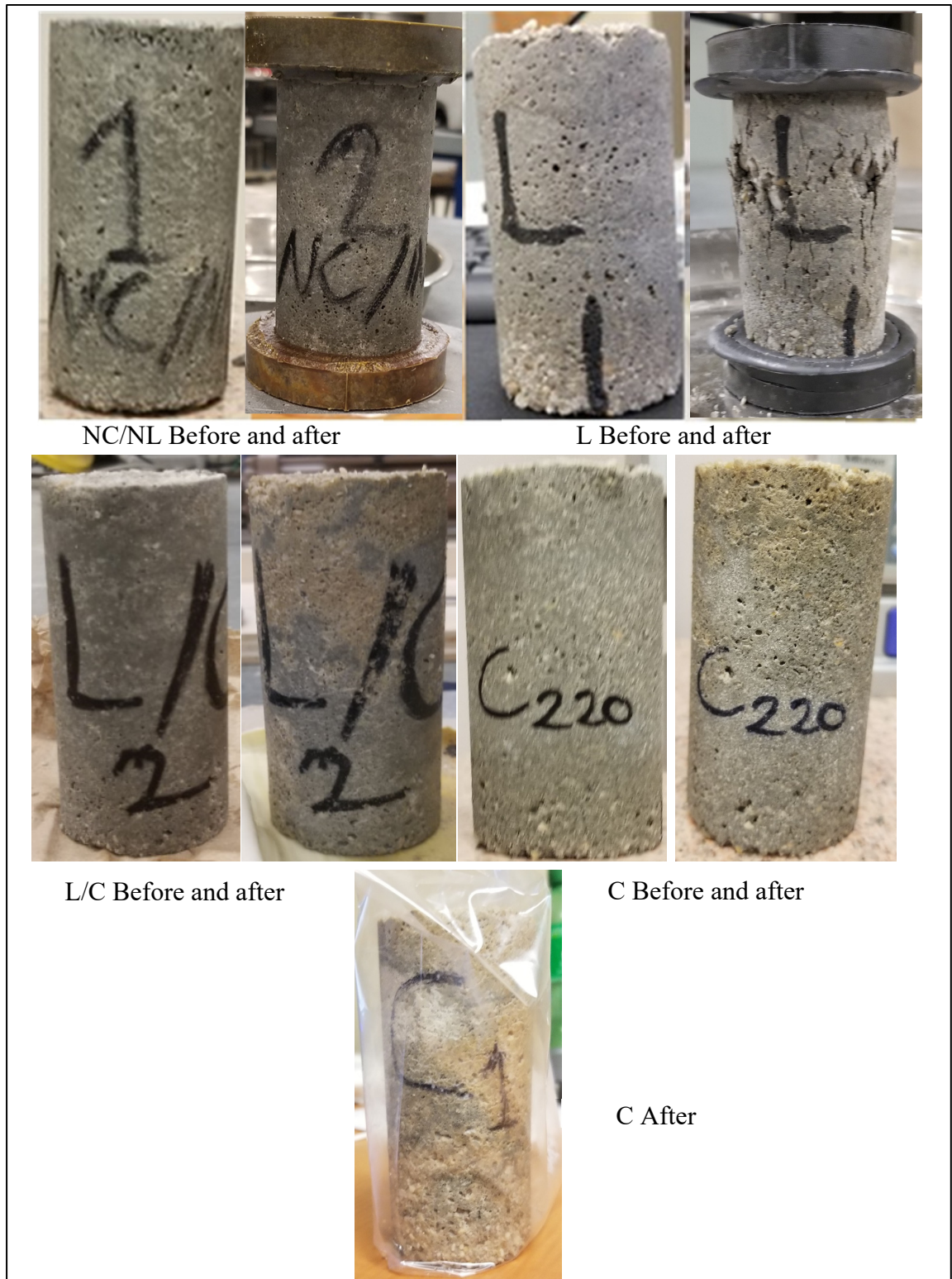


Figure 3.31 Comparison of the changes in sample colour in each test scenario: carbonated samples (buff) and un-carbonated samples (gray)

CHAPTER 4

ANALYSIS OF EXPERIMENTAL RESULTS

The test results that were presented in chapter 3 show the influence of leaching, mechanical strain and carbonation on the properties of the solidified materials and on leachate composition. The scenarios that combine two stressors also show their interactions (C/L, L/C). This chapter discusses the results that were presented in the previous chapter in terms of mechanisms and the literature.

4.1 Leaching

The NC/NL scenario was supposed to isolate the influence of leaching on the solidified material. The porosity determined from CT scans varied between 22.9 % before the test and 23.6 % after leaching. Considering the range of porosity values that was obtained by varying the threshold used for pore segmentation (Table 3.4), the influence of the NC/NL scenario on porosity is not significant. The influence of this scenario on the amount of CaCO_3 in the sample is also insignificant with weight proportions of 1.5 and 1.4 % before and after the leaching test. As expected based on these results, the influence of leaching on the solidified material microstructure is not visible to the naked eye when the initial and final CT scans for the NC/NL scenario are compared (figure 4.1). In addition, the CT images revealed the presence of three distinct regions: small white granular regions with higher density, corresponding to minerals present in the silica sand; gray-colored regions with varying brightness values, representing the cement and aggregates; and black regions corresponding to pores and cracks.

The NC/NL scenario led to a slight decrease in hydraulic conductivity of 3 % for the continuous water injection protocol and 27 % for the intermittent water injection protocol (after ten days of water injection). These small changes in hydraulic conductivity contrast with previous leaching experiments with cementitious material (e. g. Saito & Deguchi 2000) which often led to a significant increase in hydraulic conductivity caused by the dissolution of

portlandite. Leaching calcium ions increases porosity in cement-based material, damaging the pore structure (Cheng et al., 2013). It is likely that the decrease in hydraulic conductivity could be due to the phenomenon of self-healing in the presence of water flow (De Belie et al., 2018; Yildirim et al., 2015). It should be noted that the leaching experiment that are presented in the literature are designed to prevent carbonation, the main cause of self-healing. For instance, Haga et al. (2005) conducted their leaching experiment in a glove box with a nitrogen atmosphere. In the presence of CO_3^{2-} , part of the portlandite leaching could lead to carbonate precipitation and a decrease in hydraulic conductivity as was observed for the NC/NL scenario. The small changes in hydraulic conductivity could also be related to the slight decrease in the proportion of larger pores shown in Figure 3.25 before and after the NC/NL scenario. Changes in the proportions of larger and smaller pores were observed for some leaching experiments (Haga et al. 2005).

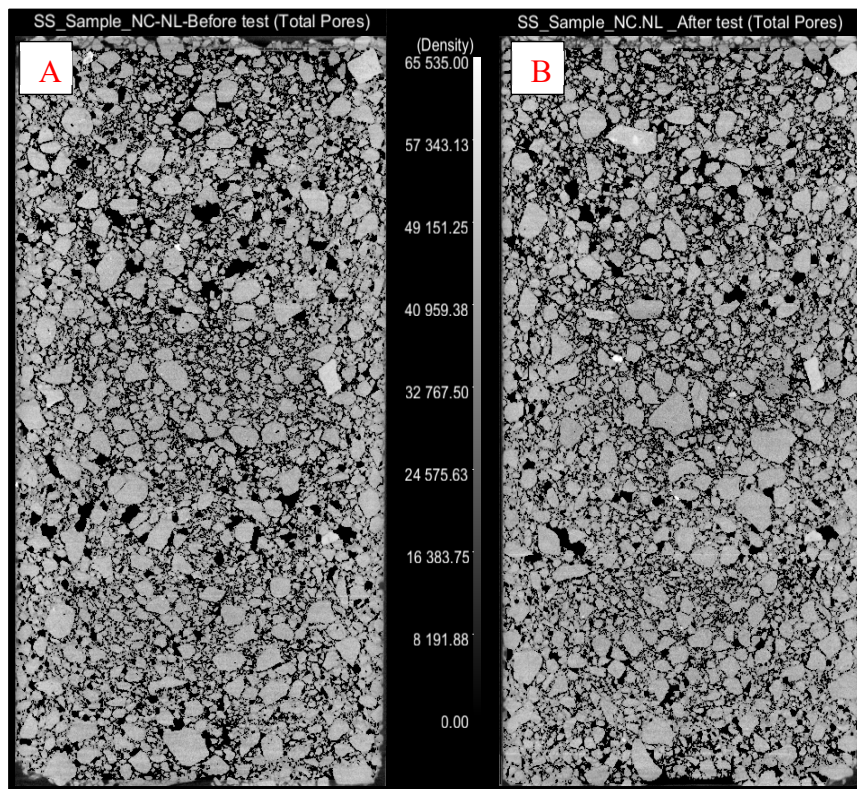


Figure 4.1 Vertical CT scan sections for the NC/NL scenario
A) before and B) after FTL test

The calcium concentration in the leachate can be associated with the dissolution of CH (Butcher et al., 2012; Haga et al., 2005; Poon et al., 2001). Figure 4.2 shows the calcium concentration with respect to the pH. The calcium concentration in the leachate allows the amount of portlandite dissolved by the leaching to be estimated. The total volume of water circulated through the sample during the NC/NL scenario for the continuous injection scenario was 2.18 L with an average Ca concentration of 740 mg/L. Assuming that the mass of leached calcium is entirely due to portlandite dissolution and based on a density of 2.24 g/cm³ for portlandite (Taylor 1997), the amount of calcium leached during the NC/NL scenario corresponds to only 0.7 % of the sample of volume or an equal increase in porosity. This porosity change is small compared to those that were observed with carbonation and loading.

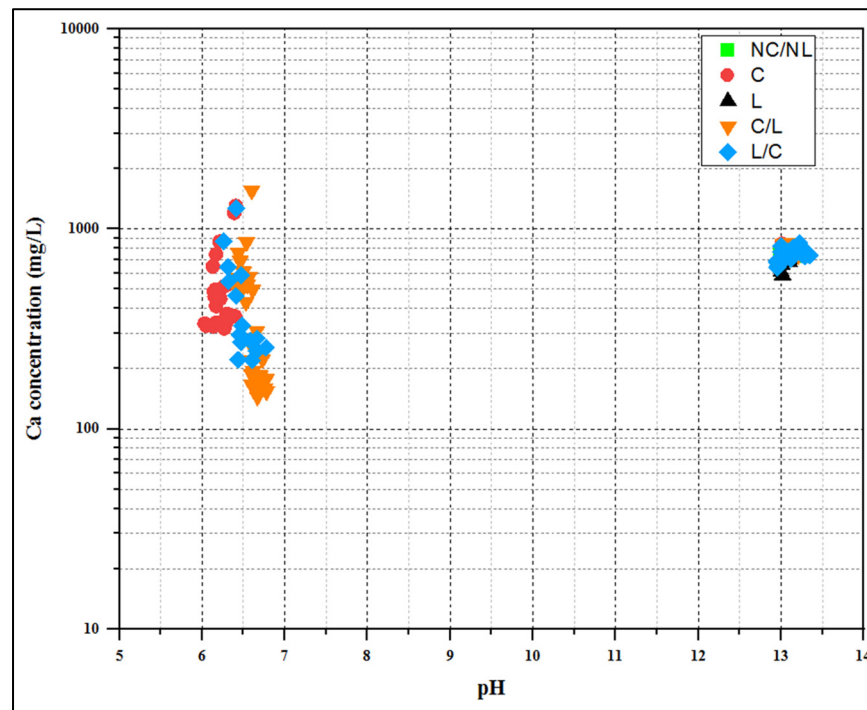


Figure 4.2 Variations of Ca concentrations as a function of pH

Figure 4.3 presents the relationship between the Si concentration and pH for the various test scenarios. Based on the low Si concentrations (below 2 mg/L) in the leachate, the leaching of C-S-H seems to be limited when the solidified matrix is alkaline. These results suggest that Si is stable when the pH value exceeds 7 (Gollmann, da Silva, Masuero & dos Santos, 2010).

According to Arribas et al. (2018), the lower silicon concentration might be attributed to silicon being incorporated into the structure of C-S-H. This discrepancy in leaching behavior can be attributed to the chemical composition of the S/S matrix, which contains a higher concentration of calcium-based compounds, such as CH, that possess greater solubility in water compared to silicon-based compounds. In line with these findings, Heukamp, Ulm, and Germaine (2003) reported that under equilibrium conditions, the dissolution of CH precedes the decalcification of C-S-H, resulting in a reduction in the calcium-to-silicon ratio.

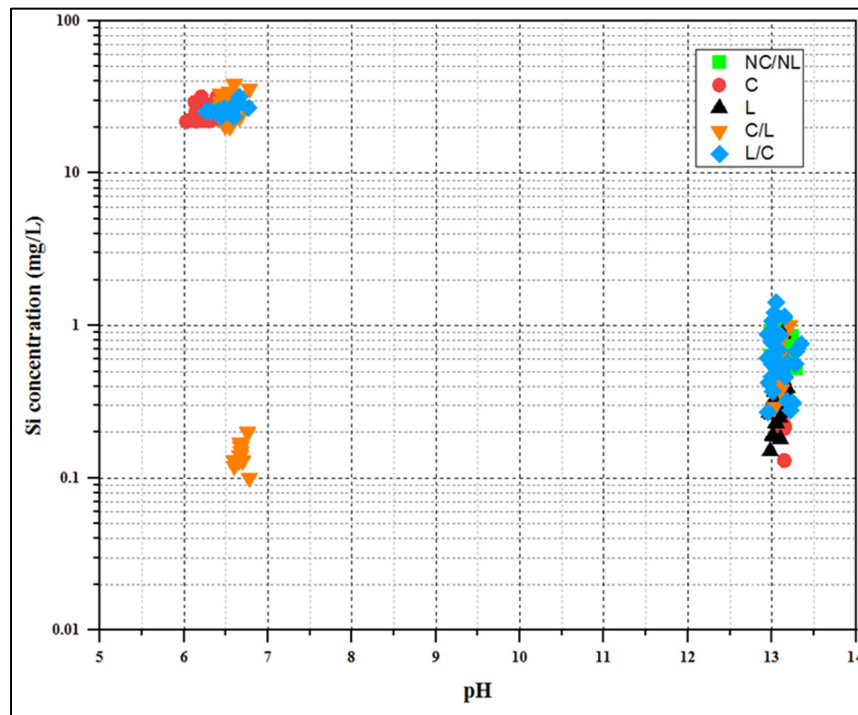


Figure 4.3 Variations of Si concentrations as a function of pH

The Cu concentration gradually declined due to continuous water injection. Additionally, in the NC/NL scenario, the release of Cu decreased and remained steady between 0.07 and 0.09 mg/L. These results suggest that as long as the leachate remains alkaline, the mobility of Cu will be low (Catalan & Wetteskind, 2002; Catalan et al., 2002). This is most likely because Cu can precipitate as copper hydroxides in alkaline conditions ($\text{pH} \geq 9$) (Komonweeraket, Cetin, Aydilek, Benson & Edil, 2015; Poon et al., 2001).

4.2 Carbonation

The impact of carbonation on the density of the solidified material was significant. The impact of carbonation can be seen by comparing visually the CT scans before and after carbonation (Figure 4.3). The initial image (A) exhibits a lower density (darker pixels) compared to the final image (B) after carbonation.

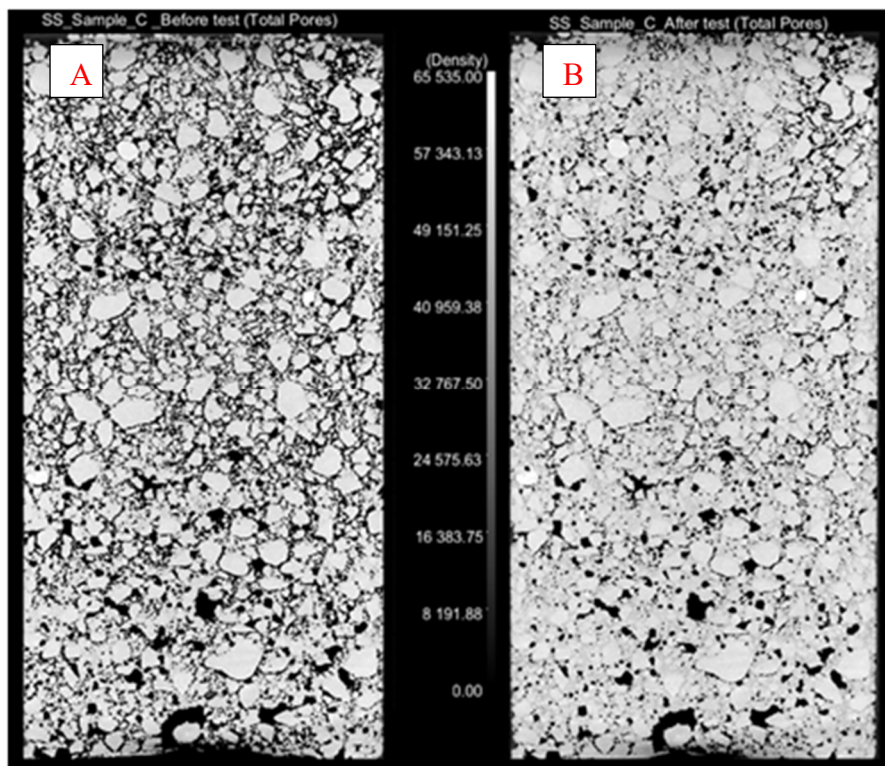


Figure 4.4 Vertical CT scan sections for the C scenario
A) before and B) after FTL test

The increased density is associated with a reduction in pore volume due to the accelerated carbonation. The porosity values obtained through the segmentation of the μ -CT scans decreased from 25.4 % before the test to 21.4 % after carbonation for the continuous injection protocol. A comparison of image A and image B also shows a noticeable decrease in the porosity for the fine-grained matrix between the larger grains. Kong et al. (2020) also observed an increased density for carbonated matrices. The decrease in porosity for scenario C is in line

with the results obtained for previous studies (Ashraf 2016; Morandea et al., 2014; Pihlajavaara, 1968; Wang et al., 2019; Ngala & Page, 1997; Song & Kwon, 2007). For example, Wang et al. (2019) observed an 84.25% decrease in the overall volume of pores exceeding 200 nm in diameter as a consequence of carbonation.

The decrease in porosity was associated with a reduction in hydraulic conductivity (Figure 3.1). Scenario C resulted in a reduction of hydraulic conductivity by 22 % for the continuous water injection protocol and 62 % for the intermittent water injection protocol. The disparity in reduction percentages for the two protocols can probably be attributed to the duration of the water injection. Water was circulated through the sample for respectively nine days and two days following carbonation for the intermittent and continuous injection protocols, respectively. These findings concerning the impact of carbonation on hydraulic conductivity align with the results reported in the literature (Claisse, El-Sayad, & Shaaban, 1999; Song & Kwon, 2007). For example, Dewaele et al. (1991) conducted a CO₂ injection under pressure and documented a reduction in permeability of several orders of magnitude following carbonation. A reduction in both porosity and hydraulic conductivity was likewise documented by Venhuis & Reardon (2001), and Song & Kwon (2007). Figure 4.5 illustrates the association between porosity and hydraulic conductivity. During carbonation, the measured hydraulic conductivity exhibited a decrease concomitant with a reduction in porosity.

The formation of calcium carbonate in the C scenario was confirmed through the thermogravimetric analysis presented in Figure 3.24. The DTG curve displayed a distinct peak after the carbonation test, indicating the conversion of calcium hydroxide to calcium carbonate by CO₂ and the acceleration of the self-healing process (Ashraf, 2016; Morandea et al., 2014). The DTG results allowed the increase in the percentage of calcite in the sample to be estimated from 1.5% before the carbonation test to 3.1% after (Table 3.3). The calcium carbonate polymorph that was precipitated was not identified in this study, but Arandigoyen, Bicer-Simsir, Alvarez, & Lange (2006) used X-ray diffraction analyses to show that calcite was the main polymorph resulting from the transformation of portlandite into calcium carbonate. These findings suggest that the pores within the solidified material underwent self-healing, leading

to pore closure and impeding smooth water flow (De Belie et al., 2018; Lange et al., 1996; Morandea et al., 2015).

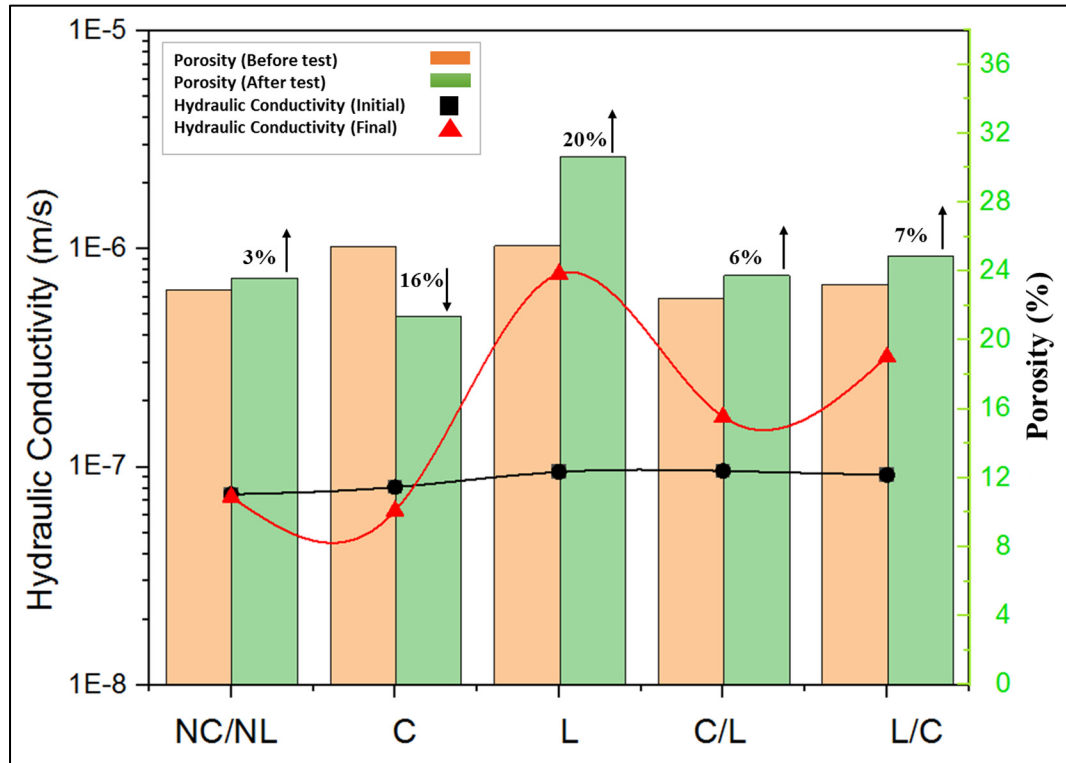


Figure 4.5 Relationship between porosity and hydraulic conductivity

Carbonation had a significant influence on the leachate pH. After carbonation, all pH measurements were between 6.03 and 6.78 for the C scenario compared with a range of 12.98 to 13.29 for the NC/NL and L scenarios. These results align with the observations of Bertos et al. (2004) and Branch et al. (2016), who documented that the presence of cement in the matrix leads to a significantly high alkaline state (pH 13). However, carbonation reduces the alkalinity of the solidified matrix.

The solubility of calcium was influenced by the effect of CO₂, leading to a momentary increase in calcium release immediately after the carbonation process, followed by a subsequent decline over time. Van Gerven, Van Baelen, Dutré, & Vandecasteele (2004) attributed the heightened calcium release from carbonated samples to the predominance of bicarbonate ions at a lower

pH. Müllauer, Beddoe, & Heinz (2012) indicated that the substantial leaching of Ca observed after carbonation could be attributed to the dissolution of portlandite and calcium-silicate-hydrate (C-S-H).

A gradual reduction in the concentration of calcium was observed over time during leaching. As depicted in Figure 3.10, the Ca concentration for the C scenario decreased to 317 mg/L at the end of the test. Because of the decreasing concentration, the total calcium mass leached during the C scenario is lower than during the NC/NL scenario. This implies that calcite precipitation during carbonation decreases the calcium mass available for leaching. The decrease in calcium concentration aligns with the findings reported by Poon & Chen (1999), who attributed the decline in calcium concentration to the continuous percolation of water through the pores of the solidified sample. Müllauer et al. (2012) observed a comparable association between carbonation and the release of calcium, which they attributed to the conversion of calcium ions into calcite, which exhibits a low solubility.

In contrast to calcium, the concentration of silicon increases following carbonation. Carbonation contributes to the increased release of silicon from the S/S matrix through chemical reactions involving carbonate compounds and silicate minerals, resulting in the dissolution of C-S-H and the formation of calcite (Branch, Kosson, Garrabrants, & He, 2016; El Bedoui et al., 2018). Carbonation led to a substantial reduction in the Ca/Si ratio of the leachate, which decreased from 1098 to 14. Müllauer et al. (2012) attributed this decrease in the Ca/Si ratio to the decalcification of C-S-H. These findings were further corroborated by Branch et al. (2016), who concluded that the increased solubility of silicon in carbonated materials provides additional evidence for the dissolution of C-S-H. These findings are corroborated by Figure 3.24. The DTG curve presented in Figure 3.24 exhibits a singular and prominent peak of mass loss, which occurred over a temperature range of 580°C to 740°C after carbonation. This distinct peak in mass loss is attributed to the transformation of the majority of portlandite and C-S-H into calcite (Arandigoyen, Bicer-Simsir, Alvarez, & Lange, 2006).

Figures 3.13 and 4.6 illustrate the leaching behavior of copper from carbonated solidified materials. The process of accelerated carbonation appears to stimulate the release of copper, with the highest concentration observed due to a decrease in pH. Specifically, the concentration of copper seems slightly higher for pH levels between 6 and 7, but the disparity before and after carbonation is relatively minor.

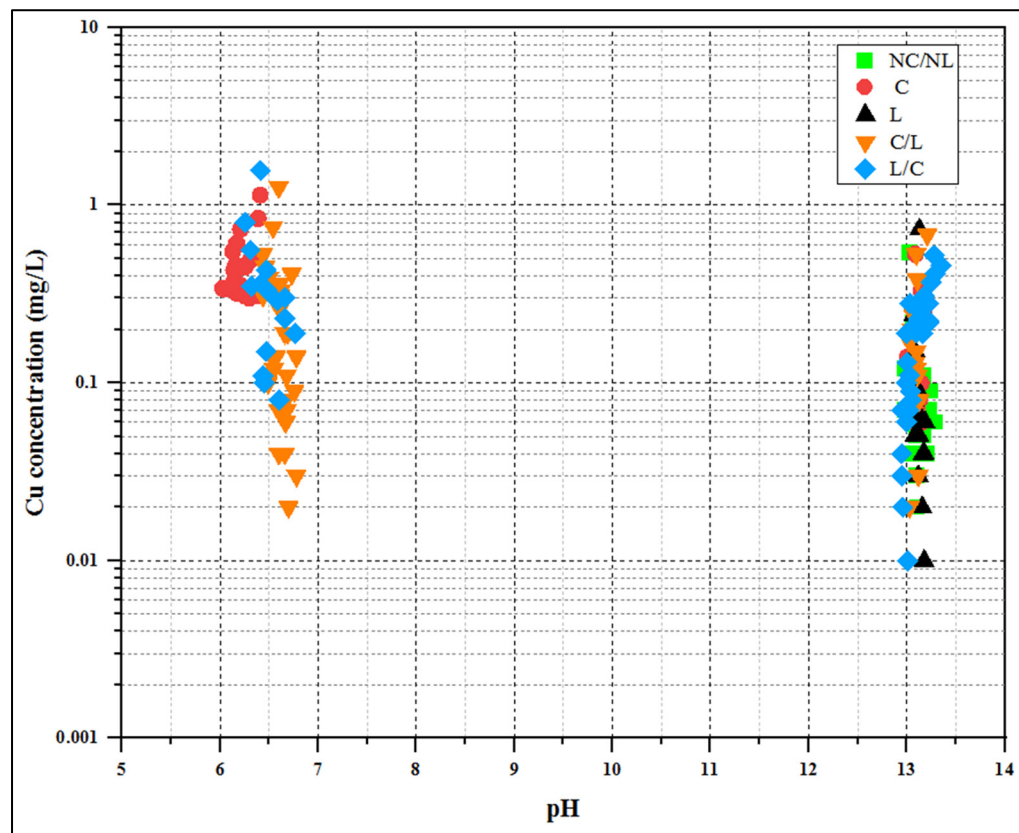


Figure 4.6 Variations of Cu concentrations as a function of pH

These findings differ from the outcomes reported by Pandey et al. (2012), who employed a different leaching procedure known as the Toxicity Characteristic Leaching Procedure (TCLP). Pandey et al. observed that non-carbonated cement showed no detectable copper, while carbonated cement exhibited a significantly poorer ability to retain copper. Bertos et al. (2004) also reported high copper leachability following carbonation, attributing this increase to the enhanced solubility of metal compounds due to pH reduction and the decomposition of ettringite.

4.3 Mechanical strain

Mechanical strains combined with leaching had a more significant influence on the solidified material properties than leaching alone. Figure 4.7 illustrates the impact of external loading combined with leaching on pore characteristics.

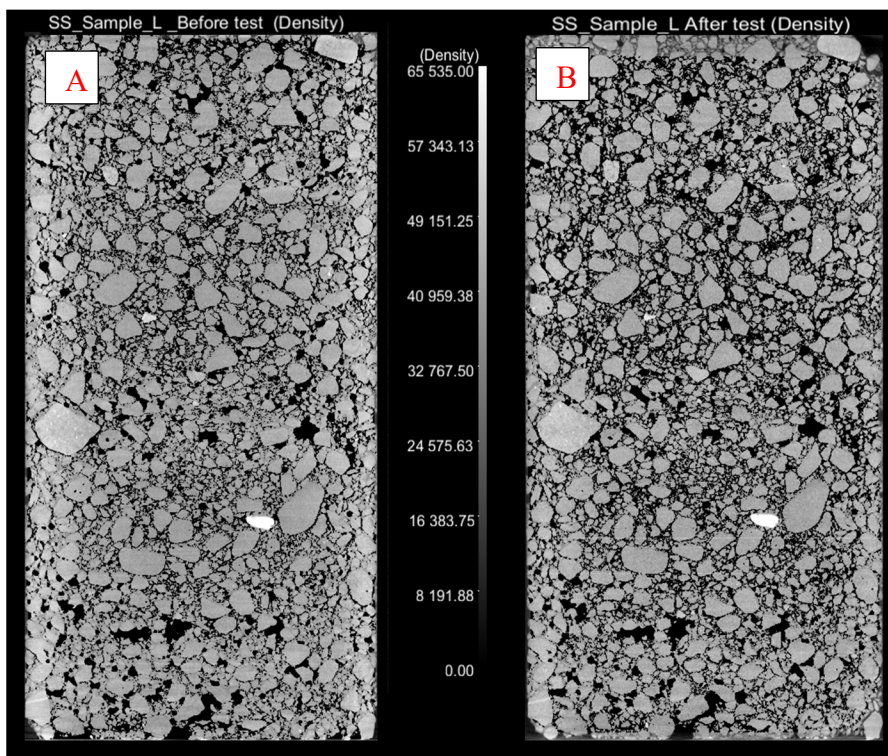


Figure 4.7 Vertical CT scan sections for the L scenario
A) before and B) after FTL test

The 2D CT scan images exhibit a significant increase in porosity after the loading test, as depicted in image B. Image A prior to loading shows comparatively brighter pixels (higher density) compared to image B where microcracks corresponding to black pixels (low density) are distributed throughout the matrix after loading. The application of mechanical strain within the S/S sample leads to the formation of microcracks and voids, ultimately resulting in a

notable augmentation of porosity. This increase encompasses both large pores, which are interconnected, and small pores, which are isolated, and can reach up to 20 %.

The higher porosity associated with loading led to an increase in hydraulic conductivity by one order of magnitude. The higher hydraulic conductivity is ascribed to the formation of new pathways and cracks within the sample. Additionally, Figure 3.27 visually demonstrates a notable rise in isolated and interconnected pores following the loading process. Aligizaki (2005) provides insight into the significant role played by interconnected porosity in influencing the transport properties of cementitious materials. Accordingly, it is postulated that large pores contribute to the interconnection of flow paths within the S/S matrix, thereby increasing hydraulic conductivity. These observations align with the findings of Hoseini et al. (2009), who similarly affirmed that the transport of fluids within cementitious materials is predominantly influenced by the interconnected pore network.

The influence of mechanical strain on hydraulic conductivity is consistent with the results that have been presented in the literature. The literature proposes that the microstructure of the solidified matrix responds sensitively to such loads, interconnecting the pore system and enhancing flow paths, thereby augmenting hydraulic conductivity (Akhavan & Rajabipour, 2012; Aligizaki, 2005; Choinska, Khelidj, Chatzigeorgiou, & Pijaudier-Cabot, 2007; Van Breugel, 2007). Wang et al. (1997) conducted measurements of the permeability coefficient of cracked materials and proposed it is dependent on the width of the crack opening, with permeability exhibiting an exponential increase for larger cracks. It is important to highlight that the measurement of crack aperture was not possible in this study due to the limited resolution of the CT scan. The crack aperture appears to be smaller than the resolution of the CT scan. Furthermore, it should be noted that the creation of cracks was conducted under controlled conditions with an axial strain of 1.96%.

The concentration of Ca in the leachate was constant for most of the test with an average concentration of 728 mg/L. The Ca concentration for scenario L was similar to scenario NC/NL, apart for the end of the test, which was marked by a gradual decrease in Ca

concentration for scenario L, as illustrated in Figure 3.10. This decrease in Ca concentration could be due to the preferential flow paths caused by cracking. These preferential flow paths could make calcium leaching slower away from the fractures. The Si and Al concentrations for the L scenarios were also similar to those of the NC/NL scenario, albeit slightly lower for the L scenario.

Figure 4.6 illustrates the evolution of copper concentration under the loading scenario, as a function of pH. The Cu concentration varies over two orders of magnitude with a relatively constant pH (between 12.97 and 13.18). The highest Cu concentration was observed at the beginning of the leaching test. As it was the case with Ca, the Cu concentration for the L scenario is similar to the concentration observed during the NC/NL scenario, but with a gradual decrease at the end of the loading scenario. As mentioned previously for calcium, this phenomenon may be due to the occurrence of cracking, which facilitates the easy flow of water along the newly formed channels. Consequently, it may take a considerable amount of time for chemical equilibrium to be established within the S/S matrix. The findings from the flow-through leaching tests are consistent with those reported by Poon & Chen (1999), who demonstrated that Cu leaching exhibited rapid initial rates followed by a gradual decline over a short period. In relation to this phenomenon, Catalan et al. (2002) explains that as long as the leachate maintains an alkaline pH, the mobility of Cu remains low. Furthermore, the observations made by Catalan et al. (2002) align with these findings, indicating a decrease in Cu concentration with an increase in leachate volume.

In the loading scenario, as water permeated through the solidified sample, a rapid recovery of hydraulic conductivity was observed, as depicted in Figure 3.1. Specifically, during the initial five cycles of water injection following the creation of new cracks, the hydraulic conductivity experienced a slight reduction of 15%. This phenomenon can be primarily attributed to self-healing mechanisms. According to De Belie et al. (2018) and as presented in Figure 1.11, in this scenario, the self-healing phenomenon can be categorized into three primary mechanisms:

- 1) **Physical blocking:** The physical blockage of cracks through the presence of fine silica and cement particles, which are direct consequences of the cracking process.
- 2) **Chemical Reactions:** When water flows through the solidified sample, it contains carbonate ions that react with calcium ions resulting in the formation and precipitation of calcite. This precipitation fills the pores and cracks, resulting in a decrease in hydraulic conductivity.
- 3) **Rehydration mechanism:** This mechanism refers to the process of continuing hydration of unhydrated cement grains during saturation or restoration, known as continued hydration. However, the occurrence of this mechanism is still a subject of debate in the current study where the research in the literature suggests that a portion of the cement matrix, up to 25%, may remain unhydrated, thus rendering the assumption of rehydration plausible (De Belie et al., 2018; Li & Yang, 2007).

The precise mechanism underlying the observed self-healing phenomenon in the current scenario has not been fully determined. However, based on the available evidence, physical blocking and chemical reactions are considered the most likely mechanisms that contribute to the self-healing process. It is noteworthy that the precipitation of calcite has a limited impact on the decrease in hydraulic conductivity. This limitation is due to the restricted availability of CO₂ during the curing process (Van Tittelboom, Gruyaert, Rahier, & De Belie, 2012), as the samples were enclosed in a sealed bag within the humidity room throughout the curing period.

4.4 Interactions between leaching, loading and carbonation.

When considering the combined effects of carbonation and loading, the hydraulic conductivity behavior exhibits less severity compared to loading alone. The C/L scenario, which involves the sequence of carbonation followed by mechanical loading, reveals two distinct stages. Figure 3.1 presents a 20% reduction in hydraulic conductivity subsequent to carbonation,

succeeded by a notable increase of 157% following the loading phase. Eventually, the value of hydraulic conductivity undergoes a gradual decline of 61% by the end of the leaching test.

The influence on hydraulic conductivity was found to be more pronounced when loading is conducted prior to carbonation, as opposed to when carbonation precedes loading. As depicted in Figure 3.1, the initial hydraulic conductivity experiences a significant increase of 552% due to the development of cracks subsequent to the loading phase. Subsequently, after subjecting the solidified sample to a period of three days involving CO₂ injection, the hydraulic conductivity demonstrates a decrease of 67% owing to pore clogging. Additionally, during a water injection period of ten days, the hydraulic conductivity exhibits a gradual decline of 30%. The combination of loading and carbonation indicates that carbonation can improve the mechanical properties of solidified sand by inducing an internal structure that mitigates the impact of external stress and minimizes fracture occurrences. This phenomenon is particularly evident in the C/L scenario, where the increase in hydraulic conductivity is lower compared to the L/C scenario. In simpler terms, when cracking occurs due to applied mechanical loading after carbonation, the impact on hydraulic conductivity is higher compared to when carbonation precedes the occurrence of cracking.

Figures 4.7 and 4.8 illustrate the impact of carbonation combined with loading on pore characteristics. Subsequent to the FTL test, it was observed that certain pores became interconnected with the cracks, resulting in a slight increase in the darkness of image B due to the augmented presence of pores. A similar phenomenon of density changes in CT images has been reported by Fukuda et al. (2012). Accordingly, Aligizaki (2005) and Hoseini et al. (2009) have confirmed that the observed increase in hydraulic conductivity can be attributed to the interconnection between pores and cracks, which consequently creates new flow paths. However, the combination of carbonation and loading resulted in a less severe increase in the porosity percentage. This hypothesis is supported by the results of the C/L and L/C scenarios.

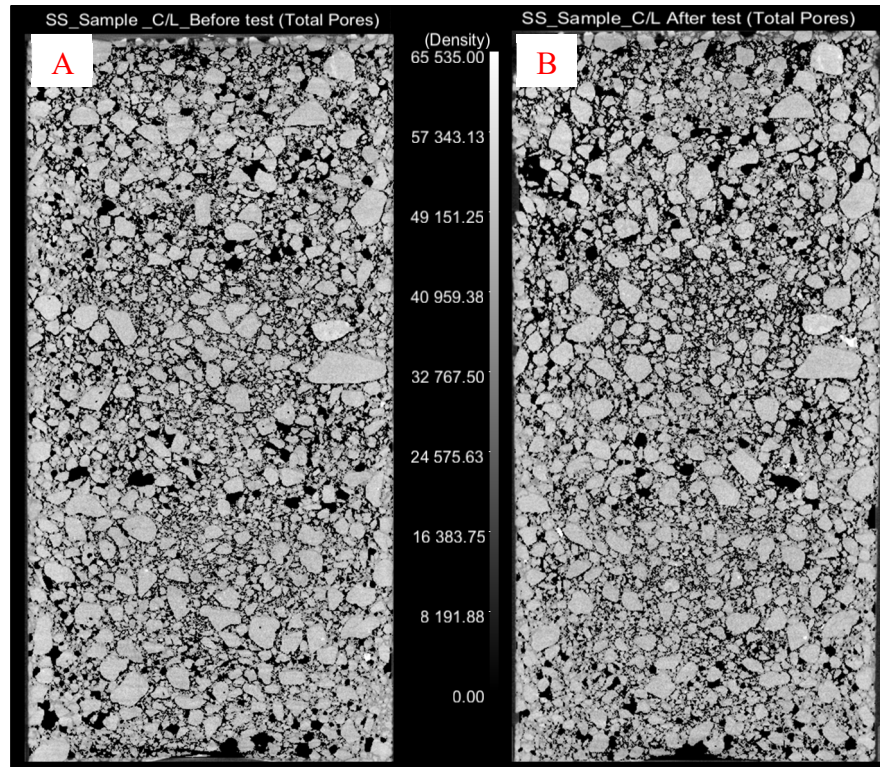


Figure 4.8 Vertical CT scan sections for the C/L scenario
A) before and B) after FTL test

Figure 4.4 illustrates that in both the C/L and L/C scenarios, there is a respective porosity increase of 6% and 7%. Put simply, the higher porosity and enhanced connectivity result in higher hydraulic conductivity, as supported by Zhong and Wille (2016) and Zhong, Xu, Netto, and Wille (2016). Despite the overall increase in total porosity observed in most cases, such as in the C/L and L/C scenarios, the hydraulic conductivity gradually decreases as water flows through the pores and cracks within the solidified/stabilized matrix. This phenomenon can be attributed to an increase in small pores, which are considered inactive, and a concurrent reduction in the larger, more active pores. This trend is visually depicted in Figures 3.29 and 3.30.

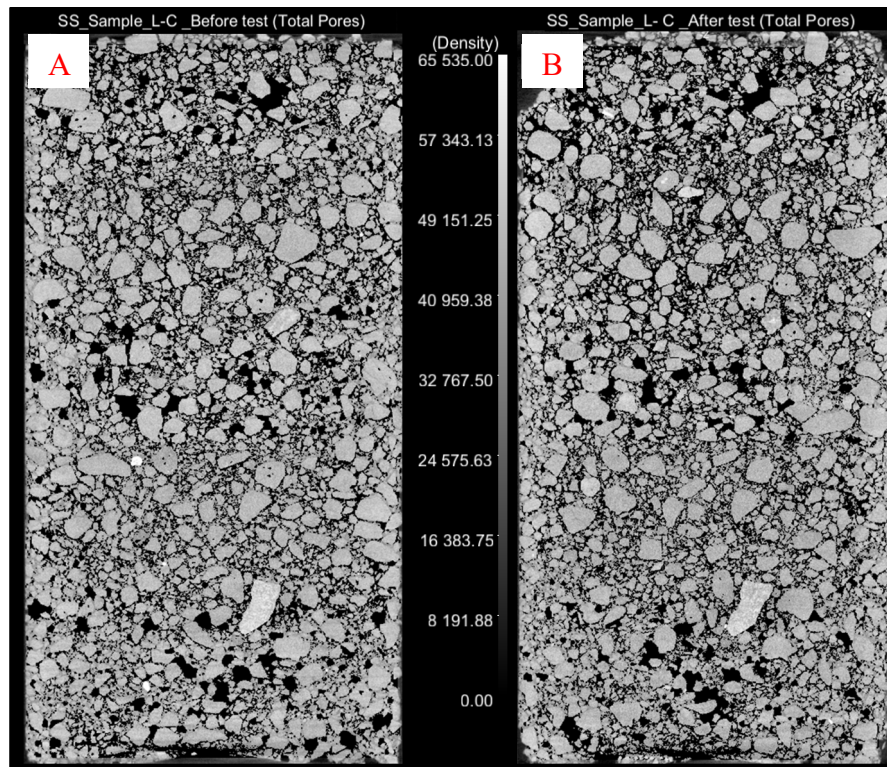


Figure 4.9 Vertical CT scan sections for the C/L scenario
A) before and B) after FTL test

The combination of carbonation and loading has provided evidence of a healing phenomenon in solidified materials, which can be ascribed to two distinct processes encompassing chemical and physical mechanisms. The chemical mechanism involves the precipitation of calcite resulting from accelerated carbonation, while the physical mechanism involves the clogging of the pores and cracks through the minute particles present on the crack surfaces subsequent to loading (De Belie et al., 2018; Ferrara et al., 2018; Herbert & Li, 2013; Nakarai & Yoshida, 2015; Heide & Schlangen, 2007). These two mechanisms, as mentioned previously, lead to a reduction in porosity, consequently resulting in a decrease in the hydraulic conductivity of the solidified matrix. The generation of carbonates through the process of accelerated carbonation induces modifications in the pore structure of the matrix, leading to an increase the density of matrix. Figure 3.24 depicts the differential thermogravimetry (DTG) curves, presenting compelling evidence that accelerated carbonation induces a substantial transformation of $\text{Ca}(\text{OH})_2$ and C-S-H gel into calcite, which is widely regarded as the primary self-healing

mechanism (De Belie et al., 2018). This observation strongly suggests that the S/S samples underwent effective carbonation (Arandigoyen, Bicer-Simsir, Alvarez, & Lange, 2006).

In general, when loading occurs after carbonation, it induces the formation of cracks, resulting in an increased gap between pores in the solidified sample. Consequently, when water is present, the reaction between Ca(OH)_2 and CO_3^{2-} may resume (Van Tittelboom et al., 2012). This hypothesis is supported by the results of the differential thermogravimetric curves, which demonstrate a higher peak of calcite in the C/L scenario compared to the L/C scenario (Figure 3.24). Furthermore, the porosity in the C/L scenario was found to be lower than in the L/C scenario, as evidenced by Figure 4.5, which also shows a decrease in hydraulic conductivity due to CaCO_3 precipitation.

For the L/C and C/L scenarios, carbonation led to a gradual reduction in Ca release, while loading did not have an impact on Ca release. The gradual decline in Ca concentration can be attributed to the effect of accelerated carbonation, resulting in the transformation of calcium ions into calcite, thereby converting the CH and C-S-H gel into CaCO_3 (Johannesson & Utgenannt, 2001; Walton et al., 1997). These findings are consistent with the release of silicon at pH 6.5, where the release of Si ions appears to increase (Branch, Kosson, Garrabrants, & He, 2016; Halim, Amal, Beydoun, Scott & Low, 2004). The increase in Si solubility after carbonation could be attributed to C-S-H dissolution (Branch et al., 2016). Gollmann, da Silva, Masuero & dos Santos (2010) reported that when the pH value exceeds 7, Si appears to remain stable. Figures 3.9 and 4.3 demonstrate a correlation between the concentration of silicon and the loading conditions. Specifically, it can be observed that the decrease in Si concentration is more pronounced in the carbonation followed by loading (C/L) scenario compared to the loading followed by carbonation (L/C) scenario at the end of the test. This reduction in Si concentration can be attributed to the subsequent occurrence of cracks in the C/L scenario. The formation of cracks facilitates preferential pathways for leaching, allowing for increased flow of leachate, which in turn leads to a decrease in Si concentration. The higher volume of leachate contributes to a more significant reduction in Si concentration within the solidified material.

As expected, carbonation has demonstrated an increase in the release of copper, reaching its peak value. This can be attributed to the dissolution and precipitation of copper hydroxide and copper oxide, as reported by Komonweeraket et al. (2015). When carbonation is combined with loading, the loading-induced decrease in copper release is noticeable, albeit remaining at a low but detectable level. These findings provide clear evidence that can be attributed to the flow of water through newly formed pathways, leaving little ambiguity for interpretation.

Most studies have reported that the mechanical properties (strength) of cement-treated soils tend to increase after a few years when compared to the initial strength measured at 28 days (Kongsukprasert, Tatsuoka, & Takahashi, 2007; Seng & Tanaka, 2011). Also, Nakarai & Yoshida (2015) report the restoration of mechanical properties, specifically an increase in the strength of cement-treated sand. They attributed this phenomenon to the formation of calcite, which occurs as a result of accelerated carbonation. Despite the observed recovery in hydraulic conductivity of solidified samples over time in all test scenarios when exposed to water (Figure 3.1), there was a decrease in the unconfined compressive strength of solidified samples across all test scenarios.

These findings align with Herbert & Li's (2013) observations from their literature review, where they noted that the presence of self-healing products can close cracks but may not necessarily imply the recovery of mechanical properties. In line with these findings, Van Tittelboom et al. (2012) observed a decrease in the coefficient of water permeability over time, but no variations in strength recovery were observed across different test series. They also concluded that the initial strength of the cementitious material was higher compared to the final strength after the healing process. These results are consistent with the current results, where the initial UCS of the solidified samples was higher than the final UCS following the leaching test as presented in Tableau 3.1. Furthermore, Herbert & Li (2013) reached the conclusion that the recovery of stiffness in samples is influenced by the duration of exposure to the healing process. As an illustration, samples that underwent healing for three months were able to regain up to 65% of their initial stiffness. This observation may provide an explanation for the absence of regained strength in the solidified samples. Additionally, it is important to note that the

samples were subjected to different conditions, including a flow-through leaching test and a loading test.

CONCLUSIONS AND RECOMMENDATIONS

This thesis was carried out to improve understanding of the physicochemical phenomenon of carbonation and loading on cement-based solidified sand samples. Using a modified triaxial cell and micro-CT scan, this study has provided valuable insight into the effects of carbonation and mechanical damage on solidified silica sand. The main experimental points that have been taken into account in the experiment preparation are as follows:

- Choosing the appropriate water/cement (W/C) ratio. A higher W/C ratio increases the percentage of connected pores, improving gas penetration, and making it easier for fluid to pass through the material.
- Choosing the appropriate method of loading. The target was to create microcracks. The variables to be considered include confinement pressure, axial loading rate, and maximum displacement.
- Choosing the gas injection protocol. The procedure was established to increase gas penetration through the sample instead of flowing around the sample. Injection time, gas flow rate, and injection pressure were the parameters to be considered.
- Choosing the appropriate leaching test to assess the long-term stability of S/S (Butcher et al., 1993; Poon et al., 1999; Zhang et al., 2009). A flow-through leaching test was used to simulate how water comes in contact with S/S materials in environmental conditions, and to ensure that the water used in the experiment is constantly renewed to mirror environmental conditions. A flow-through leaching test allows using the same sample for other tests.
- The modified triaxial cell can leach full-scale solidified samples without any size reduction. Additionally, the characteristics of the internal microstructure can be obtained before and after the leaching test.

This project's aims can be classified into two categories: The first objective is to evaluate the impact of loading and carbonation on the physical alteration of S/S matrices, such as hydraulic conductivity, compressive strength, and alteration of interior microstructure, namely pore size distribution. The second objective is to evaluate the impact of these environmental conditions on chemical alteration, such as the leachability of some major and trace elements. Consequently, two experimental protocols have been set up. The first test protocol is continuous water injection. The second test protocol is intermittent water injection. In addition, each test protocol consisted of the following five test scenarios, namely NC/NL, C, L, C/L, and L/C: 1) No carbonation / no loading (NC/NL); in this scenario, the sample was subjected to FTL/K tests; 2) carbonation (C), the sample was subjected to FTL/K tests then carbonation followed by FTL/K tests; 3) mechanical loading (L), the sample was subjected to FTL/K tests then loading test followed by FTL/K tests; 4) carbonation followed by mechanical loading (C/L), the sample was subjected to FTL/K tests, carbonation, FTL/K tests, loading test, and FTL/K tests; 5) mechanical loading followed by carbonation (L/C), the sample was subjected to FTL/K tests, loading, FTL/K tests, carbonation, and FTL/K tests.

The variations in hydraulic conductivity and porosity of solidified samples after being exposed to various test scenarios are as follows:

- a) In the first experimental scenario (control), there was a negligible decrease in hydraulic conductivity followed by a slight increase in small pores. This reduction is because the sample heals itself with water flowing into it (De Belie et al., 2018).
- b) After the carbonation process, the hydraulic conductivity was reduced. The porosity images obtained by the CT scan showed an apparent decrease in porosity, resulting in self-healing. Carbonation led to the precipitation of calcite, which closed the pores, resulting in self-healing. The healing phenomenon is strongly linked to the growth of calcite. By the end of the test, the hydraulic conductivity had gone down by a further 20 %.

- c) The third test scenario involved mechanical loading. Due to microcracking, the hydraulic conductivity increased by slightly more than one order of magnitude. In addition, after ten days of water injection, the hydraulic conductivity was reduced by 10 % because of self-healing. This percentage is similar to the value obtained by Yıldırım et al. (2015).
- d) The fourth test scenario combined the effects of carbonation and loading. This test scenario led to a 20 % decrease of hydraulic conductivity after carbonation. This decrease was due to calcite precipitation in the connected voids. After loading, the hydraulic conductivity was increased by 1.13 orders of magnitude. The subsequent measurements of hydraulic conductivity progressively decreased by 21 %, i.e., the healing continued until the end of the tests.
- e) The last test scenario increased hydraulic conductivity by 1.1 orders of magnitude when the microcracks grew under mechanical loading conditions. These microcracks might increase CO₂ penetration. As a result, they diffuse CO₂ through the pores faster than in the previous test scenario. Also, during the first water injection cycle, the hydraulic conductivity sharply decreased by up to 77 %. This hydraulic conductivity reduction gradually slowed until it was relatively constant during the last four cycles.

However, in C/L and L/C scenarios, loading did not slow healing despite crack growth, resulting in hydraulic conductivity at the end of the test equal to or even a little higher than the initial result. Also, completely eliminating these fractures is impossible, but carbonation might minimize these factors by reducing the void percentage through self-healing. According to the results of hydraulic conductivity, it would seem that the more time to healing increases, the greater the amount of calcite formed on the crack surface. It can also be noted that the gains in mechanical resistance of the samples are zero. The resistance is lower for cracked samples such as the L scenario than for the carbonation scenario.

The pH values during the flow-through leaching test showed pH stability during the NC/NL and L scenario at 13. In contrast, significant drops in the pH of the pore solution to 6 were observed after carbonation in C, C/L, and L/C scenarios. In the scenario of NC/NL, the results show that light variations in the leachability of copper and silicon indicate that this metal is still well immobilized within the solidified sand samples. However, when the sample was exposed to carbonation, three phases of copper leaching were observed: significant increase, then partial decrease, and finally, a steady state. Generally, the insolubility of copper in alkaline media was more significant than in acidic media. The main hypothesis is a more increased dissolution and mobility of copper in acidic solutions at pH 6.

Mechanical loading tended to minimize copper leaching, and after a short period, no copper concentration was detected in the leachate of L scenario. However, these observations are not reflected in the scenarios of C/L and L/C. On the other hand, it was impossible to determine whether it came from the matrix's cracking or a new chemical reaction. However, this might indicate that chemical equilibrium did not occur because the water flows through the new paths due to loading. However, the release of copper was very low and did not exceed 2 mg/L. The contents of copper in the solution as average values are 0.08, 0.33, 0.06, 0.25, and 0.27 mg/L for NC/NL, C, L, C/L, and L/C scenarios, respectively. In general, under the experimental conditions (flow-through leaching conditions) used with DI water as leachant, the retention of Cu was good, with minimal leaching observed.

The release of calcium was different via various test scenarios. For example, in the absence of carbonation, such as in NC/NL and L scenarios, the results of calcium leaching remained stable at 750 mg/L for a long time. This phenomenon can be explained as follows: when deionized water reacts with solid hydrates in the pore solution, it modifies the pore solution's chemical equilibrium. Consequently, it induces the dissolution of $\text{Ca}(\text{OH})_2$; thus, it diffuses ions out of the material (Gérard, Le Bellego & Bernard, 2002). Again, to reach the state of chemical equilibrium, more hydrates materials (e.g., $\text{Ca}(\text{OH})_2$ and CSH-phases) are dissociated and dissolved immediately from the essential constituent of the matrix (Kuhl, Bangert & Meschke, 2004). The process of calcium dissolution primarily diminishes the physical properties of the

S/S matrix, which can have detrimental effects over the lifetime. Also, loading did not increase Cu, Al, Ca, and Si leachability. However, a significant reduce in calcium leaching was observed in the presence of carbonation during the C, C/L, and L/C scenarios. This can be explained as when CO₂ penetrates the sample, it dissolves in the pore solution and reacts with hydrated materials to form calcite. The leaching of calcium exhibits a higher rate compared to that of copper, silicon, and aluminum, indicating that the solidified sample may experience degradation before the complete leaching of metals occurs (Poon et al., 2001).

The carbonation tests were carried out by using 100% carbon dioxide. The penetration of CO₂ varied between test scenarios. The carbonation depth in the scenario of C/L is slightly greater than that in the L/C scenario. Additionally, the carbonation detection result was confirmed by the phenolphthalein test. This might also be explained by saying that increasing the healing period increases the depth of carbonation. Indeed, the process of carbon dioxide diffusion through the crack is significantly dependent on crack openings and rupture mechanics.

There are significant differences in porosity observed in the microstructure between non-leached and leached samples (based on test scenarios). Also, the initial microstructure of all test scenarios shows a similar or little difference in the percentage of porosity. As a result of the flow-through leaching test, a slight increase in pore volume was observed in the scenario of NC/NL. Moreover, carbonation significantly reduces the total porosity and hydraulic conductivity. The conformity in hydraulic conductivity and the porosity indicates that the pores are clogging due to calcite formation, which modifies the microstructure. Also, there was a clear relationship between increased hydraulic conductivity and total porosity in the scenarios of L, C/L, and L/C. This increase is related to the loading effect. Given the sensitivity of the CT analysis and despite the lack of data, the results of CT data show a good agreement with the experimental results. Thus, even if we could not achieve satisfying results in terms of determining the diffusion of CO₂ and healing products such as calcite, it turns out that the CT scans prove to be a promising tool for studying the microstructure of the solidified matrix.

The following technical and scientific recommendations can be formulated to better understand the behaviour of cement-based solidified sand contaminated with metals, considering the observations, results, and conclusions made within the framework of this research:

- This study focused on a single trace element, It would be interesting to carry out similar studies for other elements such as Zn, Pb, As. Similarly, these studies must be supplemented by solidified samples from the real field containing the trace elements studied to see the relationship between results for the standard laboratory tests and actual long-term performances in the field.
- As far as stability and durability studies are concerned, the scenarios that were presented in this thesis must be supplemented by tests involving other environmental stressors and variable experimental conditions, such as using different levels of confining stress. In addition, the potential risks of other environmental attacks, such as freeze/thaw cycles, should be examined.
- The results show that carbon dioxide is primarily responsible for self-healing. One of the questions raised by the study results is the effect of microcracks on carbon dioxide penetration. However, the diffusion of carbon dioxide through the crack is significantly increased, slowed down, or even stopped according to the crack opening. Thus, it is necessary to consider the measurement of crack size and rupture mechanics. Also, to understand the self-healing phenomenon and identify the healing products (i.e., calcite). Additional analysis, such as Energy Dispersion Spectrometry, is necessary to identify the presence of calcite within the pores.

The major contributions of this thesis can be summarized into four primary points: experimental scenarios, modified triaxial cell, flow-through leaching test, and Ct analysis. To simulate the environmental conditions, the development of experimental scenarios is needed. These series of proposed test scenarios are unique. Applying carbon dioxide combined with microcracks into the solidified sample under confining stresses is another distinctive feature of

this research. Regarding laboratory leaching tests, the flow-through leaching test remains limited. For predicting the long-term behaviour of solidified matrices, the CT scan is considered an essential tool. Also, the experimental results obtained in an aggressive environment will facilitate the development of numerical models to simulate the long-term performance of S/S. The stabilization/solidification technique is seldom used in Quebec, partly because of the absence of experimental data on the long-term performances of this technique. The aim of this experimental study is to enhance our understanding of stabilization/solidification technique by examining the effectiveness, applicability, and limitations of this method.

BIBLIOGRAPHY

- Ahn, T.-H., & Kishi, T. (2010). Crack self-healing behavior of cementitious composites incorporating various mineral admixtures. *Journal of Advanced Concrete Technology*, 8(2), 171-186.
- Akhavan, A., Shafaatian, S.-M.-H., & Rajabipour, F. (2012). Quantifying the effects of crack width, tortuosity, and roughness on water permeability of cracked mortars. *Cement and Concrete Research*, 42(2), 313-320.
- Al-Tabbaa, A., & Boes, N. (2002). Pilot in situ auger mixing treatment of a contaminated site. Part 4. Performance at five years. *Proceedings of the Institution of Civil Engineers-Geotechnical Engineering*, 155(3), 187-202.
- Al Tabbaa, A., & Stegemann, J. A. (2011). *Stabilisation/Solidification Treatment and Remediation: Proceedings of the International Conference on Stabilisation/Solidification Treatment and Remediation, 12-13 April 2005*, Cambridge, UK. CRC Press.
- Aligizaki, K. K. (2005). *Pore structure of cement-based materials: testing, interpretation and requirements*. CRC Press.
- Antemir, A., Hills, C., Carey, P., Magnie, M., & Poletini, A. (2010). Investigation of 4-year-old stabilised/solidified and accelerated carbonated contaminated soil. *Journal of hazardous materials*, 181(1-3), 543-555.
- Arandigoyen, M., Bicer-Simsir, B., Alvarez, J. I., & Lange, D. A. (2006). Variation of microstructure with carbonation in lime and blended pastes. *Applied surface science*, 252(20), 7562-7571.
- Arribas, I., Vegas, I., García, V., De La Villa, R. V., Martínez-Ramírez, S., & Frías, M. (2018). The deterioration and environmental impact of binary cements containing thermally activated coal mining waste due to calcium leaching. *Journal of Cleaner Production*, 183, 887-897.
- ASTM International. *Standard test method for sieve analysis of fine and coarse aggregates*. International standard, ASTM C136M-19, West Conshohocken (PA): ASTM, 2019, 5 p.

- ASTM International. *Standard practice for classification of soils for engineering purposes (unified soil classification system)*. International standard, ASTM D2487-17, West Conshohocken (PA): ASTM, 2017, 10 p.
- ASTM International. *Standard practice for making and curing concrete test specimens in the laboratory*. International standard, ASTM C192M-19, West Conshohocken (PA): ASTM, 2019, 8 p.
- ASTM International. *Standard practice for capping cylindrical concrete specimens*. International standard, ASTM C617M-15, West Conshohocken (PA): ASTM, 2015, 6 p.
- ASTM International. *Standard test methods for measurement of hydraulic conductivity of saturated porous materials using a flexible wall permeameter*. International standard, ASTM D5084-16a, West Conshohocken (PA): ASTM, 2016, 24 p.
- ASTM International. *Standard test method for compressive strength of cylindrical concrete specimens*. International standard, ASTM C39M-21, West Conshohocken (PA): ASTM, 2021, 8 p.
- ASTM International. *Standard performance specification for hydraulic cement*. International standard, ASTM C1157-08, West Conshohocken (PA): ASTM, 2008, 5 p.
- Ashraf, W. (2016). Carbonation of cement-based materials: Challenges and opportunities. *Construction and Building Materials*, 120, 558-570.
- Auroy, M., Poyet, S., Le Bescop, P., Torrenti, J.-M., Charpentier, T., Moskura, M., & Bourbon, X. (2015). Impact of carbonation on unsaturated water transport properties of cement-based materials. *Cement and Concrete Research*, 74, 44-58.
- Badreddine, R., Humez, A.-N., Mingelgrin, U., Benchara, A., Meducin, F., & Prost, R. (2004). Retention of trace metals by solidified/stabilized wastes: assessment of long-term metal release. *Environmental science & technology*, 38(5), 1383-1398.
- Bahafid, S., Ghabezloo, S., Duc, M., Faure, P., & Sulem, J. (2017). Effect of the hydration temperature on the microstructure of Class G cement: CSH composition and density. *Cement and Concrete Research*, 95, 270-281.
- Banthia, N., Biparva, A., & Mindess, S. (2005). Permeability of concrete under stress. *Cement and Concrete Research*, 35(9), 1651-1655.

- Banthia, N., & Mindess, S. (1989). Water permeability of cement paste. *Cement and Concrete Research*, 19(5), 727-736.
- Bao, J., Wang, L., & Xiao, M. (2016). Changes in speciation and leaching behaviors of heavy metals in dredged sediment solidified/stabilized with various materials. *Environmental Science and Pollution Research*, 23(9), 8294-8301.
- Barenblatt, G. I. (1959). The formation of equilibrium cracks during brittle fracture. General ideas and hypotheses. Axially-symmetric cracks. *Journal of Applied Mathematics and Mechanics*, 23(3), 622-636.
- Barnard, L., Boardman, D., Rogers, C., Hills, C., Carey, P., Canning, K., & MacLeod, C. (2005). Influence of soil and binder properties on the efficacy of accelerated carbonation. Dans *Proceedings of the International Conference on Stabilisation/Solidification Treatment and Remediation* (pp. 285-296).
- Bates, E., & Hills, C. (2015). Stabilization and solidification of contaminated soil and waste: A manual of practice. *Hyggc Media*.
- Bech, J., Duran, P., Roca, N., Poma, W., Sánchez, I., Roca-Pérez, L., & Poschenrieder, C. (2012). Accumulation of Pb and Zn in *Bidens triplinervia* and *Senecio* sp. spontaneous species from mine spoils in Peru and their potential use in phytoremediation. *Journal of Geochemical Exploration*, 123, 109-113.
- Bentz, D. P., Haecker, C.-J., Peltz, M. A., & Snyder, K. A. (2008). X-ray absorption studies of drying of cementitious tile adhesive mortars. *Cement and concrete composites*, 30(5), 361-373.
- Bertos, M. F., Simons, S., Hills, C., & Carey, P. (2004). A review of accelerated carbonation technology in the treatment of cement-based materials and sequestration of CO₂. *Journal of hazardous materials*, 112(3), 193-205.
- Bisschop, J., & Wittel, F. K. (2011). Contraction gradient induced microcracking in hardened cement paste. *Cement and concrete composites*, 33(4), 466-473.
- Black, L., Garbev, K., & Gee, I. (2008). Surface carbonation of synthetic CSH samples: A comparison between fresh and aged CSH using X-ray photoelectron spectroscopy. *Cement and Concrete Research*, 38(6), 745-750.
- Blackman Jr, W. C. (2016). *Basic hazardous waste management*. CRC press.

- Bone, B., Barnard, L., Boardman, D., Carey, P., Hills, C., Jones, H., Tyrer, M. (2004). Review of scientific literature on the use of stabilisation/solidification for the treatment of contaminated soil, solid waste and sludges (SC980003/SR2). *The Environment Agency, Bristol*.
- Bonen, D., & Sarkar, S. L. (1995). The superplasticizer adsorption capacity of cement pastes, pore solution composition, and parameters affecting flow loss. *Cement and Concrete Research*, 25(7), 1423-1434.
- Branch, J., Kosson, D., Garrabrants, A., & He, P. (2016). The impact of carbonation on the microstructure and solubility of major constituents in microconcrete materials with varying alkalinities due to fly ash replacement of ordinary Portland cement. *Cement and Concrete Research*, 89, 297-309.
- Brouwers, H. (2003). Alkali concentrations of pore solution in hydrating OPC. *Cement and Concrete Research*, 33(2), 191-196.
- Bukowski, J., & Berger, R. L. (1979). Reactivity and strength development of CO₂ activated non-hydraulic calcium silicates. *Cement and Concrete Research*, 9(1), 57-68.
- Bullard, J. W., Jennings, H. M., Livingston, R. A., Nonat, A., Scherer, G. W., Schweitzer, J. S., Thomas, J. J. (2011). Mechanisms of cement hydration. *Cement and Concrete Research*, 41(12), 1208-1223.
- Burlion, N., Bernard, D., & Chen, D. (2006). X-ray microtomography: application to microstructure analysis of a cementitious material during leaching process. *Cement and Concrete Research*, 36(2), 346-357.
- Butcher, E., Borwick, J., Collier, N., & Williams, S. (2012). Long term leachate evolution during flow-through leaching of a vault backfill (NRVB). *Mineralogical Magazine*, 76(8), 3023-3031.
- Butcher, E., Cheeseman, C., Sollars, C., & Perry, R. (1993). Flow-through leach testing of solidified waste using a modified triaxial cell. *Environmental technology*, 14(2), 113-124.
- Butcher, E. J., Cheeseman, C. R., Sollars, C. J., & Perry, R. (1996). Flow-through leach testing applied to stabilized/solidified wastes. Dans *Stabilization and Solidification of Hazardous, Radioactive, and Mixed Wastes: 3rd Volume*. ASTM International.

- Caldwell, R., Rawlinson, S., Butcher, E., & Godfrey, L. (2011). Characterisation of full-scale historic inactive cement-based intermediate level nuclear wasteforms. *Stabilisation/Solidification Treatment and Remediation, Advances for S/S in Waste Contaminated Land*, 139-148.
- Carlson, W. D., Denison, C., & Ketcham, R. A. (2000). High-resolution X-ray computed tomography as a tool for visualization and quantitative analysis of igneous textures in three dimensions. *Visual Geosciences*, 4(3), 1-14.
- Castellote, M., Fernandez, L., Andrade, C., & Alonso, C. (2009). Chemical changes and phase analysis of OPC pastes carbonated at different CO₂ concentrations. *Materials and Structures*, 42(4), 515-525.
- Catalan, L., & Wetteskind, K. (2002). Alkalinity depletion by flow-through leaching in stabilized/solidified natrojarosite waste. *WIT Transactions on Ecology and the Environment*, 56.
- Catalan, L. J., Merlière, E., & Chezick, C. (2002). Study of the physical and chemical mechanisms influencing the long-term environmental stability of natrojarosite waste treated by stabilization/solidification. *Journal of hazardous materials*, 94(1), 63-88.
- Chang, S.-H., & Lee, C.-I. (2004). Estimation of cracking and damage mechanisms in rock under triaxial compression by moment tensor analysis of acoustic emission. *International Journal of Rock Mechanics and Mining Sciences*, 41(7), 1069-1086.
- Chen, J. J., Thomas, J. J., & Jennings, H. M. (2006). Decalcification shrinkage of cement paste. *Cement and Concrete Research*, 36(5), 801-809.
- Chen, Q., Hills, C., Tyrer, M., Slipper, I., Shen, H., & Brough, A. (2007). Characterisation of products of tricalcium silicate hydration in the presence of heavy metals. *Journal of hazardous materials*, 147(3), 817-825.
- Chen, Q., Tyrer, M., Hills, C. D., Yang, X., & Carey, P. (2009). Immobilisation of heavy metal in cement-based solidification/stabilisation: a review. *Waste management*, 29(1), 390-403.
- Chen, Q., Zhang, L., Ke, Y., Hills, C., & Kang, Y. (2009). Influence of carbonation on the acid neutralization capacity of cements and cement-solidified/stabilized electroplating sludge. *Chemosphere*, 74(6), 758-764.
- Chen, Y., Liu, P., & Yu, Z. (2018). Effects of environmental factors on concrete carbonation depth and compressive strength. *Materials*, 11(11), 2167.

- Cheng, A., Chao, S.-J., & Lin, W.-T. (2013). Effects of leaching behavior of calcium ions on compression and durability of cement-based materials with mineral admixtures. *Materials*, 6(5), 1851-1872.
- Chiu, A. C., Akeseh, R., & Amokwaw, G. (2018). Laboratory Assessment of Impact of Copper and Lead on Solidified/Stabilized Material. *KSCE Journal of Civil Engineering*, 22(10), 3783-3790.
- Choinska, M., Khelidj, A., Chatzigeorgiou, G., & Pijaudier-Cabot, G. (2007). Effects and interactions of temperature and stress-level related damage on permeability of concrete. *Cement and Concrete Research*, 37(1), 79-88.
- Claisse, P. A., El-Sayad, H., & Shaaban, I. G. (1999). Permeability and pore volume of carbonated concrete. *ACI Materials Journal*, 96(3), 378-381.
- Clear, C. A (1985). *The effects of autogenous healing upon the leakage of water through cracks in concrete*. Cement and Concrete Association: Technical Report No. 559.
- Cnudde, V., & Boone, M. N. (2013). High-resolution X-ray computed tomography in geosciences: A review of the current technology and applications. *Earth-Science Reviews*, 123, 1-17.
- Collier, N. C. (2016). Transition and decomposition temperatures of cement phases—a collection of thermal analysis data. *Ceramics-Silikaty*, 60(4), pp. 338-343.
- Conner, J. R., & Hoeffner, S. L. (1998). A critical review of stabilization/solidification technology. *Critical reviews in environmental science and technology*, 28(4), 397-462.
- Conner, J. R., & Hoeffner, S. L. (1998). The history of stabilization/solidification technology. *Critical reviews in environmental science and technology*, 28(4), 325-396.
- Constantinides, G., & Ulm, F.-J. (2004). The effect of two types of CSH on the elasticity of cement-based materials: Results from nanoindentation and micromechanical modeling. *Cement and Concrete Research*, 34(1), 67-80.
- Coumes, C. C. D., Courtois, S., Nectoux, D., Leclercq, S., & Bourbon, X. (2006). Formulating a low-alkalinity, high-resistance and low-heat concrete for radioactive waste repositories. *Cement and Concrete Research*, 36(12), 2152-2163.
- Cui, H., Tang, W., Liu, W., Dong, Z., & Xing, F. (2015). Experimental study on effects of CO₂ concentrations on concrete carbonation and diffusion mechanisms. *Construction and Building Materials*, 93, 522-527.

- Czarnecki, L., & Woyciechowski, P. (2015). Modelling of concrete carbonation; is it a process unlimited in time and restricted in space? *Bulletin of the Polish Academy of Sciences: Technical Sciences*, (1).
- Dalton, J. L., Gardner, K. H., Seager, T. P., Weimer, M. L., Spear, J. C., & Magee, B. J. (2004). Properties of Portland cement made from contaminated sediments. *Resources, conservation and recycling*, 41(3), 227-241.
- De Argandona, V. R., Rey, A. R., Celorio, C., Del Río, L. S., Calleja, L., & Llavona, J. (1999). Characterization by computed X-ray tomography of the evolution of the pore structure of a dolomite rock during freeze-thaw cyclic tests. *Physics and Chemistry of the Earth, Part A: Solid Earth and Geodesy*, 24(7), 633-637.
- De Belie, N., Gruyaert, E., Al-Tabbaa, A., Antonaci, P., Baera, C., Bajare, D., Jefferson, T. (2018). A review of self-healing concrete for damage management of structures. *Advanced materials interfaces*, 5(17), 1800074.
- De Ceukelaire, L., & Van Nieuwenburg, D. (1993). Accelerated carbonation of a blast-furnace cement concrete. *Cement and Concrete Research*, 23(2), 442-452.
- Dermatas, D., Xu, X., Cao, X., Shen, G., Menounou, N., Arienti, P., & Delaney, J. (2005). An evaluation of pozzolanic lead immobilization mechanisms in firing range soils. A. Al-Tabbaa, Stagemann (Eds.), *Stabilization/Solidification Treatment and Remediation*, Taylor & Francis, pp. 45-56
- Dewaele, P., Reardon, E., & Dayal, R. (1991). Permeability and porosity changes associated with cement grout carbonation. *Cement and Concrete Research*, 21(4), 441-454.
- Dhaliwal, S. S., Singh, J., Taneja, P. K., & Mandal, A. (2020). Remediation techniques for removal of heavy metals from the soil contaminated through different sources: a review. *Environmental Science and Pollution Research*, 27(2), 1319-1333.
- Dias, W. (2000). Reduction of concrete sorptivity with age through carbonation. *Cement and Concrete Research*, 30(8), 1255-1261.
- Dow, C., & Glasser, F. P. (2003). Calcium carbonate efflorescence on Portland cement and building materials. *Cement and Concrete Research*, 33(1), 147-154.
- Du, Y.-J., Liu, S.-Y., Liu, Z.-B., Chen, L., Zhang, F., & Jin, F. (2010). An overview of stabilization/solidification technique for heavy metals contaminated soils. *Advances in environmental Geotechnics*, 760-766.

- Du, Y.-J., Wei, M.-L., Reddy, K. R., & Wu, H.-I. (2016). Effect of carbonation on leachability, strength and microstructural characteristics of KMP binder stabilized Zn and Pb contaminated soils. *Chemosphere*, *144*, 1033-1042.
- Dullien, F. A. (2012). *Porous media: fluid transport and pore structure*. Academic press.
- Ekolu, S. (2016). A review on effects of curing, sheltering, and CO₂ concentration upon natural carbonation of concrete. *Construction and Building Materials*, *127*, 306-320.
- Ekström, T. (2003). *Leaching of concrete. The leaching process and its effects*. (Doctoral thesis, Lund University, Lund, Sweden).
- El Bedoui, S., Duhaime, F., & Dubé, J.-S. (2018). Impact of carbonation on chemical and mineralogical properties of stabilized and solidified matrices, paper presented at 71th Canadian Geotechnical Conference, GeoEdmonton 2018. Edmonton, AB.
- Elsalamawy, M., Mohamed, A. R., & Kamal, E. M. (2019). The role of relative humidity and cement type on carbonation resistance of concrete. *Alexandria Engineering Journal*, *58*(4), 1257-1264.
- Fattuhi, N. (1988). Concrete carbonation as influenced by curing regime. *Cement and Concrete Research*, *18*(3), 426-430.
- Ferrara, L., Van Mullem, T., Alonso, M. C., Antonaci, P., Borg, R. P., Cuenca, E., Roig-Flores, M. (2018). Experimental characterization of the self-healing capacity of cement based materials and its effects on the material performance: A state of the art report by COST Action SARCOS WG2. *Construction and Building Materials*, *167*, 115-142.
- Fukuda, D., Nara, Y., Kobayashi, Y., Maruyama, M., Koketsu, M., Hayashi, D., . . . Kaneko, K. (2012). Investigation of self-sealing in high-strength and ultra-low-permeability concrete in water using micro-focus X-ray CT. *Cement and Concrete Research*, *42*(11), 1494-1500.
- Garrabrants, A., Sanchez, F., & Kosson, D. (2004). Changes in constituent equilibrium leaching and pore water characteristics of a Portland cement mortar as a result of carbonation. *Waste management*, *24*(1), 19-36.
- Gartner, E., Young, J., Damidot, D., & Jawed, I. (2002). Hydration of Portland cement. *Structure and performance of cements*, *2*, 57-113.
- Gérard, B., Le Bellego, C., & Bernard, O. (2002). Simplified modelling of calcium leaching of concrete in various environments. *Materials and Structures*, *35*(10), 632-640.

- Gerges, N. N., Issa, C. A., & Fawaz, S. (2015). Effect of construction joints on the splitting tensile strength of concrete. *Case Studies in Construction Materials*, 3, 83-91.
- Glasser, F. (1997). Fundamental aspects of cement solidification and stabilisation. *Journal of hazardous materials*, 52(2-3), 151-170.
- Głowacki, A., Bouin, C., Ethier, Y., Dubé, J.-S., & Duhaime, F. (2018). Using CT-scanning to study internal erosion in soils, paper presented at 71th Canadian Geotechnical Conference, GeoEdmonton 2018. Edmonton, AB.
- Gollmann, M. A., da Silva, M. M., Masuero, Â. B., & dos Santos, J. H. Z. (2010). Stabilization and solidification of Pb in cement matrices. *Journal of hazardous materials*, 179(1-3), 507-514.
- Granger, S., Loukili, A., Pijaudier-Cabot, G., & Chanvillard, G. (2007). Experimental characterization of the self-healing of cracks in an ultra high performance cementitious material: Mechanical tests and acoustic emission analysis. *Cement and Concrete Research*, 37(4), 519-527.
- Groves, G., Rodway, D., & Richardson, I. (1990). The carbonation of hardened cement pastes. *Advances in Cement research*, 3(11), 117-125.
- Haach, V. G., Vasconcelos, G., & Lourenço, P. B. (2011). Influence of aggregates grading and water/cement ratio in workability and hardened properties of mortars. *Construction and Building Materials*, 25(6), 2980-2987.
- Haga, K., Sutou, S., Hironaga, M., Tanaka, S., & Nagasaki, S. (2005). Effects of porosity on leaching of Ca from hardened ordinary Portland cement paste. *Cement and Concrete Research*, 35(9), 1764-1775.
- Halim, C. E., Amal, R., Beydoun, D., Scott, J. A., & Low, G. (2004). Implications of the structure of cementitious wastes containing Pb (II), Cd (II), As (V), and Cr (VI) on the leaching of metals. *Cement and Concrete Research*, 34(7), 1093-1102.
- Hearn, N. (1998). Self-sealing, autogenous healing and continued hydration: What is the difference? *Materials and Structures*, 31(8), 563-567.
- Hearn, N. (1999). Effect of shrinkage and load-induced cracking on water permeability of concrete. *Materials Journal*, 96(2), 234-241.
- Herbert, E. N., & Li, V. C. (2013). Self-healing of microcracks in engineered cementitious composites (ECC) under a natural environment. *Materials*, 6(7), 2831-2845.

- Heukamp, F. H., Ulm, F.-J., & Germaine, J. T. (2003). Poroplastic properties of calcium-leached cement-based materials. *Cement and Concrete Research*, 33(8), 1155-1173.
- Hillerborg, A., Modéer, M., & Petersson, P.-E. (1976). Analysis of crack formation and crack growth in concrete by means of fracture mechanics and finite elements. *Cement and Concrete Research*, 6(6), 773-781.
- Hills, C., Sweeney, R., & Buenfeld, N. (1999). Microstructural study of carbonated cement-solidified synthetic heavy metal waste. *Waste management*, 19(5), 325-331.
- Hjelmar, O. (1996). Disposal strategies for municipal solid waste incineration residues. *Journal of hazardous materials*, 47(1-3), 345-368.
- Hornain, H., Marchand, J., Ammouche, A., Commene, J., & Moranville, M. (1996). Microscopic observation of cracks in concrete—A new sample preparation technique using dye impregnation. *Cement and Concrete Research*, 26(4), 573-583.
- Horpibulsuk, S., Katkan, W., Sirilerdwattana, W., & Rachan, R. (2006). Strength development in cement stabilized low plasticity and coarse grained soils: Laboratory and field study. *Soils and Foundations*, 46(3), 351-366.
- Hoseini, M., Bindiganavile, V., & Banthia, N. (2009). The effect of mechanical stress on permeability of concrete: A review. *Cement and concrete composites*, 31(4), 213-220.
- Houst, Y. F. (1997). Carbonation shrinkage of hydrated cement paste. Dans *Proc. 4th CANMET/ACI International Conference on Durability of Concrete* (pp. 481-491). CANMET, Ottawa, Canada.
- Hu, J., Ge, Z., & Wang, K. (2014). Influence of cement fineness and water-to-cement ratio on mortar early-age heat of hydration and set times. *Construction and Building Materials*, 50, 657-663.
- Huang, H., Ye, G., & Damidot, D. (2014). Effect of blast furnace slag on self-healing of microcracks in cementitious materials. *Cement and Concrete Research*, 60, 68-82.
- Hussain, M., Pu, L., & Underwood, J. (1974). Strain Energy Release Rate for. Dans *Proceedings of the 1973 National Symposium on Fracture Mechanics, University of Maryland, College Park, Md., 27-29 Aug. 1973* (Vol. 559, pp. 2).
- Imran, I., & Pantazopoulou, S. J. (1996). Experimental study of plain concrete under triaxial stress. *ACI Materials Journal-American Concrete Institute*, 93(6), 589-601.

- Isgor, O. B., & Razaqpur, A. G. (2004). Finite element modeling of coupled heat transfer, moisture transport and carbonation processes in concrete structures. *Cement and concrete composites*, 26(1), 57-73.
- ISO. (2007). ISO 11885: 2007: Water quality—determination of selected elements by inductively coupled plasma optical emission spectrometry (ICP-OES): ISO Geneva, Switzerland.
- Iyer, S., & Sinha, S. K. (2005). A robust approach for automatic detection and segmentation of cracks in underground pipeline images. *Image and Vision Computing*, 23(10), 921-933.
- Jackson, D. R., Garrett, B. C., & Bishop, T. A. (1984). Comparison of batch and column methods for assessing leachability of hazardous waste. *Environmental science & technology*, 18(9), 668-673.
- Jacobsen, S., & Sellevold, E. J. (1996). Self healing of high strength concrete after deterioration by freeze/thaw. *Cement and Concrete Research*, 26(1), 55-62.
- Jiangying, L., Dimin, X., Xiong, L., Hills, C., Carey, P., & Gardner, K. (2008). Comparison of properties of traditional and accelerated carbonated solidified/stabilized contaminated soils. *Journal of Environmental Sciences*, 20(5), 593-598.
- Jing, P., Song, X., Zhang, J., & Nowamooz, H. (2022). A review of hydro-mechanical coupling behaviour of cement-treated materials. *Construction and Building Materials*, 322, 126446.
- Johannesson, B., & Utgenannt, P. (2001). Microstructural changes caused by carbonation of cement mortar. *Cement and Concrete Research*, 31(6), 925-931.
- Johnson, D., MacLeod, C., Carey, P., & Hills, C. (2003). Solidification of stainless steel slag by accelerated carbonation. *Environmental technology*, 24(6), 671-678.
- Jolous Jamshidi, R. (2014). *Evaluation of cement-treated soils subjected to cycles of freezing and thawing*. (Doctoral thesis, Dalhousie University of Halifax, Nova Scotia, Canada).
- Kaddhour, G., Andò, E., Salager, S., Bésuelle, P., Viggiani, C., Hall, S., & Desrues, J. (2013). Application of X-ray tomography to the characterisation of grain-scale mechanisms in sand. Dans *Multiphysical testing of soils and shales* (pp. 195-200). Springer.

- Kakali, G., Tsvivilis, S., & Tsialtas, A. (1998). Hydration of ordinary portland cements made from raw mix containing transition element oxides. *Cement and Concrete Research*, 28(3), 335-340.
- Kangni-Foli, E., Poyet, S., Le Bescop, P., Charpentier, T., Bernachy-Barbé, F., Dauzères, A., de Lacaillerie, J.-B. d. E. (2021). Carbonation of model cement pastes: The mineralogical origin of microstructural changes and shrinkage. *Cement and Concrete Research*, 144, 106446.
- Kantro, D. L. (1975). Tricalcium silicate hydration in the presence of various salts. *ASTM Journal of Testing and Evaluation*, 3(4).
- Katsuura, H., Inoue, T., Hiraoka, M., & Sakai, S. (1996). Full-scale plant study on fly ash treatment by the acid extraction process. *Waste management*, 16(5-6), 491-499.
- Khan, M. I., & Lynsdale, C. (2002). Strength, permeability, and carbonation of high-performance concrete. *Cement and Concrete Research*, 32(1), 123-131.
- Klich, I., Batchelor, B., Wilding, L., & Drees, L. (1999). Mineralogical alterations that affect the durability and metals containment of aged solidified and stabilized wastes. *Cement and Concrete Research*, 29(9), 1433-1440.
- Kogbara, R. B. (2014). A review of the mechanical and leaching performance of stabilized/solidified contaminated soils. *Environmental reviews*, 22(1), 66-86.
- Kogbara, R. B., Al-Tabbaa, A., Yi, Y., & Stegemann, J. A. (2013). Cement–fly ash stabilisation/solidification of contaminated soil: Performance properties and initiation of operating envelopes. *Applied Geochemistry*, 33, 64-75.
- Komonweeraket, K., Cetin, B., Aydilek, A. H., Benson, C. H., & Edil, T. B. (2015). Effects of pH on the leaching mechanisms of elements from fly ash mixed soils. *Fuel*, 140, 788-802.
- Kovalčíková, M., & Eštoková, A. (2014). Leaching of calcium and silicon from cement composites in the aggressive environment. *Pollack Periodica*, 9(2), 123-130.
- Kong, W., Wei, Y., Wang, S., Chen, J., & Wang, Y. (2020). Research progress on cement-based materials by X-ray computed tomography. *International Journal of Pavement Research and Technology*, 13, 366-375.

- Kongsukprasert, L., Tatsuoka, F., & Takahashi, H. (2007). Effects of curing period and stress conditions on the strength and deformation characteristics of cement-mixed soil. *Soils and Foundations*, 47(3), 577-596.
- Kuhl, D., Bangert, F., & Meschke, G. (2004). Coupled chemo-mechanical deterioration of cementitious materials. Part I: Modeling. *International Journal of Solids and Structures*, 41(1), 15-40.
- Lange, L., Hills, C., & Poole, A. (1996). The effect of accelerated carbonation on the properties of cement-solidified waste forms. *Waste management*, 16(8), 757-763.
- Lange, L. C., Hills, C. D., & Poole, A. B. (1995). Preliminary investigation into the effects of carbonation on cement-solidified hazardous wastes. *Environmental science & technology*, 30(1), 25-30.
- Lanzón, M., Cnudde, V., De Kock, T., & Dewanckele, J. (2012). X-ray microtomography (μ -CT) to evaluate microstructure of mortars containing low density additions. *Cement and concrete composites*, 34(9), 993-1000.
- Lee, K. J., & Lee, T. G. (2012). A review of international trends in mercury management and available options for permanent or long-term mercury storage. *Journal of hazardous materials*, 241, 1-13.
- Lerigoleur, E. (2014). Effect of early age carbonation curing on the microstructure of cement paste.
- Levy, D., Barbarick, K., Siemer, E., & Sommers, L. (1992). Distribution and partitioning of trace metals in contaminated soils near Leadville, Colorado. *Journal of Environmental Quality*, 21(2), 185-195.
- Li, V. C., & Yang, E.-H. (2007). Self healing in concrete materials. Dans *Self healing materials* (pp. 161-193). Springer.
- Li, X., Poon, C. S., Sun, H., Lo, I., & Kirk, D. W. (2001). Heavy metal speciation and leaching behaviors in cement based solidified/stabilized waste materials. *Journal of hazardous materials*, 82(3), 215-230.
- Loo, Y., Chin, M., Tam, C., & Ong, K. (1994). A carbonation prediction model for accelerated carbonation testing of concrete. *Magazine of Concrete Research*, 46(168), 191-200.
- Ma, X., Pan, J., Cai, J., Zhang, Z., & Han, J. (2021). A review on cement-based materials used in steel structures as fireproof coating. *Construction and Building Materials*, 125623.

- Mainguy, M., Tognazzi, C., Torrenti, J.-M., & Adenot, F. (2000). Modelling of leaching in pure cement paste and mortar. *Cement and Concrete Research*, 30(1), 83-90.
- Meredith, P., Donald, A., Meller, N., & Hall, C. (2004). Tricalcium aluminate hydration: Microstructural observations by in-situ electron microscopy. *Journal of materials science*, 39(3), 997-1005.
- Metalssi, O. O., Aït-Mokhtar, A., Turcry, P., & Ruot, B. (2012). Consequences of carbonation on microstructure and drying shrinkage of a mortar with cellulose ether. *Construction and Building Materials*, 34, 218-225.
- Mohammadi, A., Ghiasvand, E., & Nili, M. (2020). Relation between mechanical properties of concrete and alkali-silica reaction (ASR); a review. *Construction and Building Materials*, 258, 119567.
- Morandau, A., Thiery, M., & Dangla, P. (2014). Investigation of the carbonation mechanism of CH and CSH in terms of kinetics, microstructure changes and moisture properties. *Cement and Concrete Research*, 56, 153-170.
- Morandau, A., Thiéry, M., & Dangla, P. (2015). Impact of accelerated carbonation on OPC cement paste blended with fly ash. *Cement and Concrete Research*, 67, 226-236.
- Morshed, A. Z., & Shao, Y. (2013). Influence of moisture content on CO₂ uptake in lightweight concrete subject to early carbonation. *Journal of Sustainable Cement-Based Materials*, 2(2), 144-160.
- Müllauer, W., Beddoe, R. E., & Heinz, D. (2012). Effect of carbonation, chloride and external sulphates on the leaching behaviour of major and trace elements from concrete. *Cement and concrete composites*, 34(5), 618-626.
- Nakarai, K., & Yoshida, T. (2015). Effect of carbonation on strength development of cement-treated Toyoura silica sand. *Soils and Foundations*, 55(4), 857-865.
- Narayanan, N., & Ramamurthy, K. (2000). Structure and properties of aerated concrete: a review. *Cement and concrete composites*, 22(5), 321-329.
- Neithalath, N., Weiss, J., & Olek, J. (2006). Characterizing enhanced porosity concrete using electrical impedance to predict acoustic and hydraulic performance. *Cement and Concrete Research*, 36(11), 2074-2085.
- Neville, A. M., & Brooks, J. J. (1987). *Concrete technology*. Longman Scientific & Technical England.

- Ngala, V., & Page, C. (1997). Effects of carbonation on pore structure and diffusional properties of hydrated cement pastes. *Cement and Concrete Research*, 27(7), 995-1007.
- Nishikawa, T., & Suzuki, K. (1994). Chemical conversion of C- S- H in concrete. *Cement and Concrete Research*, 24(1), 176-182.
- Ortolan, V., Mancio, M., & Tutikian, B. (2016). Evaluation of the influence of the pH of concrete pore solution on the corrosion resistance of steel reinforcement. *Journal of Building Pathology and Rehabilitation*, 1(1), 1-7.
- Otsu, N. (1979). A threshold selection method from gray-level histograms. *IEEE transactions on systems, man, and cybernetics*, 9(1), 62-66.
- Pandey, B., Kinrade, S. D., & Catalan, L. J. (2012). Effects of carbonation on the leachability and compressive strength of cement-solidified and geopolymer-solidified synthetic metal wastes. *Journal of Environmental Management*, 101, 59-67.
- Pang, B., Zhou, Z., Hou, P., Du, P., Zhang, L., & Xu, H. (2016). Autogenous and engineered healing mechanisms of carbonated steel slag aggregate in concrete. *Construction and Building Materials*, 107, 191-202.
- Paria, S., & Yuet, P. K. (2006). Solidification–stabilization of organic and inorganic contaminants using portland cement: a literature review. *Environmental reviews*, 14(4), 217-255.
- Park, C.-K. (2000). Hydration and solidification of hazardous wastes containing heavy metals using modified cementitious materials. *Cement and Concrete Research*, 30(3), 429-435.
- Perera, A., Al-Tabbaa, A., Reid, J., & Stegemann, J. (2011). Part IV: Testing and performance criteria. *Stabilisation/Solidification Treatment and Remediation Advances in S/S for Waste and Contaminated Land*, 415-435.
- Phung, Q. T., Maes, N., Jacques, D., Bruneel, E., Van Driessche, I., Ye, G., & De Schutter, G. (2015). Effect of limestone fillers on microstructure and permeability due to carbonation of cement pastes under controlled CO₂ pressure conditions. *Construction and Building Materials*, 82, 376-390.
- Picandet, V., Khelidj, A., & Bellegou, H. (2009). Crack effects on gas and water permeability of concretes. *Cement and Concrete Research*, 39(6), 537-547.

- Pihlajavaara, S. (1968). Some results of the effect of carbonation on the porosity and pore size distribution of cement paste. *Matériaux et Construction*, 1(6), 521-527.
- Plassard, F., Winiarski, T., & Petit-Ramel, M. (2000). Retention and distribution of three heavy metals in a carbonated soil: comparison between batch and unsaturated column studies. *Journal of Contaminant Hydrology*, 42(2-4), 99-111.
- Plummer, L. N., & Busenberg, E. (1982). The solubilities of calcite, aragonite and vaterite in CO₂-H₂O solutions between 0 and 90 C, and an evaluation of the aqueous model for the system CaCO₃-CO₂-H₂O. *Geochimica et cosmochimica acta*, 46(6), 1011-1040.
- Poon, C., Qiao, X., & Cheeseman, C. (2011). Applications of rejected fly ash in stabilization and solidification processes. Dans *Stabilisation/Solidification Treatment and Remediation: Proceedings of the International Conference on Stabilisation/Solidification Treatment and Remediation, 12-13 April 2005, Cambridge, UK* (pp. 63). CRC Press.
- Poon, C. S., & Chen, Z. Q. (1999). Comparison of the characteristics of flow-through and flow-around leaching tests of solidified heavy metal wastes. *Chemosphere*, 38(3), 663-680.
- Poon, C. S., Chen, Z. Q., & Wai, O. (1999). A flow-through leaching model for monolithic chemically stabilized/solidified hazardous waste. *Journal of the Air & Waste Management Association*, 49(5), 569-575.
- Poon, C. S., Chen, Z. Q., & Wai, O. W. (2001). The effect of flow-through leaching on the diffusivity of heavy metals in stabilized/solidified wastes. *Journal of hazardous materials*, 81(1-2), 179-192.
- Popovics, S., & Ujhelyi, J. (2008). Contribution to the concrete strength versus water-cement ratio relationship. *Journal of materials in civil engineering*, 20(7), 459-463.
- Poursaeed, A. (2016). Corrosion of steel in concrete structures. Dans *Corrosion of steel in concrete structures* (pp. 19-33). Elsevier.
- Ramm, W., & Biscop, M. (1998). Autogenous healing and reinforcement corrosion of water-penetrated separation cracks in reinforced concrete. *Nuclear Engineering and Design*, 179(2), 191-200.

- Ranachowski, Z., Józwiak-Niedźwiedzka, D., Ranachowski, P., Rejmund, F., Dąbrowski, M., Kudela Jr, S., & Dvorak, T. (2014). Application of X-ray microtomography and optical microscopy to determine the microstructure of concrete penetrated by carbon dioxide/Zastosowanie Mikrotomografii Komputerowej I Mikroskopii Optycznej Do Oceny Mikrostruktury Betonów Poddanych Działaniu Co₂. *Archives of Metallurgy and Materials*, (4).
- Rani, D. A., Boccaccini, A., Deegan, D., & Cheeseman, C. (2008). Air pollution control residues from waste incineration: current UK situation and assessment of alternative technologies. *Waste management*, 28(11), 2279-2292.
- Rao, N. V., & Meena, T. (2017). A review on carbonation study in concrete. Dans *IOP Conference Series: Materials Science and Engineering* (Vol. 263, pp. 032011). IOP Publishing.
- Reinhardt, H.-W., & Jooss, M. (2003). Permeability and self-healing of cracked concrete as a function of temperature and crack width. *Cement and Concrete Research*, 33(7), 981-985.
- Rha, C. Y., Kang, S. K., & Kim, C. E. (2000). Investigation of the stability of hardened slag paste for the stabilization/solidification of wastes containing heavy metal ions. *Journal of hazardous materials*, 73(3), 255-267.
- Rose, J., Benard, A., El Mrabet, S., Masion, A., Moulin, I., Briois, V., . . . Bottero, J.-Y. (2006). Evolution of iron speciation during hydration of C4AF. *Waste management*, 26(7), 720-724.
- Saito, H., & Deguchi, A. (2000). Leaching tests on different mortars using accelerated electrochemical method. *Cement and Concrete Research*, 30(11), 1815-1825.
- Sakai, E., Yamada, K., & Ohta, A. (2003). Molecular structure and dispersion-adsorption mechanisms of comb-type superplasticizers used in Japan. *Journal of Advanced Concrete Technology*, 1(1), 16-25.
- Salman, M., Mathavan, S., Kamal, K., & Rahman, M. (2013). Pavement crack detection using the Gabor filter. Dans *Intelligent Transportation Systems-(ITSC)*, 2013 16th International IEEE Conference on (pp. 2039-2044). IEEE.
- Salami, O. T. (2014). *Synthesis and Working Mechanism of Humic Acid Graft Copolymer Fluid Loss Additives Suitable for Cementing High Pressure/High Temperature Oil and Gas Wells* (Technische Universität München).

- Sanchez, F., Garrabrants, A., Vandecasteele, C., Moszkowicz, P., & Kosson, D. (2003). Environmental assessment of waste matrices contaminated with arsenic. *Journal of hazardous materials*, 96(2), 229-257.
- Sanchez, F., Gervais, C., Garrabrants, A., Barna, R., & Kosson, D. (2002). Leaching of inorganic contaminants from cement-based waste materials as a result of carbonation during intermittent wetting. *Waste management*, 22(2), 249-260.
- Sanchez, L., Drimalas, T., Fournier, B., Mitchell, D., & Bastien, J. (2018). Comprehensive damage assessment in concrete affected by different internal swelling reaction (ISR) mechanisms. *Cement and Concrete Research*, 107, 284-303.
- Sanjuán, M., Andrade, C., & Cheyrezy, M. (2003). Concrete carbonation tests in natural and accelerated conditions. *Advances in Cement research*, 15(4), 171-180.
- Šavija, B., & Luković, M. (2016). Carbonation of cement paste: Understanding, challenges, and opportunities. *Construction and Building Materials*, 117, 285-301.
- Sawell, S., Hetherington, S., & Chandler, A. (1996). An overview of municipal solid waste management in Canada. *Waste management*, 16(5-6), 351-359.
- Schlangen, E., Heide, N. t., & Breugel, K. v. (2006). Crack healing of early age cracks in concrete. Dans *Measuring, monitoring and modeling concrete properties* (pp. 273-284). Springer.
- Scrivener, K., & Capmas, A. (2003). *Calcium aluminate cements*. Advanced concrete technology, 1-31.
- Scrivener, K., Ouzia, A., Juilland, P., & Mohamed, A. K. (2019). Advances in understanding cement hydration mechanisms. *Cement and Concrete Research*, 124, 105823.
- Seng, S., & Tanaka, H. (2011). Properties of cement-treated soils during initial curing stages. *Soils and Foundations*, 51(5), 775-784.
- Shao, N., Li, S., Yan, F., Su, Y., Liu, F., & Zhang, Z. (2020). An all-in-one strategy for the adsorption of heavy metal ions and photodegradation of organic pollutants using steel slag-derived calcium silicate hydrate. *Journal of hazardous materials*, 382, 121120.
- Shi, C., & Fernández-Jiménez, A. (2006). Stabilization/solidification of hazardous and radioactive wastes with alkali-activated cements. *Journal of hazardous materials*, 137(3), 1656-1663.

- Shi, C., & Spence, R. (2004). Designing of cement-based formula for solidification/stabilization of hazardous, radioactive, and mixed wastes. *Critical reviews in environmental science and technology*, 34(4), 391-417.
- Snoeck, D., Dewanckele, J., Cnudde, V., & De Belie, N. (2016). X-ray computed microtomography to study autogenous healing of cementitious materials promoted by superabsorbent polymers. *Cement and concrete composites*, 65, 83-93.
- Snoeck, D., Van Tittelboom, K., Steuperaert, S., Dubruel, P., & De Belie, N. (2014). Self-healing cementitious materials by the combination of microfibres and superabsorbent polymers. *Journal of Intelligent Material Systems and Structures*, 25(1), 13-24.
- Song, H.-W., Kwon, S.-J., Byun, K.-J., & Park, C.-K. (2006). Predicting carbonation in early-aged cracked concrete. *Cement and Concrete Research*, 36(5), 979-989.
- Song, H.-W., & Kwon, S.-J. (2007). Permeability characteristics of carbonated concrete considering capillary pore structure. *Cement and Concrete Research*, 37(6), 909-915.
- Statistics Canada. (2008). Waste management industry survey: Business and government sectors, 2006.
- St-Laurent, S., Burelle, S., Ouellette, H., Bonneau, L., & Larue, M. (2012). *Lignes directrices sur la gestion des matières résiduelles et des sols contaminés traités par stabilisation et solidification*. Développement durable, environnement et parcs Québec.
- Suo, C., Yao, X., Song, Z., & Dong, X. (2022). Mechanical and leaching characteristics of red mud residue solidified/stabilized high Cu (II)-contaminated soil. *Environmental Earth Sciences*, 81(1), 1-11.
- Sweeney, R., Hills, C., & Buenfeld, N. (1998). Investigation into the carbonation of stabilised/solidified synthetic waste. *Environmental technology*, 19(9), 893-902.
- Szelağ, M. (2018). Development of cracking patterns in modified cement matrix with microsilica. *Materials*, 11(10), 1928.
- Talab, A. M. A., Huang, Z., Xi, F., & HaiMing, L. (2016). Detection crack in image using Otsu method and multiple filtering in image processing techniques. *Optik-International Journal for Light and Electron Optics*, 127(3), 1030-1033.
- Taina, I., Heck, R., & Elliot, T. (2008). Application of X-ray computed tomography to soil science: A literature review. *Canadian Journal of Soil Science*, 88(1), 1-19.

- Tashiro, C., & Oba, J. (1979). The effects of Cr₂O₃, Cu (OH) ₂, ZnO and PbO on the compressive strength and the hydrates of the hardened C3A paste. *Cement and Concrete Research*, 9(2), 253-258.
- Taylor, H. F. (1997). *Cement chemistry* (Vol. 2). Thomas Telford London.
- Taylor, K. W., & Chénier, R. (2003). Introduction to ecological risk assessments of priority substances under the Canadian Environmental Protection Act, 1999. *Human and Ecological Risk Assessment*, 9(2), 447-451.
- Tchounwou, P. B., Yedjou, C. G., Patlolla, A. K., & Sutton, D. J. (2012). Heavy metal toxicity and the environment. *Molecular, clinical and environmental toxicology*, 133-164.
- Ter Heide, N., & Schlangen, E. (2007). Self-healing of early age cracks in concrete. Dans *Proceedings of 1st international conference on self healing materials, Noordwijk aan Zee, The Netherlands* (pp. 18-20).
- Thiery, M., Villain, G., Dangla, P., & Platret, G. (2007). Investigation of the carbonation front shape on cementitious materials: Effects of the chemical kinetics. *Cement and Concrete Research*, 37(7), 1047-1058.
- Thomas, N., Jameson, D. A., & Double, D. (1981). The effect of lead nitrate on the early hydration of Portland cement. *Cement and Concrete Research*, 11(1), 143-153.
- Tracz, T., & Zdeb, T. (2019). Effect of hydration and carbonation progress on the porosity and permeability of cement pastes. *Materials*, 12(1), 192.
- USEPA. (2019). Leaching environmental assessment framework (LEAF) how-to guide: Understanding the LEAF approach and how and when to use it: USEPA Washington, DC. <https://www.epa.gov/hw-sw846/how-guide-leaching-environmental-assessment-framework>.
- Valls, S., & Vazquez, E. (2001). Accelerated carbonatation of sewage sludge–cement–sand mortars and its environmental impact. *Cement and Concrete Research*, 31(9), 1271-1276.
- Valsaraj, K. T., & Melvin, E. M. (2000). *Elements of environmental engineering: thermodynamics and kinetics*. CRC Press.
- Van Breugel, K. (2007). Is there a market for self-healing cement-based materials. Dans *Proceedings of the first international conference on self-healing materials* (pp. 1-9).

- Van Der Zwaag, S. (2007). Self-healing materials: an alternative approach to 20 centuries of material science. *Delft: Springer*.
- Van Geet, M., Lagrou, D., & Swennen, R. (2003). Porosity measurements of sedimentary rocks by means of microfocus X-ray computed tomography (μ CT). *Geological Society, London, Special Publications*, 215(1), 51-60.
- Van Gerven, T., Van Baelen, D., Dutré, V., & Vandecasteele, C. (2004). Influence of carbonation and carbonation methods on leaching of metals from mortars. *Cement and Concrete Research*, 34(1), 149-156.
- Van Tittelboom, K., & De Belie, N. (2013). Self-healing in cementitious materials—A review. *Materials*, 6(6), 2182-2217.
- Van Tittelboom, K., Gruyaert, E., Rahier, H., & De Belie, N. (2012). Influence of mix composition on the extent of autogenous crack healing by continued hydration or calcium carbonate formation. *Construction and Building Materials*, 37, 349-359.
- Venhuis, M. A., & Reardon, E. J. (2001). Vacuum method for carbonation of cementitious wastefoms. *Environmental science & technology*, 35(20), 4120-4125.
- Vidal, M., Ostra, M., Imaz, N., García-Lecina, E., & Ubide, C. (2016). Analysis of SEM digital images to quantify crack network pattern area in chromium electrodeposits. *Surface and Coatings Technology*, 285, 289-297.
- Vogel, H. J. (2005). Applications of X-ray Computed Tomography in the Geosciences. Geological Society of London. *European Journal of Soil Science*, 56(2), 277-278.
- Walker, T. R., MacAskill, D., & Weaver, P. (2013). Environmental recovery in Sydney Harbour, Nova Scotia: Evidence of natural and anthropogenic sediment capping. *Marine pollution bulletin*, 74(1), 446-452.
- Walton, J. C., Bin-Shafique, S., Smith, R. W., Gutierrez, N., & Tarquin, A. (1997). Role of carbonation in transient leaching of cementitious wastefoms. *Environmental science & technology*, 31(8), 2345-2349.
- Wang, F., Wang, H., & Al-Tabbaa, A. (2014). Leachability and heavy metal speciation of 17-year old stabilised/solidified contaminated site soils. *Journal of hazardous materials*, 278, 144-151.

- Wang, F., Wang, H., Jin, F., & Al-Tabbaa, A. (2015). The performance of blended conventional and novel binders in the in-situ stabilisation/solidification of a contaminated site soil. *Journal of hazardous materials*, 285, 46-52.
- Wang, J., Dewanckele, J., Cnudde, V., Van Vlierberghe, S., Verstraete, W., & De Belie, N. (2014). X-ray computed tomography proof of bacterial-based self-healing in concrete. *Cement and concrete composites*, 53, 289-304.
- Wang, J., Xu, H., Xu, D., Du, P., Zhou, Z., Yuan, L., & Cheng, X. (2019). Accelerated carbonation of hardened cement pastes: Influence of porosity. *Construction and Building Materials*, 225, 159-169.
- Wang, K., Jansen, D. C., Shah, S. P., & Karr, A. F. (1997). Permeability study of cracked concrete. *Cement and Concrete Research*, 27(3), 381-393.
- Wang, W., & Noguchi, T. (2020). Alkali-silica reaction (ASR) in the alkali-activated cement (AAC) system: A state-of-the-art review. *Construction and Building Materials*, 252, 119105.
- Wang, Y., Hu, Y., Xue, C., Khan, A., Zheng, X., & Cai, L. (2022). Risk assessment of lead and cadmium leaching from solidified/stabilized MSWI fly ash under long-term landfill simulation test. *Science of the total environment*, 816, 151555.
- Whitaker, S. (1986). Flow in porous media I: A theoretical derivation of Darcy's law. *Transport in porous media*, 1(1), 3-25.
- Wiles, C. C. (1987). A review of solidification/stabilization technology. *Journal of hazardous materials*, 14(1), 5-21.
- Wong, H., Zobel, M., Buenfeld, N., & Zimmerman, R. (2009). Influence of the interfacial transition zone and microcracking on the diffusivity, permeability and sorptivity of cement-based materials after drying. *Magazine of Concrete Research*, 61(8), 571-589.
- Wu, J., West, L., & Stewart, D. (2002). Effect of humic substances on Cu (II) solubility in kaolin-sand soil. *Journal of hazardous materials*, 94(3), 223-238.
- Wu, L., Farzadnia, N., Shi, C., Zhang, Z., & Wang, H. (2017). Autogenous shrinkage of high performance concrete: A review. *Construction and Building Materials*, 149, 62-75.
- Wuana, R. A., & Okieimen, F. E. (2011). Heavy metals in contaminated soils: a review of sources, chemistry, risks and best available strategies for remediation. *Isrn Ecology*, 2011.

- Xue, J., Liu, S., Ma, X., Teng, Y., & Guan, X. (2022). Effect of different gypsum dosage on the chloride binding properties of C4AF hydrated paste. *Construction and Building Materials*, 315, 125562.
- Yaman, I., Aktan, H., & Hearn, N. (2002). Active and non-active porosity in concrete part II: evaluation of existing models. *Materials and Structures*, 35(2), 110-116.
- Yaman, I., Hearn, N., & Aktan, H. (2002). Active and non-active porosity in concrete part I: experimental evidence. *Materials and Structures*, 35(2), 102-109.
- Yang, B.-h., Wu, A.-x., Miao, X.-x., & Liu, J.-z. (2014). 3D characterization and analysis of pore structure of packed ore particle beds based on computed tomography images. *Transactions of Nonferrous Metals Society of China*, 24(3), 833-838.
- Yang, E.-H. (2008). *Designing Added Functions in Engineered Cementitious Composites*.
- Yi, S.-T., Hyun, T.-Y., & Kim, J.-K. (2011). The effects of hydraulic pressure and crack width on water permeability of penetration crack-induced concrete. *Construction and Building Materials*, 25(5), 2576-2583.
- Yıldırım, G., Keskin, Ö. K., Keskin, S. B., Şahmaran, M., & Lachemi, M. (2015). A review of intrinsic self-healing capability of engineered cementitious composites: Recovery of transport and mechanical properties. *Construction and Building Materials*, 101, 10-21.
- Yiyang, Z. (2014). The design of glass crack detection system based on image preprocessing technology. Dans *Information Technology and Artificial Intelligence Conference (ITAIC), 2014 IEEE 7th Joint International* (pp. 39-42). IEEE.
- Young, J. (1972). A review of the mechanisms of set-retardation in Portland cement pastes containing organic admixtures. *Cement and Concrete Research*, 2(4), 415-433.
- Yousuf, M., Mollah, A., Vempati, R. K., Lin, T.-C., & Cocke, D. L. (1995). The interfacial chemistry of solidification/stabilization of metals in cement and pozzolanic material systems. *Waste management*, 15(2), 137-148.
- Yvon, J., Antenucci, D., Jdid, E.-A., Lorenzi, G., Dutre, V., Leclercq, D., Veschkens, M. (2006). Long-term stability in landfills of Municipal Solid Waste Incineration fly ashes solidified/stabilized by hydraulic binders. *Journal of Geochemical Exploration*, 90(1-2), 143-155.
- Zdravkov, B., Čermák, J., Šefara, M., & Janků, J. (2007). Pore classification in the characterization of porous materials: A perspective. *Open Chemistry*, 5(2), 385-395.

- Zha, F.-s., Liu, J.-j., Xu, L., & Cui, K.-r. (2013). Effect of cyclic drying and wetting on engineering properties of heavy metal contaminated soils solidified/stabilized with fly ash. *Journal of Central South University*, 20(7), 1947-1952.
- Zhang, D., & Shao, Y. (2016). Effect of early carbonation curing on chloride penetration and weathering carbonation in concrete. *Construction and Building Materials*, 123, 516-526.
- Zhang, H., Wang, B., Dong, X., Feng, L., & Fan, Z. (2009). Leachability of heavy metals from solidified sludge. *Science in China Series E: Technological Sciences*, 52(7), 1906-1912.
- Zhong, R., & Wille, K. (2016). Linking pore system characteristics to the compressive behavior of pervious concrete. *Cement and concrete composites*, 70, 130-138.
- Zhong, R., Xu, M., Netto, R. V., & Wille, K. (2016). Influence of pore tortuosity on hydraulic conductivity of pervious concrete: Characterization and modeling. *Construction and Building Materials*, 125, 1158-1168.
- Zhong, W., & Yao, W. (2008). Influence of damage degree on self-healing of concrete. *Construction and Building Materials*, 22(6), 1137-1142.
- Zhongping, Y., Yao, W., Xuyong, L., Shupe, R., Hui, X., & Jiazhao, C. (2021). The effect of long-term freeze-thaw cycles on the stabilization of lead in compound solidified/stabilized lead-contaminated soil. *Environmental Science and Pollution Research*, 28(28), 37413-37423.